

Anatomy of the Real Higgs Triplet Model

Saiyad Ashanujjaman^{a,b,c,d} Sumit Banik^{e,f} Guglielmo Coloretti^{e,f} Andreas Crivellin^{e,f} Siddharth P. Maharathy^{g,h} Bruce Mellado^{g,i}

^a*Institut für Theoretische Teilchenphysik, Karlsruhe Institute of Technology, Engesserstraße 7, D-76128 Karlsruhe, Germany*

^b*Institut für Astroteilchenphysik, Karlsruhe Institute of Technology, Hermann-von-Helmholtz-Platz 1, D-76344 Eggenstein-Leopoldshafen, Germany*

^c*Institute of High Energy Physics, Chinese Academy of Sciences, Beijing 100049, China*

^d*Kaiping Neutrino Research Center, Jiangmen 529399, China*

^e*Laboratory for Particle Physics, PSI Center for Neutron and Muon Sciences, Forschungsstrasse 111, 5232 Villigen PSI, Switzerland*

^f*Physik-Institut, Universität Zurich, Winterthurerstrasse 190, CH-8057 Zurich*

^g*School of Physics and Institute for Collider Particle Physics, University of the Witwatersrand, Johannesburg, Wits 2050, South Africa*

^h*Indian Institute of Science Education and Research Pune, Dr. Homi Bhabha Road, Pune 411008, India*

ⁱ*Themba LABS, National Research Foundation, PO Box 722, Somerset West 7129, South Africa*

E-mails: saiyad.ashanujjaman@kit.edu, sumit.banik@psi.ch, guglielmo.coloretti@physik.uzh.ch, andreas.crivellin@psi.ch, siddharth.m@students.iiserpune.ac.in, bmellado@mail.cern.ch

ABSTRACT: In this article, we examine the Standard Model extended by a $Y = 0$ real Higgs triplet, the Δ SM. It contains a CP -even neutral Higgs (Δ^0) and two charged Higgs bosons (Δ^\pm), which are quasi-degenerate in mass. We first study the theoretical constraints from vacuum stability and perturbative unitarity and then calculate the Higgs decays, including the loop-induced modes such as di-photons ($\gamma\gamma$) and $Z\gamma$. In the limit of a small mixing between the SM Higgs and Δ^0 , the latter decays dominantly to WW and can have a sizable branching ratio to di-photon. The model predicts a positive definite shift in the W mass, which agrees with the current global electroweak fit. At the Large Hadron Collider, it leads to a (i) stau-like signature from $pp \rightarrow \Delta^+\Delta^- \rightarrow \tau^+\tau^-\nu\bar{\nu}$, (ii) multi-lepton final states from $pp \rightarrow \gamma^* \rightarrow \Delta^+\Delta^- \rightarrow W^+W^-ZZ$ and $pp \rightarrow W^* \rightarrow \Delta^\pm\Delta^0 \rightarrow W^\pm ZW^+W^-$ as well as (iii) associated di-photon production from $pp \rightarrow W^* \rightarrow \Delta^\pm(\Delta^0 \rightarrow \gamma\gamma)$. Concerning (i), the reinterpretation of the recent supersymmetric tau partner search by ATLAS and CMS excludes $m_{\Delta^\pm} < 110$ GeV at 95% CL. From (ii), some of the signal regions of multi-lepton searches lead to bounds close to the predicted cross-section, but electroweak scale masses are still allowed. For (iii), the recast of the

associated di-photon searches by ATLAS and a combined log-likelihood fit of signal and background to data find that out of the 25 signal regions, 10 provide relevant limits on $\text{Br}(\Delta^0 \rightarrow \gamma\gamma)$ at the per cent level. Interestingly, 6 signal regions show excesses at around 152 GeV, leading to a preference for a non-zero di-photon branching ratio of about 0.7% with the corresponding significance amounting to about 4σ . While the minimalistic ΔSM does not fully describe the discrepancies between the data and the SM, this study indicates that the Drell-Yan production mechanisms can contribute to the explanation of the narrow excesses at 152 GeV at the LHC. Furthermore, extended models involving the triplet are capable of explaining the multi-lepton anomalies. In the appendix, we provide the Feynman rules for the model along with an analysis of charge-breaking minima.

Contents

1	Introduction	2
2	The ΔSM	3
2.1	Masses and couplings	5
2.2	Vacuum stability and perturbative unitarity	7
3	Higgs Production and Decays	10
3.1	Production	10
3.2	Decays of the SM-like Higgs	11
3.3	Decays of the triplet-like Higgses Δ^0 and Δ^\pm	14
4	Phenomenology	20
4.1	W mass	20
4.2	Multi-lepton signature from DY production	20
4.3	Associated production of the triplet-like Higgs and resonant di-photon signatures: $\gamma\gamma + X$	24
4.4	Higgs to $Z\gamma$ search in the $\ell^+\ell^-\gamma$ final state	34
5	Summary and Outlook	35
A	Feynman rules for the ΔSM	37
B	Loop functions	42
C	Stability and charge-breaking minima	44

1 Introduction

The Standard Model (SM) of particle physics is the currently accepted theory describing the fundamental constituents of matter and their interactions. It has been tested with high accuracy [1–3], and the discovery of the 125 GeV Brout-Englert-Higgs boson [4–7] at the Large Hadron Collider (LHC) [8, 9] provided its last missing piece. Therefore, any observation of new (fundamental) particles would prove the existence of physics beyond the SM (BSM). In fact, the SM cannot be the ultimate fundamental theory of Nature as it fails to account for several experimental observations, such as neutrino masses and mixing or the existence of Dark Matter. Therefore, the SM must be extended by new particles and new interactions.

While one can account for Dark Matter and neutrino masses in many ways and at very different energies, anomalies, *i.e.* deviations from the SM predictions, point towards new physics at or below the TeV scale (see Ref. [10] for a review). In fact, many of these anomalies can be explained by extensions of the SM Higgs sector, whose minimality, *i.e.* the presence of a single $SU(2)_L$ doublet scalar that simultaneously gives mass to the electroweak (EW) gauge bosons and all fermions, is not guaranteed by any guiding principle or symmetry. Furthermore, while the measured properties of the 125 GeV Higgs are consistent with the SM expectations [11–15], this does not exclude the existence of additional scalar bosons as long as their role in electroweak symmetry breaking is minute. A plethora of models going beyond the SM Higgs sector have been proposed in the literature, including the addition of $SU(2)_L$ singlets [16–18], doublets [19–23] and triplets [24–29], etc. While, in the past, the main focus has been on singlet and doublet extensions that preserve the custodial symmetry at tree level (*i.e.* $\rho = 1$), the larger-than-expected W mass measured by the CDF-II collaboration [30] has led to a renaissance of scalar multiplet models [31–52]. In particular, the Higgs triplet with hypercharge $Y = 0$ is the most minimal extension of the SM that leads to a positive shift in the W mass at tree-level [33–41, 50, 53–67].

Though the intensified LHC searches for new particles, particularly new Higgses, have not led to any discovery yet, several “multi-lepton anomalies”—statistically significant deviations from the SM predictions in final states with multiple leptons, missing energy and possibly (b -)jets [68–75]—have emerged; see Refs. [10, 76] for a review. They are compatible with the production of a ≈ 270 GeV Higgs decaying into a pair of lighter Higgses (S and S'), which dominantly decay to WW and $b\bar{b}$, respectively. The opposite-sign di-lepton invariant mass from the leptonic W decays is sensitive to the mass m_S and fitting the invariant mass spectra, Ref. [69] found $m_S = 150 \pm 5$ GeV. In this context, it is important to note that the neutral component of the $Y = 0$ triplet naturally has a dominant branching ratio to W bosons.

Refs. [77, 78], analyzing the sidebands of the SM Higgs boson searches by the ATLAS and CMS collaborations [79–86], find that the data suggest the presence of a

new narrow resonance in the di-photon and $Z\gamma$ spectra with a mass around 152 GeV produced in association with leptons, (b -)jets and missing energy. The overall global significance of this resonant excess, using the Fischer method, has surpassed the 5σ mark within a simplified model.¹ Since there is no excess in ZZ final states, it is therefore interesting to explore the phenomenology of the Real Higgs Triplet model in this context. As such, Refs. [87–89] showed that the latest ATLAS analyses [90, 91] targeting associated productions of the SM Higgs in various di-photon channels, are consistent with the Drell-Yan production of a ≈ 152 GeV Higgs triplet with a corresponding significance of around 4σ .²

We take the above phenomenological motivations to perform a comprehensive study of the $Y = 0$ Higgs triplet model [31, 53–60], which after spontaneous symmetry breaking contains, in addition to the SM Higgs, a CP -even Higgs (Δ^0) and two charged Higgs bosons (Δ^\pm). The outline of this article is as follows. We present in Sec. 2 details of the model, followed by the vacuum stability and perturbative unitarity constraints. The decay rates of the triplet Higgses are discussed in Sec. 3 and the phenomenology in Sec. 4. Finally, we summarise our findings in Sec. 5. Further, we collect the relevant Feynman rules in Appendix A, and in Appendix C, we discuss possible vacua configurations and the stability of the neutral ones against the charge-breaking ones.

2 The Δ SM

The Higgs sector of the real Higgs triplet model, called the Δ SM, is composed of the SM Higgs $SU(2)_L$ doublet (Φ) with $Y = 1/2$ (in our convention)

$$\Phi = \begin{pmatrix} h_\Phi^+ \\ \frac{1}{\sqrt{2}}(v_\Phi + h_\Phi^0 + iG^0) \end{pmatrix}, \quad (2.1)$$

and the Higgs triplet (Δ) with $Y = 0$ transforming in the adjoint representation of $SU(2)_L$

$$\Delta = \frac{1}{2} \begin{pmatrix} v_\Delta + h_\Delta^0 & \sqrt{2}h_\Delta^+ \\ \sqrt{2}h_\Delta^- & -(v_\Delta + h_\Delta^0) \end{pmatrix}, \quad (2.2)$$

where $h_{\Phi,\Delta}^0$ are real scalar fields, $h_{\Phi,\Delta}^- = (h_{\Phi,\Delta}^+)^*$, and v_Φ and v_Δ are the respective vacuum expectation values (VEVs). With these conventions, the canonically

¹This is obtained by adding the ATLAS excess in $\gamma\gamma + \tau$ ($\approx 3\sigma$) [91] to the combination of Ref. [78].

²Hints for the existence of a neutral scalar with a mass around 95 GeV were presented by the CMS collaboration [92–94], not excluded by the ATLAS experiment [95, 96] and consistent with a mild excess reported by the LEP experiments [97]. As a possible explanation for these excesses, the scalar triplet with $Y = 0$ was proposed in Ref. [66, 98]. However, we will find here that the updated ATLAS stau search with full run 2 luminosity excludes this possibility.

normalised gauge-kinetic part of the Lagrangian involving the triplet is

$$\mathcal{L} \supset \text{Tr}[(D_\mu \Delta)^\dagger (D^\mu \Delta)], \quad (2.3)$$

where $D_\mu \Delta = \partial_\mu \Delta + ig \left[\frac{1}{2} \sigma^k W_\mu^k, \Delta \right]$, with g being the $SU(2)_L$ gauge coupling, σ^k the Pauli matrices, and the square bracket denotes the commutator.

After EW symmetry breaking, the $SU(2)_L$ doublet Higgs contributes to both W and Z boson masses at the tree level, preserving the so-called custodial symmetry, i.e. $\rho = 1$. However, the Higgs triplet only contributes to the W -boson mass (at the tree level), thereby breaking the custodial symmetry maximally such that

$$\rho_{\text{tree}} = \frac{m_W^2}{m_Z^2 \cos^2 \theta_w} = \frac{\frac{1}{4} g^2 (v_\Phi^2 + 4v_\Delta^2)}{\frac{1}{4} (g^2 + g'^2) v_\Phi^2 \cos^2 \theta_w} \approx 1 + \frac{4v_\Delta^2}{v^2}, \quad (2.4)$$

where g' is the $U(1)_Y$ gauge coupling, θ_w is the Weinberg angle, and $v \approx v_\Phi \approx 246$ GeV. Note that the electroweak precision data require ρ to be close to unity at the sub-percent level, allowing us to expand in v_Δ/v_Φ in the last step.

At the phenomenological level, the W -boson mass is usually calculated in the so-called “ G_F scheme” input scheme using the Z -boson mass, the fine-structure constant α , and the Fermi constant G_F from muon decay, resulting in

$$m_W^2 \left(1 - \frac{m_W^2}{m_Z^2} \right) = \frac{\pi \alpha}{\sqrt{2} G_F} (1 + \Delta r). \quad (2.5)$$

Here, m_W and m_Z are renormalised masses in the on-shell scheme, and $\Delta r = \Delta \alpha - \frac{c_W^2}{s_W^2} \Delta \rho + \Delta r_{\text{rem}}$ represents radiative corrections to α , the ρ parameter, and the remaining part of the gauge boson two-point functions as well as the vertex and box diagram corrections to the light fermion scattering process [99]. Combining the expressions above, we have

$$m_W^2 = \frac{m_Z^2}{2} \left[1 + \sqrt{1 - \frac{4\pi \alpha_{\text{em}}}{\sqrt{2} G_F m_Z^2} (1 + \Delta r(m_W^2))} \right]. \quad (2.6)$$

Taking into account that the triplet Higgs contribution to Δr at one-loop is suppressed on account of its small mixing with the SM Higgs and its degenerate masses (see later), the only relevant contribution to Δr appears through ρ at tree-level. Thus, to first-order in v_Δ , Eq. (2.6) implies a shift in ρ_{tree} : $\delta \rho = \rho_{\text{tree}} - 1$, which translates to a shift in m_W [67, 99]

$$\Delta m_W \approx \frac{m_W}{2} \frac{\cos^2 \theta_w}{\cos^2 \theta_w - \sin^2 \theta_w} \delta \rho. \quad (2.7)$$

2.1 Masses and couplings

The most general scalar potential of the Δ SM model is

$$V = -\mu_\Phi^2 \Phi^\dagger \Phi + \frac{\lambda_\Phi}{4} (\Phi^\dagger \Phi)^2 - \mu_\Delta^2 \text{Tr}(\Delta^\dagger \Delta) + \frac{\lambda_\Delta}{4} [\text{Tr}(\Delta^\dagger \Delta)]^2 + A \Phi^\dagger \Delta \Phi + \lambda_{\Phi\Delta} \Phi^\dagger \Phi \text{Tr}(\Delta^\dagger \Delta). \quad (2.8)$$

Without loss of generality, all couplings can be assumed to be real. Consequently, the potential is CP -conserving. Note that in the limit $A \rightarrow 0$, the potential possesses a global $O(4)_\Phi \times O(3)_\Delta$ symmetry and the discrete $Z_{2,\Delta}$ ($\Delta \rightarrow -\Delta$) symmetry. Therefore, a non-zero A leads to a soft breaking of this symmetry such that small values of it are natural in the sense 't Hooft defined it [100].

Minimizing the potential in Eq. (2.8), we find the conditions

$$\mu_\Phi^2 = -\frac{Av_\Delta}{2} + \frac{1}{4}v_\Phi^2\lambda_\Phi + \frac{1}{2}\lambda_{\Phi\Delta}v_\Delta^2, \quad (2.9)$$

$$\mu_\Delta^2 = -\frac{Av_\Phi^2}{4v_\Delta} + \frac{1}{2}v_\Phi^2\lambda_{\Phi\Delta} + \frac{1}{4}\lambda_\Delta v_\Delta^2, \quad (2.10)$$

which can be used to replace μ_Φ^2 and μ_Δ^2 such that the mass matrices for the (CP -even) neutral and charged Higgses read

$$M_0^2 = \begin{pmatrix} \frac{\lambda_\Phi v_\Phi^2}{2} & (\lambda_{\Phi\Delta} v_\Delta - \frac{A}{2}) v_\Phi \\ (\lambda_{\Phi\Delta} v_\Delta - \frac{A}{2}) v_\Phi & \frac{\lambda_\Delta v_\Delta^2}{2} + \frac{Av_\Phi^2}{4v_\Delta} \end{pmatrix}, \quad (2.11)$$

$$M_\pm^2 = \begin{pmatrix} Av_\Delta & \frac{Av_\Phi}{2} \\ \frac{Av_\Phi}{2} & \frac{Av_\Phi^2}{4v_\Delta} \end{pmatrix}, \quad (2.12)$$

in the interaction basis $(h_\phi^{0,\pm}, h_\Delta^{0,\pm})$. We diagonalize these mass matrices by rotating the interaction states to the physical basis where the mass matrices are diagonal. These mass eigenstates are given by

$$\begin{pmatrix} h \\ \Delta^0 \end{pmatrix} = \begin{pmatrix} \cos \alpha & \sin \alpha \\ -\sin \alpha & \cos \alpha \end{pmatrix} \begin{pmatrix} h_\Phi^0 \\ h_\Delta^0 \end{pmatrix}, \quad (2.13)$$

$$\begin{pmatrix} G^\pm \\ \Delta^\pm \end{pmatrix} = \begin{pmatrix} \cos \beta & \sin \beta \\ -\sin \beta & \cos \beta \end{pmatrix} \begin{pmatrix} h_\Phi^\pm \\ h_\Delta^\pm \end{pmatrix}, \quad (2.14)$$

with the eigenvalues

$$m_h^2 = \frac{\lambda_\Phi v_\Phi^2}{2} + \tan \alpha \left(\lambda_{\Phi\Delta} v_\Delta - \frac{A}{2} \right) v_\Phi, \quad (2.15)$$

$$m_{\Delta^0}^2 = \frac{\lambda_\Delta v_\Delta^2}{2} + \frac{Av_\Phi^2}{4v_\Delta} - \tan \alpha \left(\lambda_{\Phi\Delta} v_\Delta - \frac{A}{2} \right) v_\Phi, \quad (2.16)$$

$$m_{\Delta^\pm}^2 = A \frac{v_\Phi^2 + 4v_\Delta^2}{4v_\Delta}, \quad (2.17)$$

$$m_{G^\pm}^2 = 0, \quad (2.18)$$

and the mixing angles

$$\tan 2\alpha = \frac{4v_\Phi v_\Delta (2\lambda_{\Phi\Delta} v_\Delta - A)}{2\lambda_\Phi v_\Phi^2 v_\Delta - 2\lambda_\Delta v_\Delta^3 - Av_\Phi^2}, \quad (2.19)$$

$$\tan 2\beta = -\frac{4v_\Phi v_\Delta}{v_\Phi^2 - 4v_\Delta^2} \quad \left(\text{equivalently, } \tan \beta = -\frac{2v_\Delta}{v_\Phi} \right). \quad (2.20)$$

Note that the mass eigenstate h is identified as the 125 GeV Higgs observed at the LHC, and the zero eigenvalue of the charged Higgs mass matrix corresponds to the *would-be* Goldstone boson. Note that we did not explicitly write down the neutral Goldstone G^0 , which comes purely from the doublet Higgs and thus has the same properties as in the SM.

From Eq. (2.16) and Eq. (2.17), we have

$$m_{\Delta^\pm}^2 - m_{\Delta^0}^2 = Av_\Delta - \frac{\lambda_\Delta v_\Delta^2}{2} + \tan \alpha \left(\lambda_{\Phi\Delta} v_\Delta - \frac{A}{2} \right) v_\Phi. \quad (2.21)$$

Therefore, Δ^0 and Δ^\pm are nearly mass-degenerate for $\alpha \approx 0$ and $v_\Delta \approx 0$. Even though α and v_Δ break this mass-degeneracy and sufficiently large values could induce sizable mass-splitting among them, the requirement of vacuum stability and perturbative unitarity (see Sec. 2.2) together with the experimental limit on the ρ parameter restrict the mass-splitting to at most a few GeV.³ However, such a small mass-splitting is of little consequence as far as the LHC phenomenology or electroweak precision observables—in particular, the oblique parameters—are concerned [36, 102, 103]. Therefore, we take $m_{\Delta^0} \approx m_{\Delta^\pm} \approx m_\Delta$ further in this work unless stated otherwise.

We can trade all trilinear and quartic couplings of the Lagrangian in Eq. (2.8) for the physical Higgs masses ($m_h \approx 125$ GeV, m_{Δ^0} , m_{Δ^\pm}), the VEVs ($v_\Phi \approx 246$ GeV, v_Δ) and the mixing angle (α):

$$\lambda_\Phi = \frac{2}{v_\Phi^2} [\cos^2 \alpha m_h^2 + \sin^2 \alpha m_{\Delta^0}^2], \quad (2.22)$$

$$\lambda_\Delta = \frac{2}{v_\Delta^2} \left[\sin^2 \alpha m_h^2 + \cos^2 \alpha m_{\Delta^0}^2 - \frac{v_\Phi^2}{v_\Phi^2 + 4v_\Delta^2} m_{\Delta^\pm}^2 \right], \quad (2.23)$$

$$\lambda_{\Phi\Delta} = \frac{1}{2v_\Phi v_\Delta} \left[\sin 2\alpha (m_h^2 - m_{\Delta^0}^2) + \frac{4v_\Phi v_\Delta}{v_\Phi^2 + 4v_\Delta^2} m_{\Delta^\pm}^2 \right], \quad (2.24)$$

³Note that EW radiative corrections, driven by the EW gauge bosons, induce a mass-splitting $m_{\Delta^\pm} - m_{\Delta^0}$ of 160–170 MeV [101].

$$A = \frac{4v_\Delta}{v_\Phi^2 + 4v_\Delta^2} m_{\Delta^\pm}^2. \quad (2.25)$$

Therefore, the Higgs sector has only four free parameters: $m_{\Delta^0}, m_{\Delta^\pm}, \alpha$ and v_Δ . To get a better analytic understanding of these equations, we expand them in $v_\Delta/v_\Phi \approx v_\Delta/v$ to obtain

$$\lambda_\Phi = \frac{2}{v^2} [\cos^2 \alpha m_h^2 + \sin^2 \alpha m_{\Delta^\pm}^2], \quad (2.26)$$

$$\lambda_\Delta = \frac{2}{v_\Delta^2} [\sin^2 \alpha m_h^2 + \cos^2 \alpha m_{\Delta^0}^2 - m_{\Delta^\pm}^2], \quad (2.27)$$

$$\lambda_{\Phi\Delta} = \frac{1}{2vv_\Delta} \sin 2\alpha (m_{\Delta^0}^2 - m_{\Delta^\pm}^2) + \frac{2}{v^2} m_{\Delta^\pm}^2, \quad (2.28)$$

$$A = \frac{4v_\Delta}{v^2} m_{\Delta^\pm}^2. \quad (2.29)$$

Further expanding in the mixing angle α , one finds

$$\lambda_\Phi = \frac{2m_h^2}{v^2}, \quad (2.30)$$

$$\lambda_\Delta = \frac{2}{v_\Delta^2} [m_{\Delta^0}^2 - m_{\Delta^\pm}^2], \quad (2.31)$$

$$\lambda_{\Phi\Delta} = \frac{\alpha}{vv_\Delta} (m_{\Delta^0}^2 - m_{\Delta^\pm}^2) + \frac{2}{v^2} m_{\Delta^\pm}^2, \quad (2.32)$$

$$A = \frac{4v_\Delta}{v^2} m_{\Delta^\pm}^2. \quad (2.33)$$

Note that the Higgs triplet field (Δ) does not couple to the SM fermions at the Lagrangian level. Therefore, the Yukawa Lagrangian is the same as that of the SM (before EW symmetry breaking),

$$\mathcal{L}_{\text{Yuk}} = -\bar{Q}_L Y_d \Phi d_R - \bar{Q}_L Y_u \Phi^c u_R - \bar{L}_L Y_l \Phi e_R \quad (2.34)$$

with the only difference arising from the mixing of the scalar states. The resulting Feynman rules concerning their gauge, Yukawa, and self-interactions are given in Appendix A.

2.2 Vacuum stability and perturbative unitarity

While writing Eq. (2.1) and Eq. (2.2), we have implicitly assumed that the EW symmetry is spontaneously broken at some electrically neutral point in the field space and that the corresponding vacuum is the global minimum of the potential. Although the conditions in Eq. (2.9) and Eq. (2.10) ensure that the desired EW vacuum corresponds to an extremum of the potential in Eq.(2.8), one still needs to check that this extremum is indeed stable, *i.e.* not a saddle-point or a local maximum.

As we show in Appendix C, the absence of tachyonic modes in the Higgs sector, *i.e.* $m_h^2 > 0$, $m_{\Delta^0}^2 > 0$ and $m_{\Delta^\pm}^2 > 0$, suffices to ensure that the desired EW vacuum corresponds to the global minimum of the potential. Further discussions on the possible vacua configurations and stability of the neutral ones against the charge-breaking ones are deferred till Appendix C.

A necessary condition for the stability of the vacuum is that the potential is bounded from below in all directions in field space. At large field values, the potential in Eq. (2.8) is dominated by the quadratic terms

$$V_4(\Phi, \Delta) = \frac{\lambda_\Phi}{4} (\Phi^\dagger \Phi)^2 + \frac{\lambda_\Delta}{4} [\text{Tr}(\Delta^\dagger \Delta)]^2 + \lambda_{\Phi\Delta} \Phi^\dagger \Phi \text{Tr}(\Delta^\dagger \Delta) \quad (2.35)$$

$$= (|\Phi|^2 \quad |\Delta|^2) \begin{pmatrix} \frac{\lambda_\Phi}{4} & \frac{\lambda_{\Phi\Delta}}{4} \\ \frac{\lambda_{\Phi\Delta}}{4} & \frac{\lambda_\Delta}{8} \end{pmatrix} \begin{pmatrix} |\Phi|^2 \\ |\Delta|^2 \end{pmatrix},$$

$$= x^T \Lambda x, \quad (2.36)$$

where $x = \begin{pmatrix} |\Phi|^2 \\ |\Delta|^2 \end{pmatrix} \geq 0$ and $\Lambda = \begin{pmatrix} \frac{\lambda_\Phi}{4} & \frac{\lambda_{\Phi\Delta}}{4} \\ \frac{\lambda_{\Phi\Delta}}{4} & \frac{\lambda_\Delta}{8} \end{pmatrix}$. The requirement $V_4(\Phi, \Delta) \geq 0$, thus, implies that Λ has to be a copositive matrix. Applying the copositivity conditions to Λ , we find

$$\lambda_\Phi > 0, \quad \lambda_\Delta > 0, \quad \sqrt{2}\lambda_{\Phi\Delta} + \sqrt{\lambda_\Phi \lambda_\Delta} > 0. \quad (2.37)$$

These conditions are sufficient and necessary to ensure that the potential is bounded from below in all directions in field space at the tree level.⁴ The constraint $\lambda_\Delta > 0$ implies that $m_{\Delta^0}^2 - m_{\Delta^\pm}^2 > \sin^2 \alpha (m_{\Delta^0}^2 - m_h^2)$, see Eq. (2.27). This, therefore, fixes the hierarchy of the triplet-like Higgs spectra for $m_{\Delta^0} > m_h$: $m_{\Delta^0} > m_{\Delta^\pm}$.

The model parameter space can also be constrained by requiring perturbative unitarity in scattering processes. This sets limits on interactions in $2 \rightarrow 2$ scalar scattering processes.⁵ The partial-wave decomposition of the scattering amplitude $\mathcal{M}_{i \rightarrow f}$ reads as

$$\mathcal{M}_{fi} = iT^{fi} = 16i\pi \sum_j (2j+1) a_j^{fi}(s) P_j(\cos \theta), \quad (2.38)$$

where a_j denotes the j -th partial-wave amplitude, θ is the polar angle between the i and f directions, and P_j is the Legendre polynomial of degree j . In the high energy (massless) limit, the most dominant contribution comes from the $j = 0$ partial-wave

⁴In this work, we do not attempt to find the possible quantum modifications to these constraints.

⁵On account of the equivalence theorem [104, 105], we can use unphysical scalar states instead of longitudinal components of the gauge bosons in the high energy limit. Compared to $2 \rightarrow 2$ scattering processes, $2 \rightarrow 3$ partial-wave amplitudes can be neglected as the latter scales as the inverse of the energy scale. Further, the amplitudes containing trilinear vertices are generally suppressed by factors accruing from the intermediate propagators.

(s -wave) at tree-level⁶

$$a_0^{fi} = -\frac{i}{16\pi} \mathcal{M}_{fi}. \quad (2.39)$$

The S -matrix unitarity for the scattering processes requires $|(a_0)| \leq 1$, $|\operatorname{Re}(a_0)| \leq \frac{1}{2}$, and $0 \leq \operatorname{Im}(a_0) \leq 1$. However, in practice, it suffices to require $|(a_0)| \leq 1$ or $|\operatorname{Re}(a_0)| \leq \frac{1}{2}$, which, in turn, implies that the eigenvalues x_i of the scattering submatrices: $|x_i| \leq \kappa\pi$, where $\kappa = 16$ or 8 depending on whether we demand the former or the latter. This is largely a matter of choice [111], and we choose the former.

In the following, we present the resulting submatrices structured in terms of net electric charge in the initial/final states, with their entries corresponding to the quartic couplings that mediate the scalar-scalar scattering processes

$$\mathcal{M}^2 = \operatorname{diag} \left(\frac{\lambda_\Phi}{2}, \frac{\lambda_\Delta}{2}, \lambda_{\Phi\Delta} \right), \quad (2.40)$$

$$\mathcal{M}^1 = \operatorname{diag} \left(\frac{\lambda_\Phi}{2}, \lambda_{\Phi\Delta}, \frac{\lambda_\Phi}{2}, \lambda_{\Phi\Delta}, \frac{\lambda_\Delta}{2}, \lambda_{\Phi\Delta} \right), \quad (2.41)$$

$$\mathcal{M}_{(a)}^0 = \operatorname{diag} \left(\lambda_{\Phi\Delta}, \lambda_{\Phi\Delta}, \lambda_{\Phi\Delta}, \frac{\lambda_\Phi}{2}, \lambda_{\Phi\Delta} \right), \quad (2.42)$$

$$\mathcal{M}_{(b)}^0 = \begin{pmatrix} \lambda_\Phi & \lambda_{\Phi\Delta} & \frac{\lambda_\Phi}{2\sqrt{2}} & \frac{\lambda_{\Phi\Delta}}{\sqrt{2}} & \frac{\lambda_\Phi}{2\sqrt{2}} \\ \lambda_{\Phi\Delta} & \lambda_\Delta & \frac{\lambda_{\Phi\Delta}}{\sqrt{2}} & \frac{\lambda_\Delta}{2\sqrt{2}} & \frac{\lambda_{\Phi\Delta}}{\sqrt{2}} \\ \frac{\lambda_\Phi}{2\sqrt{2}} & \frac{\lambda_{\Phi\Delta}}{\sqrt{2}} & \frac{3\lambda_\Phi}{4} & \frac{\lambda_{\Phi\Delta}}{2} & \frac{\lambda_\Phi}{4} \\ \frac{\lambda_{\Phi\Delta}}{\sqrt{2}} & \frac{\lambda_\Delta}{2\sqrt{2}} & \frac{\lambda_{\Phi\Delta}}{2} & \frac{3\lambda_\Delta}{4} & \frac{\lambda_{\Phi\Delta}}{2} \\ \frac{\lambda_\Phi}{2\sqrt{2}} & \frac{\lambda_{\Phi\Delta}}{\sqrt{2}} & \frac{\lambda_\Phi}{4} & \frac{\lambda_{\Phi\Delta}}{2} & \frac{3\lambda_\Phi}{4} \end{pmatrix}, \quad (2.43)$$

where the submatrices, respectively, correspond to scattering processes with initial and final states $\left(\frac{1}{\sqrt{2}} h_\Phi^+ h_\Phi^+, \frac{1}{\sqrt{2}} h_\Delta^+ h_\Delta^+, h_\Phi^+ h_\Delta^+ \right)$, $\left(h_\Phi^0 h_\Phi^+, h_\Delta^0 h_\Phi^+, G^0 h_\Phi^+, h_\Phi^0 h_\Delta^+, h_\Delta^0 h_\Delta^+, G^0 h_\Delta^+ \right)$, $\left(h_\Phi^+ h_\Delta^-, h_\Delta^+ h_\Phi^-, h_\Phi^0 h_\Delta^0, h_\Phi^0 G^0, h_\Delta^0 G^0 \right)$ and $\left(h_\Phi^+ h_\Phi^-, h_\Delta^+ h_\Delta^-, \frac{1}{\sqrt{2}} h_\Phi^0 h_\Phi^0, \frac{1}{\sqrt{2}} h_\Delta^0 h_\Delta^0, \frac{1}{\sqrt{2}} G^0 G^0 \right)$; $\sqrt{2}$ accounts for identical particle statistics. Now, requiring the moduli of the eigenvalues of the submatrices in Eq. (2.40)–Eq. (2.43) to be $\leq \kappa\pi$, we get

$$|\lambda_\Phi| \leq 2\kappa\pi, \quad |\lambda_\Delta| \leq 2\kappa\pi, \quad (2.44)$$

$$|\lambda_{\Phi\Delta}| \leq \kappa\pi, \quad |6\lambda_\Phi + 5\lambda_\Delta \pm \sqrt{(6\lambda_\Phi - 5\lambda_\Delta)^2 + 192\lambda_{\Phi\Delta}^2}| \leq 8\kappa\pi. \quad (2.45)$$

These conditions ensure that perturbative unitarity is respected in all $2 \rightarrow 2$ scalar scattering processes and put non-trivial constraints on the parameter space. In

⁶While the loop corrections to $2 \rightarrow 2$ scattering amplitudes might affect the allowed parameter space, the difference is expected to be marginal. We checked numerically using `Vevacious` [106, 107], `SPheno` [108, 109] and `BSMart` [110] that the inclusion of the one-loop effective potential and meta stability, indeed, has only a marginal effect on vacuum stability and perturbative unitarity.

particular, the conditions $|\lambda_\Delta| \leq 2\kappa\pi$ and $|\lambda_{\Phi\Delta}| \leq \kappa\pi$ restricts the mass-splitting $m_{\Delta^\pm} - m_{\Delta^0}$ to a few GeV, see Eq. (2.27) and Eq. (2.28).

3 Higgs Production and Decays

3.1 Production

The SM-like Higgs h is dominantly produced via gluon-gluon fusion (ggF) and vector-boson fusion (VBF) processes, and the cross-sections are obtained in the Δ SM by multiplying the corresponding SM cross-sections (48.58 pb [112] and 3.78 pb [113]) by $\cos^2 \alpha$ and

$$g_{WW}^h = \frac{v_\Phi \cos \alpha + 4v_\Delta \sin \alpha}{v} \approx \cos \alpha + \frac{4v_\Delta}{v} \sin \alpha, \quad (3.1)$$

respectively.⁷ The triplet-like neutral Higgs Δ^0 is also produced via ggF and VBF processes by mixing with the SM Higgs. The cross-sections are obtained from SM Higgs cross-sections by a rescaling with $\sin^2 \alpha$ and

$$g_{WW}^{\Delta^0} = \frac{-v_\Phi \sin \alpha + 4v_\Delta \cos \alpha}{v} \approx -\sin \alpha + \frac{4v_\Delta}{v} \cos \alpha, \quad (3.2)$$

respectively.⁸

In the Δ SM, an additional production mechanism is relevant: the Drell-Yan (DY) production of Higgs pairs via γ^*/Z^* and $W^{\pm*}$

$$q\bar{q}' \rightarrow W^{\pm*} \rightarrow \Delta^0 \Delta^\pm, \quad q\bar{q} \rightarrow \gamma^*/Z^* \rightarrow \Delta^+ \Delta^-.$$

Fig. 1 shows the dominant Feynman diagrams for the production of the triplet-like Higgs states.⁹ Fig. 2 shows the Drell-Yan production cross-sections for the triplet-like Higgs states at the 13 TeV LHC, including the higher-order corrections via k factor, as a function of their common mass. The SM-like Higgs h is also DY-produced in

⁷As occasioned by the EW precision data, $v_\Delta \ll v$; therefore, $v_\Phi \approx v$. In what follows, we neglect the corrections in v_Φ/v while writing analytical expressions for the decay widths.

⁸The triplet-like Higgs states are also pair-produced via VBF processes. Likewise, the charged Higgs states are also pair-produced via the t/u -channel photon-photon fusion processes. However, such processes are sub-dominant and can be safely neglected.

⁹We obtain the leading-order Drell-Yan production cross-sections by using the UFO modules generated from SARAH [114, 115] and Feynrules [116–118] in MadGraph5_aMC_v3.5.3 [119, 120] with the NNPDF23_nlo_as_0118_qed parton distribution function [121]. The higher-order corrections can be included via a k factor, which at the next-to-leading order (NLO) in QCD matched with next-to-next-to-leading-logarithmic (NNLL) threshold resummation is ≈ 1.15 for the mass range of our interest [122, 123]. Further, Refs. [122, 123] showed that the NLO+NNLL differential k -factors for heavy lepton kinematics are substantially flat, suggesting that naive scaling by an overall k -factor is a very good approximation.

the Δ SM. However, the corresponding cross-sections are suppressed by the square of the small mixing angles α and β .

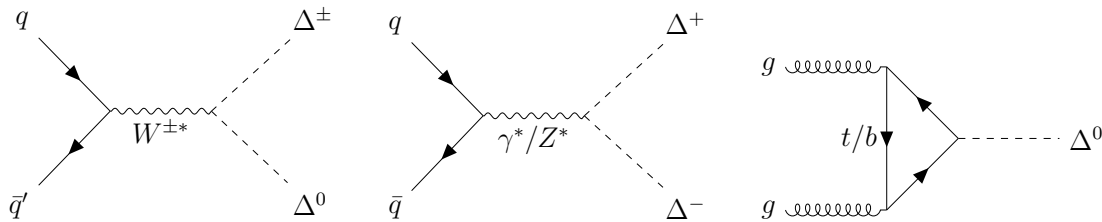


Figure 1. Example Feynman diagrams showing the production of the triplet-like Higgses at the LHC: Drell-Yan (left and middle) and ggF (right).

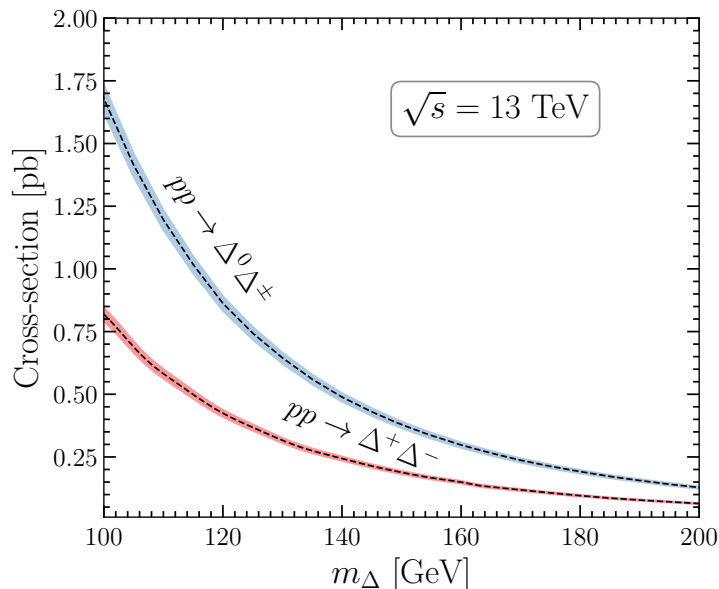


Figure 2. Drell-Yan production cross-sections for the triplet-like Higgses, including the NLO+NNLL QCD corrections and uncertainties of Refs. [122, 123], at the 13 TeV LHC. Here, we disregarded small corrections due to the mixing angles α and β .

3.2 Decays of the SM-like Higgs

The properties of the SM-like Higgs boson h have been studied in detail at the LHC [11–15, 124, 125]. These data, particularly on $h \rightarrow \gamma\gamma$ and $h \rightarrow ZZ^*$, provide nontrivial constraints on New Physics (NP) impacting the SM Higgs. It is customary to define the corresponding signal strengths for a decay mode $h \rightarrow XY$, normalised to the SM value

$$\mu_{XY} = \frac{\sigma_h}{\sigma_h^{\text{SM}}} \times \frac{\Gamma_{h \rightarrow XY}}{\Gamma_{h \rightarrow XY}^{\text{SM}}} \times \frac{\Gamma_{h,\text{tot}}^{\text{SM}}}{\Gamma_{h,\text{tot}}} \quad (3.3)$$

where $\sigma_h/\sigma_h^{\text{SM}} \approx \cos^2 \alpha$ is the production cross-section of h normalised to its SM value and $\Gamma_{h,\text{tot}}^{\text{SM}} = 4.07 \text{ MeV}$ is the total decay width in the SM. For $\gamma\gamma$ and $Z\gamma$, the partial widths are given by [126]

$$\Gamma_{h \rightarrow \gamma\gamma}^{(\text{SM})} = \frac{\alpha_{\text{EM}}^2 g_2^2 m_h^3}{1024 \pi^3 m_W^2} |g_{h\gamma\gamma}^{\text{SM}}|^2, \quad (3.4)$$

$$\Gamma_{h \rightarrow Z\gamma}^{(\text{SM})} = \frac{\alpha_{\text{EM}} g_2^4 m_h^3}{2048 \pi^4 m_W^2} \left(1 - \frac{m_Z^2}{m_h^2}\right)^3 |g_{hZ\gamma}^{\text{SM}}|^2, \quad (3.5)$$

where the fine-structure constant α_{EM} should be taken at the scale $q^2 = 0$ (since the photons are on-shell), and

$$\begin{aligned} g_{h\gamma\gamma}^{\text{SM}} &= \sum_f N_f^c Q_f^2 \beta_{\gamma\gamma}^{1/2} \left(\frac{4m_f^2}{m_h^2}\right) + \beta_{\gamma\gamma}^1 \left(\frac{4m_W^2}{m_h^2}\right), \\ g_{h\gamma\gamma} &= \sum_f N_f^c Q_f^2 g_{f\bar{f}}^h \beta_{\gamma\gamma}^{1/2} \left(\frac{4m_f^2}{m_h^2}\right) + g_{WW}^h \beta_{\gamma\gamma}^1 \left(\frac{4m_W^2}{m_h^2}\right) + \frac{\lambda_{h\Delta^+\Delta^-} v}{2m_{\Delta^\pm}^2} \beta_{\gamma\gamma}^0 \left(\frac{4m_{\Delta^\pm}^2}{m_h^2}\right), \\ g_{hZ\gamma}^{\text{SM}} &= \sum_f \frac{2N_f^c}{\cos \theta_w} Q_f (I_{3f} - 2Q_f \sin^2 \theta_w) \beta_{Z\gamma}^{1/2} \left(\frac{4m_f^2}{m_h^2}, \frac{4m_f^2}{m_Z^2}\right) + \beta_{Z\gamma}^1 \left(\frac{4m_W^2}{m_h^2}, \frac{4m_W^2}{m_Z^2}\right), \\ g_{hZ\gamma} &= \sum_f \frac{2N_f^c}{\cos \theta_w} Q_f (I_{3f} - 2Q_f \sin^2 \theta_w) g_{f\bar{f}}^h \beta_{Z\gamma}^{1/2} \left(\frac{4m_f^2}{m_h^2}, \frac{4m_f^2}{m_Z^2}\right) + g_{WW}^h \beta_{Z\gamma}^1 \left(\frac{4m_W^2}{m_h^2}, \frac{4m_W^2}{m_Z^2}\right) \\ &\quad - \left(\sin^2 \beta + \frac{2 \cos^2 \theta_w}{\cos 2\theta_w} \cos^2 \beta\right) \frac{\lambda_{h\Delta^+\Delta^-} v}{2m_{\Delta^\pm}^2} \beta_{Z\gamma}^0 \left(\frac{4m_{\Delta^\pm}^2}{m_h^2}, \frac{4m_{\Delta^\pm}^2}{m_Z^2}\right) \end{aligned}$$

Here Q_f and I_{3f} are the electric charge and the third component of the electroweak isospin of the SM fermion f ¹⁰ running in the loop, respectively, N_f^c is the number of colours (3 for quarks and 1 for leptons). We also defined

$$\begin{aligned} \lambda_{h\Delta^+\Delta^-} &= \sin \alpha \left\{ \frac{1}{2} \lambda_{\Delta} v_{\Delta} \cos^2 \beta + \left(\lambda_{\Phi\Delta} v_{\Delta} + \frac{1}{2} A \right) \sin^2 \beta \right\} \\ &\quad + \cos \alpha \left\{ \frac{1}{2} \lambda_{\Phi} v_{\Phi} \sin^2 \beta + \lambda_{\Phi\Delta} v_{\Phi} \cos^2 \beta - \frac{1}{2} A \sin 2\beta \right\}; \quad (3.6) \end{aligned}$$

the functions $\beta_{\gamma\gamma, Z\gamma}^{0,1/2,1}$ are collected in Appendix B, and the Higgs coupling to fermions normalised to its SM value is

$$g_{f\bar{f}}^h = \cos \alpha, \quad (3.7)$$

¹⁰In our notation, $I_{3f} = \pm \frac{1}{2}(0)$ for the left(right)-handed fermions in weak isodoublets (isosinglets).

The other SM Higgs signal strengths ($b\bar{b}$, $c\bar{c}$, $\tau\tau$, gg , and ZZ^*) are given by $\cos^4\alpha$, and the one for WW^* is given by $\cos^2\alpha(g_{WW}^h)^2$.

These expressions must be compared to the measurements of CMS and ATLAS for the $h \rightarrow \gamma\gamma$, $h \rightarrow Z\gamma$ and $h \rightarrow ZZ^*$ signal strengths using the full run 2 data at the 13 TeV LHC. Combining their most recent $h \rightarrow \gamma\gamma$ measurements: $\mu_{\gamma\gamma}^{\text{CMS}} = 1.12_{-0.09}^{+0.09}$ [127] and $\mu_{\gamma\gamma}^{\text{ATLAS}} = 1.04_{-0.09}^{+0.10}$ [128], we get the weighted average

$$\mu_{\gamma\gamma}^{\text{LHC}} = 1.08_{-0.06}^{+0.07}. \quad (3.8)$$

On the other hand, the collaborations themselves performed a combined analysis of their $h \rightarrow Z\gamma$ measurements [129, 130] in Ref. [131] and reported

$$\mu_{Z\gamma}^{\text{LHC}} = 2.2 \pm 0.7. \quad (3.9)$$

Note that this measured value is in mild tension ($\approx 1.9\sigma$) with the SM expectation. The PDG average [1] of the $h \rightarrow ZZ^*$ signal strength based on the LHC measurements [13, 125, 132] gives

$$\mu_{ZZ^*}^{\text{LHC}} = 1.02 \pm 0.08. \quad (3.10)$$

While the $h \rightarrow ZZ^*$ signal strength puts a constraint on the mixing angle

$$|\alpha| \lesssim 0.25(0.38)[0.49] \text{ at } 1\sigma(2\sigma)[3\sigma] \text{ level}, \quad (3.11)$$

the $h \rightarrow \gamma\gamma$ and $h \rightarrow Z\gamma$ signal strengths impose non-trivial constraints on m_{Δ^0} , $m_{\Delta^\pm} - m_{\Delta^0}$ and α . Note that their dependence on $m_{\Delta^\pm} - m_{\Delta^0}$ stems from the $h\Delta^+\Delta^-$ coupling, see Eq. (3.6). Figs. 3 and 4 show their dependence on α and $m_{\Delta^\pm} - m_{\Delta^0}$ plane for $m_{\Delta^0} = 152 \text{ GeV}$ and $v_\Delta = 3.4 \text{ GeV}$ (left) and $v_\Delta = 2.3 \text{ GeV}$ (right).¹¹ As we see, $\alpha > 0$ is favored by the $\mu \rightarrow \gamma\gamma$ measurements for $m_{\Delta^0} = 152 \text{ GeV}$. The same follows for $m_{\Delta^0} > m_h$. The reverse that $\alpha < 0$ is favoured by the $\mu \rightarrow \gamma\gamma$ measurements is largely true for $m_{\Delta^0} < m_h$ (corresponding plot not shown for brevity). As expected, a positive correlation between $\mu_{\gamma\gamma}$ and $\mu_{Z\gamma}$ in the α vs $m_{\Delta^\pm} - m_{\Delta^0}$ plane can be seen. That is the parameter space predicting a larger-than-expected $\mu_{\gamma\gamma}$ predicts a larger-than-expected $\mu_{Z\gamma}$, and vice-versa. However, since the latter is beset with quite a large error, it is not difficult to simultaneously accommodate both measurements.

¹¹Understandably, the chosen values for m_{Δ^0} and v_Δ might seem arbitrary at this point. However, as we see later in Section 4.1, these values for v_Δ are preferred by the W -mass world average, including/excluding the CDF-II measurement. Further, we find later in Section. 4.3 that ATLAS di-photon data strongly prefer a Higgs triplet with $m_{\Delta^0} = 152 \text{ GeV}$.

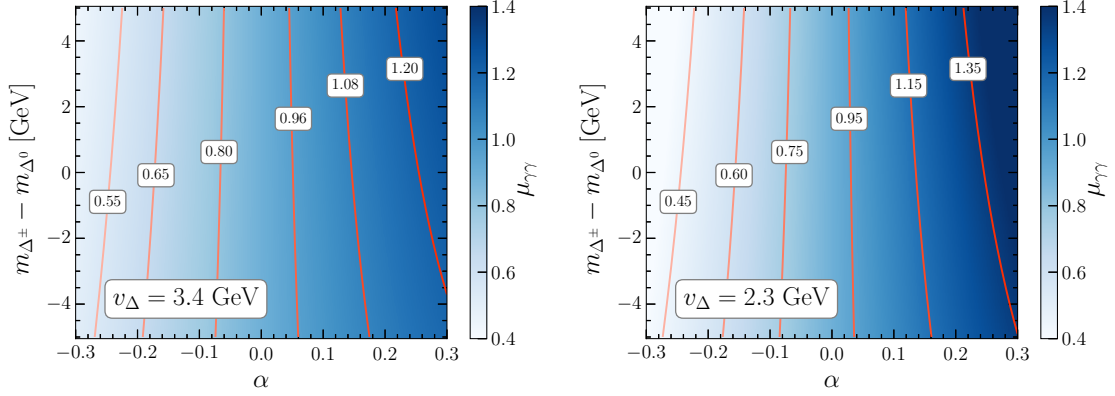


Figure 3. $h \rightarrow \gamma\gamma$ signal strength in the α vs $m_{\Delta^\pm} - m_{\Delta^0}$ plane for $m_{\Delta^0} = 152$ GeV and $v_\Delta = 3.4$ GeV (left) and $v_\Delta = 2.3$ GeV (right).

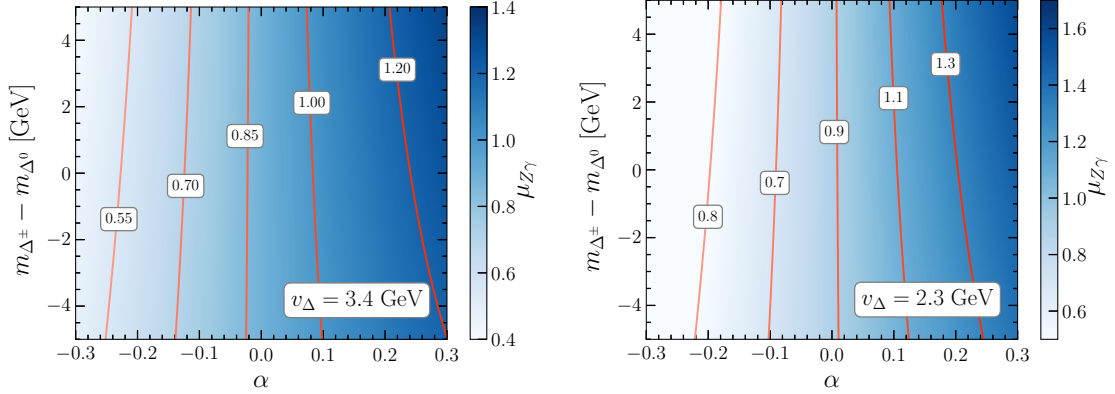


Figure 4. $h \rightarrow Z\gamma$ signal strength in the α vs $m_{\Delta^\pm} - m_{\Delta^0}$ plane for $m_{\Delta^0} = 152$ GeV and $v_\Delta = 3.4$ GeV (left) and $v_\Delta = 2.3$ GeV (right).

3.3 Decays of the triplet-like Higgses Δ^0 and Δ^\pm

The triplet-like Higgs states Δ^0 and Δ^\pm have two dominant classes of decays:

- (i) Δ^0 decays into two SM particles (on-shell or off-shell), either at tree-level to $f\bar{f}$, $WW^{(*)}$, $ZZ^{(*)}$, $hh^{(*)}$, or at the loop level to gg , $\gamma\gamma$, $Z\gamma$. Likewise Δ^\pm decays to ff' , $W^{(*)}Z^{(*)}$, $h^{(*)}W^{(*)}$. The asterisk signals a possible off-shellness.
- (ii) Even though kinematically suppressed due to the small mass splitting, Δ^0 and Δ^\pm could decay into one another and an off-shell W -boson, often referred to as cascade decays.

The tree-level decay rates for the triplet-like Higgs Δ^0 are given by

$$\Gamma(\Delta^0 \rightarrow f\bar{f}) = \frac{N_c m_f^2 m_{\Delta^\pm}}{8\pi v_\Phi^2} \sin^2 \alpha \left[\beta \left(\frac{m_f^2}{m_{\Delta^0}^2}, \frac{m_f^2}{m_{\Delta^0}^2} \right) \right]^{3/2},$$

$$\begin{aligned}
\Gamma(\Delta^0 \rightarrow WW) &= \frac{g^4 m_{\Delta^\pm}^3}{256\pi m_W^4} (-v_\Phi \sin \alpha + 4v_\Delta \cos \alpha)^2 \beta_V \left(\frac{m_W^2}{m_{\Delta^0}^2} \right), \\
\Gamma(\Delta^0 \rightarrow ZZ) &= \frac{g^4 m_{\Delta^\pm}^3}{512\pi m_W^4} (-v_\Phi \sin \alpha)^2 \beta_V \left(\frac{m_Z^2}{m_{\Delta^0}^2} \right), \\
\Gamma(\Delta^0 \rightarrow WW^*) &= \frac{3g^6 m_{\Delta^\pm}}{2048\pi^3 m_W^2} (-v_\Phi \sin \alpha + 4v_\Delta \cos \alpha)^2 \beta'_V \left(\frac{m_W^2}{m_{\Delta^0}^2} \right), \\
\Gamma(\Delta^0 \rightarrow ZZ^*) &= \frac{3g^6 m_{\Delta^\pm}}{2048\pi^3 \cos^6 \theta_w m_Z^2} (-v_\Phi \sin \alpha)^2 \left(\frac{7}{12} - \frac{10}{9} \sin^2 \theta_W + \frac{40}{27} \sin^4 \theta_W \right) \beta'_V \left(\frac{m_Z^2}{m_{\Delta^0}^2} \right), \\
\Gamma(\Delta^0 \rightarrow hh) &= \frac{1}{32\pi m_{\Delta^0}} \lambda_{\Delta^0 hh}^2 \left[\beta \left(\frac{m_h^2}{m_{\Delta^0}^2}, \frac{m_h^2}{m_{\Delta^0}^2} \right) \right]^{1/2}, \\
\Gamma(\Delta^0 \rightarrow hh^* \rightarrow h\bar{b}\bar{b}) &= \frac{3m_b^2 \cos^2 \alpha}{32\pi^3 v_\Phi^2 m_H} \lambda_{\Delta^0 hh}^2 \beta_S \left(\frac{m_h^2}{m_{\Delta^0}^2} \right), \\
\Gamma(\Delta^0 \rightarrow hh^* \rightarrow h\tau^+ \tau^-) &= \frac{m_\tau^2 \cos^2 \alpha}{32\pi^3 v_\Phi^2 m_H} \lambda_{\Delta^0 hh}^2 \beta_S \left(\frac{m_h^2}{m_{\Delta^0}^2} \right), \\
\Gamma(\Delta^0 \rightarrow \Delta^\pm W^\mp) &= \frac{9g^2 m_{\Delta^0}}{128\pi^3} \lambda_{\Delta^0 \Delta^\pm W^\mp}^2 G \left(\frac{m_{\Delta^\pm}^2}{m_{\Delta^0}^2}, \frac{m_W^2}{m_{\Delta^0}^2} \right),
\end{aligned}$$

where

$$\begin{aligned}
\lambda_{\Delta^0 hh} &= \left(\lambda_{\Phi\Delta} v_\Delta - \frac{1}{2} A \right) \cos^3 \alpha + \left(2\lambda_{\Phi\Delta} - \frac{3}{2} \lambda_\Phi \right) v_\Phi \cos^2 \alpha \sin \alpha \\
&\quad + \left(\frac{3}{2} \lambda_\Delta v_\Delta - 2\lambda_{\Phi\Delta} v_\Delta + A \right) \cos \alpha \sin^2 \alpha - \lambda_{\Phi\Delta} v_\Phi \sin^3 \alpha, \\
\lambda_{\Delta^0 \Delta^\pm W^\mp} &= -\frac{g}{2} (2 \cos \alpha \cos \beta - \sin \alpha \sin \beta),
\end{aligned}$$

and the loop-induced decays, with at least one massless gauge boson in the final state, are given by

$$\begin{aligned}
\Gamma(\Delta^0 \rightarrow gg) &= \frac{\alpha_s^2 g^2 m_{\Delta^0}^3}{288\pi^3 m_W^2} |g_{\Delta^0 gg}|^2, \\
\Gamma(\Delta^0 \rightarrow \gamma\gamma) &= \frac{\alpha_{\text{EM}}^2 g_2^2 m_{\Delta^0}^3}{1024\pi^3 m_W^2} |g_{\Delta^0 \gamma\gamma}|^2, \\
\Gamma(\Delta^0 \rightarrow Z\gamma) &= \frac{\alpha_{\text{EM}} g_2^4 m_{\Delta^0}^3}{2048\pi^4 m_W^2} \left(1 - \frac{m_Z^2}{m_h^2} \right)^3 |g_{\Delta^0 Z\gamma}|^2,
\end{aligned}$$

where α_s is the strong coupling constant,

$$g_{\Delta^0 gg} = \frac{3}{4} \sum_q g_{ff}^{\Delta^0} \beta_{\gamma\gamma}^{1/2} \left(\frac{4m_q^2}{m_{\Delta^0}^2} \right),$$

$$\begin{aligned}
g_{\Delta^0\gamma\gamma} &= \sum_f N_c Q_f^2 g_{ff}^{\Delta^0} \beta_{\gamma\gamma}^{1/2} \left(\frac{4m_f^2}{m_{\Delta^0}^2} \right) + g_{WW}^{\Delta^0} \beta_{\gamma\gamma}^1 \left(\frac{4m_W^2}{m_{\Delta^0}^2} \right) + \frac{\lambda_{\Delta^+\Delta^-\Delta^0} v_{\text{SM}}}{2m_{\Delta^\pm}^2} \beta_{\gamma\gamma}^0 \left(\frac{4m_{\Delta^\pm}^2}{m_{\Delta^0}^2} \right), \\
g_{\Delta^0 Z\gamma} &= \sum_f \frac{2N_f^c}{\cos\theta_w} Q_f (I_{3f} - 2Q_f \sin^2\theta_w) g_{ff}^{\Delta^0} \beta_{Z\gamma}^{1/2} \left(\frac{4m_f^2}{m_{\Delta^0}^2}, \frac{4m_f^2}{m_Z^2} \right) + g_{WW}^{\Delta^0} \beta_{Z\gamma}^1 \left(\frac{4m_W^2}{m_{\Delta^0}^2}, \frac{4m_W^2}{m_Z^2} \right) \\
&\quad - \left(\sin^2\beta + \frac{2\cos^2\theta_w}{\cos 2\theta_w} \cos^2\beta \right) \frac{\lambda_{\Delta^0\Delta^+\Delta^-} v}{2m_{\Delta^\pm}^2} \beta_{Z\gamma}^0 \left(\frac{4m_{\Delta^\pm}^2}{m_{\Delta^0}^2}, \frac{4m_{\Delta^\pm}^2}{m_Z^2} \right),
\end{aligned}$$

with

$$\begin{aligned}
\lambda_{\Delta^0\Delta^+\Delta^-} &= \cos\alpha \left\{ \frac{1}{2} \lambda_{\Delta} v_{\Delta} \cos^2\beta + \left(\lambda_{\Phi\Delta} v_{\Delta} + \frac{1}{2} A \right) \sin^2\beta \right\} \\
&\quad - \sin\alpha \left\{ \frac{1}{2} \lambda_{\Phi} v_{\Phi} \sin^2\beta + \lambda_{\Phi\Delta} v_{\Phi} \cos^2\beta - \frac{1}{2} A \sin 2\beta \right\}, \\
g_{ff}^{\Delta^0} &= -\sin\alpha;
\end{aligned}$$

and all the loop functions or form factors used in the Higgs decays are collected in Section B.

Finally, for masses slightly below the $t\bar{t}$ threshold, Δ^0 can decay into one on-shell and one off-shell top quarks, $\Delta^0 \rightarrow t\bar{t}^* \rightarrow t\bar{b}W$. As in the MSSM or 2HDM, the below-threshold branching ratios can be significant only very close to the $t\bar{t}$ threshold. Therefore, this decay is negligible in the mass region of our interest and thus not considered further for brevity.

While we provide the leading order decay rates here, QCD corrections can be sizable. To estimate them, we use the higher-order corrections reported in the CERN Yellow Report 3 [113] for $h \rightarrow b\bar{b}, c\bar{c}, \tau\tau, WW, ZZ$ and appropriately apply them to Δ^0 decays for our numerical estimation.

The dominant decay rates for the triplet-like charged Higgs Δ^\pm are given by [133–137]

$$\begin{aligned}
\Gamma(\Delta^\pm \rightarrow ff') &= \frac{N_c m_{\Delta^\pm}^3 \sin^2\beta}{8\pi v_{\Phi}^2} \beta_{ff'} \left(\frac{m_f^2}{m_{\Delta^\pm}^2}, \frac{m_{f'}^2}{m_{\Delta^\pm}^2} \right), \\
\Gamma(\Delta^\pm \rightarrow t^*\bar{b}/\bar{t}^*b \rightarrow W^\pm b\bar{b}) &= \frac{3m_t^4 m_{\Delta^\pm} \sin^2\beta}{128\pi^3 v_{\Phi}^4} \beta_t \left(\frac{m_t^2}{m_{\Delta^\pm}^2}, \frac{m_W^2}{m_{\Delta^\pm}^2} \right) \\
\Gamma(\Delta^\pm \rightarrow W^\pm Z) &= \frac{\lambda_{\Delta^\pm W^\mp Z}^2}{16\pi m_{\Delta^\pm}} \left[\beta \left(\frac{m_W^2}{m_{\Delta^\pm}^2}, \frac{m_Z^2}{m_{\Delta^\pm}^2} \right) \right]^{1/2} \left[2 + \frac{m_{\Delta^\pm}^4}{4m_W^2 m_Z^2} \left(1 - \frac{m_W^2}{m_{\Delta^\pm}^2} - \frac{m_Z^2}{m_{\Delta^\pm}^2} \right)^2 \right], \\
\Gamma(\Delta^\pm \rightarrow W^\pm Z^*) &= \frac{9g^2 \lambda_{\Delta^\pm W^\mp Z}^2}{128\pi^3 \cos^2\theta_w m_{\Delta^\pm}} \left(\frac{7}{12} - \frac{10}{9} \sin^2\theta_w + \frac{40}{27} \sin^4\theta_w \right) H \left(\frac{m_W^2}{m_{\Delta^\pm}^2}, \frac{m_Z^2}{m_{\Delta^\pm}^2} \right), \\
\Gamma(\Delta^\pm \rightarrow W^{\pm*} Z) &= \frac{9g^2 \lambda_{\Delta^\pm W^\mp Z}^2}{256\pi^3 m_{\Delta^\pm}} H \left(\frac{m_Z^2}{m_{\Delta^\pm}^2}, \frac{m_W^2}{m_{\Delta^\pm}^2} \right),
\end{aligned}$$

$$\begin{aligned}\Gamma(\Delta^\pm \rightarrow hW^\pm) &= \frac{m_{\Delta^\pm}^3}{16\pi m_W^2} \lambda_{\Delta^\pm hW^\mp}^2 \left[\beta \left(\frac{m_W^2}{m_{\Delta^\pm}^2}, \frac{m_h^2}{m_{\Delta^\pm}^2} \right) \right]^{3/2}, \\ \Gamma(\Delta^\pm \rightarrow hW^{\pm*}) &= \frac{9g^2 m_{\Delta^\pm}}{128\pi^3} \lambda_{\Delta^\pm hW^\mp}^2 G \left(\frac{m_h^2}{m_{\Delta^\pm}^2}, \frac{m_W^2}{m_{\Delta^\pm}^2} \right), \\ \Gamma(\Delta^\pm \rightarrow \Delta^0 W^{\pm*}) &= \frac{9g^2 m_{\Delta^\pm}}{128\pi^3} \lambda_{\Delta^0 \Delta^\pm W^\mp}^2 G \left(\frac{m_{\Delta^0}^2}{m_{\Delta^\pm}^2}, \frac{m_W^2}{m_{\Delta^\pm}^2} \right),\end{aligned}$$

where

$$\begin{aligned}\lambda_{\Delta^\pm W^\mp Z} &= -\frac{g^2}{2 \cos \theta_w} (2v_\Delta \cos^2 \theta_w \cos \beta - v_\Phi \sin^2 \theta_w \sin \beta), \\ \lambda_{\Delta^\pm hW^\mp} &= -\frac{g}{2} (2 \sin \alpha \cos \beta + \cos \alpha \sin \beta).\end{aligned}$$

Having provided all the decay rate expressions, a brief discussion on their dependence on the free model parameters is in order. Note that, for the mass range of our interest, any of the heavy SM particles can be off-shell. However, for brevity, we omit the asterisk sign signaling this hereinafter. The tree-level decays of Δ^0 depend on three parameters, namely m_{Δ^0} , v_Δ and α , while those of Δ^\pm depend on m_{Δ^\pm} and v_Δ only, except for $\Delta^\pm \rightarrow hW^\pm$ which also depends on α . The cascade and loop-induced decays depend additionally on the mass-splitting $m_{\Delta^\pm} - m_{\Delta^0}$. As discussed in Sec. 2.2, the requirement of vacuum stability and perturbative unitarity, together with the EW precision data, restricts the mass-splitting to a few GeV. Therefore, on account of this small mass-splitting, the cascade decays are generally suppressed. Further, the dependence of the tree-level decays on v_Δ drops out as long as $v_\Delta \sim \mathcal{O}(1)$ GeV. Consequently, for the v_Δ -range favoured by W -mass measurements (see Sec. 4.1), the tree-level decays are reasonably independent of v_Δ . However, the loop-induced decays crucially depend on v_Δ .

In Fig. 5, we show the variation of the dominant branching ratios of the triplet-like Higgs Δ^0 , including the corresponding uncertainties, as a function of its mass m_{Δ^0} (left) and the mixing angle α (right). The uncertainties are estimated by propagating the errors on the $\tau\tau$, $b\bar{b}$, WW^* and ZZ^* decays of a hypothetical SM-like Higgs with mass m_{Δ^0} reported in the CERN Yellow Report [113]. For definiteness, we take $v_\Delta = 3.4$ GeV. Further, we take $\alpha = 0.1$ for the left plot and $m_{\Delta^0} = 152$ GeV for the right one. While Δ^0 exclusively decays into WW for $\alpha \approx 0$, the other modes become relevant for $\alpha \neq 0$. In particular, for $\alpha > 0$, the $b\bar{b}$ mode dominates over the rest for m_{Δ^0} up to close to the WW kinematic threshold, beyond which the gauge-boson modes WW and ZZ become the primary ones. While for $\alpha < 0$ (corresponding plot not shown for brevity), the $b\bar{b}$ and WW modes are relevant, with the latter dominating over the former much before the WW threshold. However, the WW mode vanishes for $\tan \alpha \approx \frac{4v_\Delta}{v}$; see the right plot. Before moving further, a brief comment on the $\Delta^0 \rightarrow hh$ decay is in order. Though this mode is not suppressed by

α , it is suppressed by the kinematic phase space for $m_{\Delta^0} < 2m_h$, thus not relevant for the mass range of our interest.

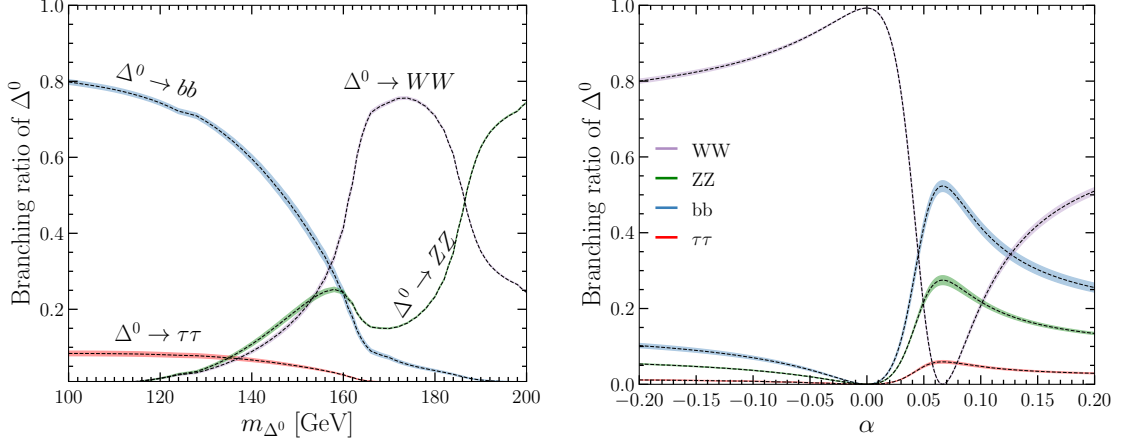


Figure 5. Dominant branching ratios of Δ^0 , including the uncertainties estimated from Ref. [113], with $\alpha = 0.1$ for the left plot, and $m_{\Delta^0} = 152$ GeV for the right one.

Figs. 6 and 7 show $\text{Br}(\Delta^0 \rightarrow \gamma\gamma)$ and $\text{Br}(\Delta^0 \rightarrow Z\gamma)$ in the α vs $m_{\Delta^\pm} - m_{\Delta^0}$ plane for $m_{\Delta^0} = 152$ GeV and $v_\Delta = 3.4$ GeV (left) and $v_\Delta = 2.3$ GeV (right). As we see, in the vicinity of degenerate mass-spectrum for the triple-like Higgs states, both the $\Delta^0 \rightarrow \gamma\gamma$ and $\Delta^0 \rightarrow Z\gamma$ branching ratios are $\sim \mathcal{O}(0.1)\%$ – $\mathcal{O}(1)\%$.

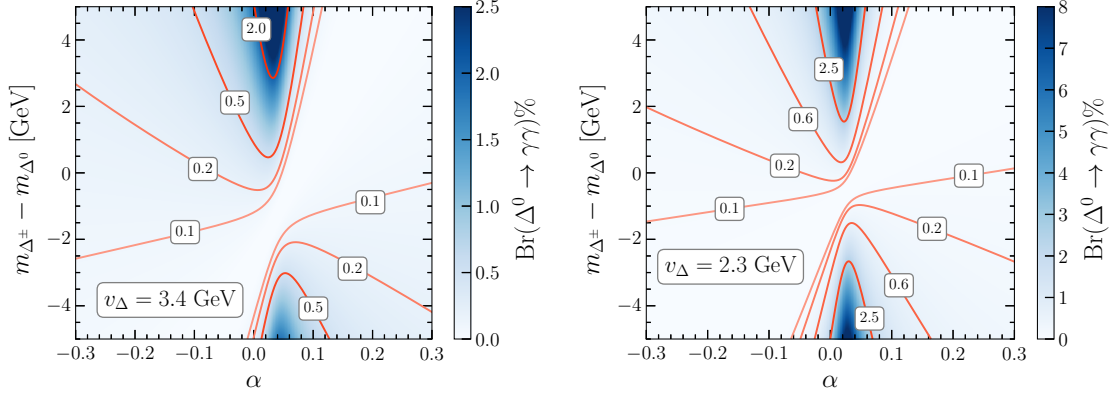


Figure 6. $\text{Br}(\Delta^0 \rightarrow \gamma\gamma)$ as a function of α vs $m_{\Delta^\pm} - m_{\Delta^0}$ for $m_{\Delta^0} = 152$ GeV and $v_\Delta = 3.4$ GeV (left) and $v_\Delta = 2.3$ GeV (right).

In Fig. 8, the dominant branching ratios of the charged Higgs Δ^\pm , including the corresponding uncertainties, are shown as a function of its mass m_{Δ^\pm} . Once again, the uncertainties are estimated by propagating the errors on the $\tau\tau$, $c\bar{c}$, $t\bar{t}$ and ZZ^* decays of a hypothetical SM-like Higgs with mass m_{Δ^\pm} reported in the CERN Yellow Report [113]. For definiteness, we take $v_\Delta = 3.4$ GeV and $\alpha = 0$. For low m_{Δ^\pm} , the most dominant decay mode is $\tau\nu$. While for intermediate m_{Δ^\pm} , which is also the

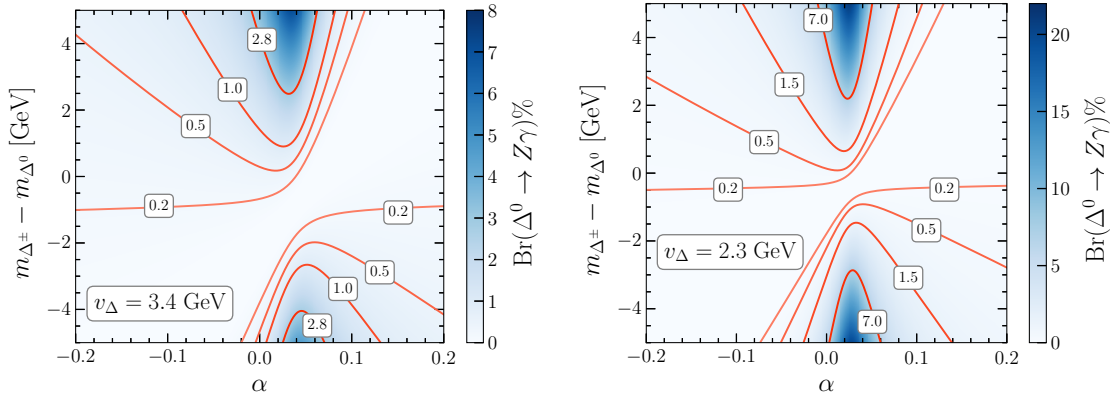


Figure 7. $\text{Br}(\Delta^0 \rightarrow Z\gamma)$ as a function of α vs $m_{\Delta^\pm} - m_{\Delta^0}$ for $m_{\Delta^0} = 152$ GeV and $v_\Delta = 3.4$ GeV (left) and $v_\Delta = 2.3$ GeV (right).

mass range of our interest, the WZ mode dominates over the rest, with the $t\bar{b}$ mode dominating for high m_{Δ^\pm} .

Finally, a brief comment on the $\Delta^\pm \rightarrow hW^\pm$ decay is in order. As mentioned earlier, among all decays of Δ^\pm , only the hW^\pm mode depends on α . This decay is suppressed by α as well as the kinematic phase space through the coupling $\lambda_{\Delta^\pm hW^\mp}$, and thus not shown in the plot. In fact, it vanishes for $\tan \alpha \approx \frac{v_\Delta}{v}$. That said, this can be relevant for sizable α and $m_{\Delta^0} > m_h$.

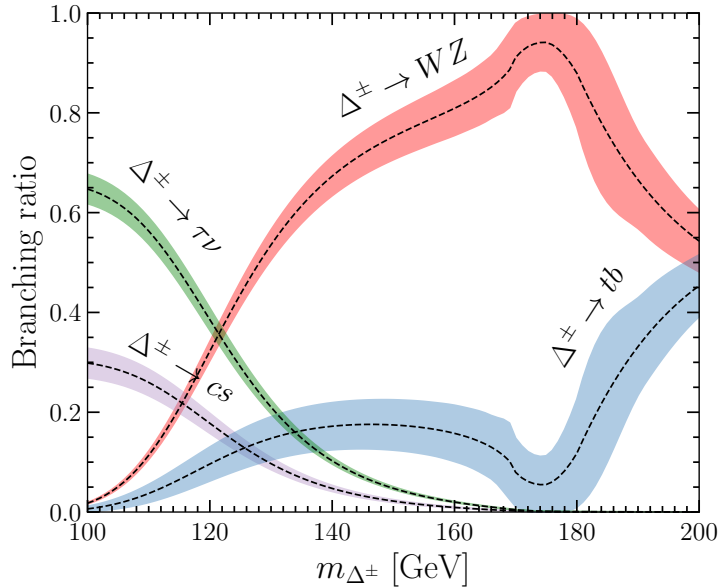


Figure 8. Dominant branching ratios of Δ^\pm , including the uncertainties estimated from Ref. [113], as a function of its mass. Note that the dependence on v_Δ drops out.

4 Phenomenology

4.1 W mass

The W mass $m_W = 80.4335(94)$ GeV as measured by the CDF II collaboration [30] is significantly larger than the ATLAS measurement $m_W = 80.360(16)$ [138] as well as the LHCb measurement $m_W = 80.354(32)$ [139]. Combining these measurements with those from the D0 experiment [139–142] at the Tevatron, and the ALEPH, DELPHI, L3 and OPAL experiments at the LEP [143], the LHC-TeV MW Working Group [144] has obtained a world average

$$m_W^{\text{avg}} = 80394.6 \pm 11.5 \text{ MeV}. \quad (4.1)$$

Comparing this with the SM prediction of $m_W^{\text{SM}} = 80.3499(56)$ GeV [145], the discrepancy of 44.7 MeV amounts to 3.5σ . Since there is a tension between the most precise CDF-II measurement and the rest, removing the former increases the compatibility within the m_W fit and leads to a lower average of

$$m_W^{\text{avg (w/o CDF II)}} = 80369.2 \pm 13.3 \text{ MeV}, \quad (4.2)$$

is obtained. Therefore, the world average, including the CDF-II measurement, requires $v_\Delta = 3.4 \pm 1.0$ GeV, while excluding CDF-II, one finds $v_\Delta = 2.3 \pm 1.7$ GeV.¹² In the rest of this work, we fix $v_\Delta = 3.4$ GeV or 2.3 GeV.

4.2 Multi-lepton signature from DY production

Drell-Yan production of the triplet-like Higgs bosons, $pp \rightarrow \Delta^0 \Delta^\pm$ and $pp \rightarrow \Delta^+ \Delta^-$, with their decays $\Delta^0 \rightarrow W^+ W^-$, ZZ , $b\bar{b}$, $\tau^+ \tau^-$ and $\Delta^\pm \rightarrow W^\pm Z$, $t\bar{b}$, $c\bar{s}$, $\tau^\pm \nu$ lead to final states with multiple charged leptons. Two representative Feynman diagrams for these processes are shown in Fig. 9.

As discussed in Sec. 3.3, low-mass triplet-like charged Higgs Δ^\pm dominantly decays to $\tau\nu$; see Fig. 8. Consequently, their pair production and subsequent decays, as shown in Fig. 10, leads to a final state with a pair of τ -leptons and missing transverse momentum, which is the identical collider signature as supersymmetric partners of τ -leptons ($\tilde{\tau}$) promptly decaying into a τ and a (massless) neutralino. This has been searched for by CMS and ATLAS collaborations [148–151].

¹²There is a recent update on the measurement of m_W by ATLAS which finds a slightly heavier $m_W = 80.3665(159)$ GeV [146] compared to their previous analysis [138] based on the same dataset. However, the said combination did not consider the updated ATLAS measurement. Furthermore, after this combination was performed, CMS published a new measurement $m_W = 80360.2 \pm 9.9$ GeV [147], which agrees well with the world average excluding the CDF-II measurement. Including these updates might significantly reduce the world average and thus would imply a slightly lower value for v_Δ . However, the specific value for v_Δ is immaterial for our analysis as long as $v_\Delta \sim \mathcal{O}(1)$ GeV.

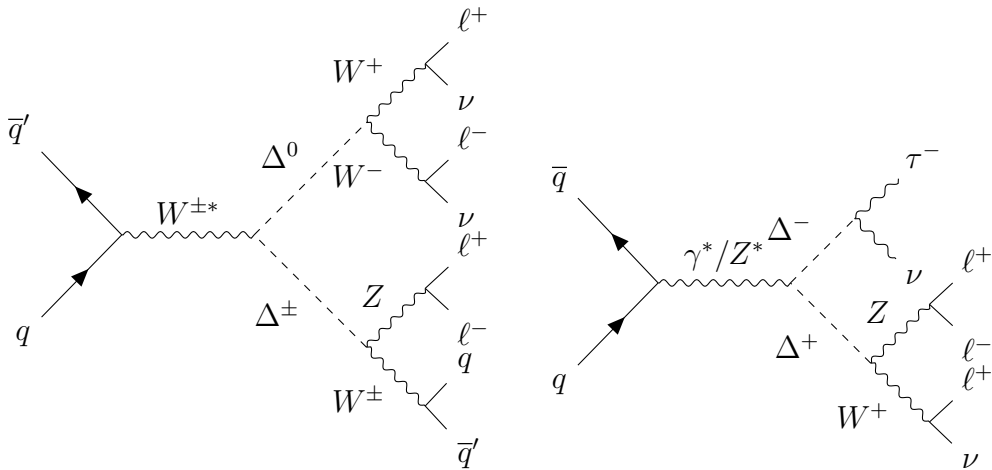


Figure 9. Representative Feynman diagrams for the Drell-Yan production of the triplet-like Higgses and their decays to SM particles leading to multi-lepton final states at the LHC.

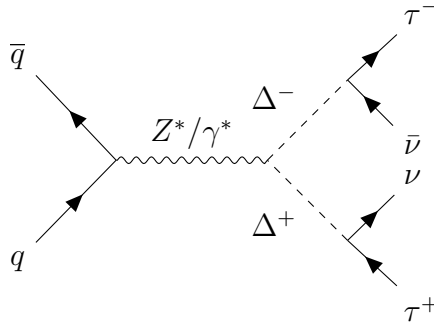


Figure 10. Pair production and subsequent decays of Δ^\pm leading to the stau-like $\tau\tau\nu\nu$ final state.

Using the full run 2 dataset at the 13 TeV LHC, CMS [150] has obtained 95% confidence level (CL) upper limits on the cross-section as a function of the $\tilde{\tau}$ mass. On the contrary, ATLAS [151] observed a stronger limit than expected; however, they do not provide upper limits on the cross-section. We thus use the CMS result in Ref. [150] to constrain the triplet-like charged Higgs Δ^\pm .

The CMS expected and observed 95% CL upper limits on the signal cross-section $\sigma(pp \rightarrow \Delta^+\Delta^- \rightarrow \tau\tau\nu\nu)$, taken from Ref. [150], are shown in Fig. 11. The inner green and outer yellow bands around the dotted line indicate the 68% and 95% CL regions. The red line and the thin-shaded band indicate the model prediction for the signal cross-section, including the NLO+NNLL QCD corrections and uncertainties. The QCD corrections are taken from Refs. [122, 123], and the uncertainties are estimated by propagating the ones on the cross-section and branching ratios reported in Refs. [122, 123] and Ref. [113], respectively. This excludes Δ^\pm with masses below 110 GeV at 95% CL.

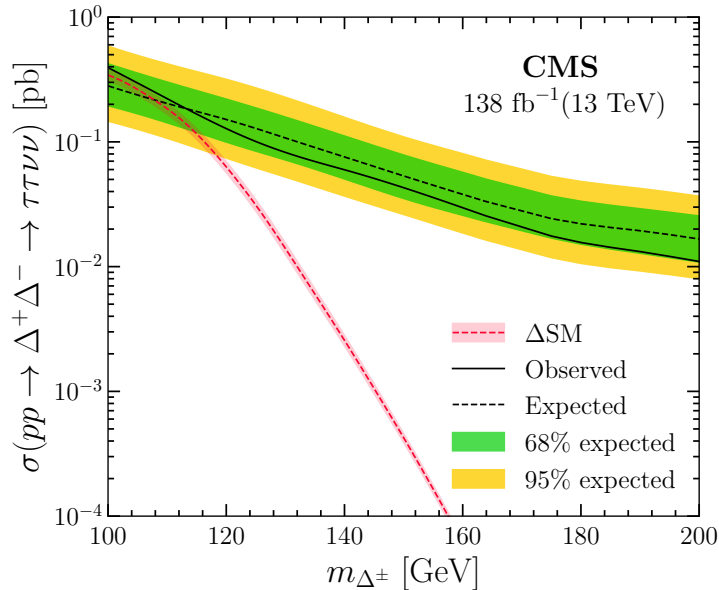


Figure 11. Expected and observed 95% CL upper limits on the cross-section $\sigma(pp \rightarrow \Delta^+ \Delta^- \rightarrow \tau\tau\nu\nu)$ taken from CMS [150]. The red line and band indicate the model prediction for the signal cross-section, including the NLO+NNLL QCD corrections and uncertainties.

For higher masses of the triplet-like Higgses, i.e. $\gtrsim 120$ GeV, the decays to WW and ZW become relevant. The most relevant signatures stem from the subsequent decays to leptons, which, compared to hadronic final states, have a considerably smaller SM background and, thus, superior constraining power. Since there is no dedicated search for this signature of our model,¹³ Ref. [62] used several SM measurements implemented in the **Contur** toolkit, and find that the four-lepton search by ATLAS [159] is the most constraining one. They excluded Δ^0 with mass in the 180–200 GeV range for small $\lambda_{\phi\Delta}$; while for sizeable $\lambda_{\phi\Delta}$, the constraints are easily avoided. Here, we will make use of the model-independent multi-lepton search by ATLAS [155], which entails inclusive event selection and thus covers a large phase space of signatures. This search considers 22 signal regions (SRs) and analyses them model-independently by putting limits on the visible cross-sections.

The three and four charged-lepton events are categorised into several orthogonal SRs based on the number of leptons, the presence/absence of a lepton pair presumably originating from a Z -boson decay (on- Z /off- Z lepton pair¹⁴) and the missing

¹³Several multi-lepton searches have been performed using the full run 2 data by CMS and ATLAS, see *e.g.* Refs. [152–158]. However, most of these searches probe specific models and, like for instance Ref. [157] and Ref. [154] consider events with high lepton invariant masses and/or high missing transverse momenta. Being tuned for specific models, these searches exploit very distinctive event features, such as resonances in invariant-mass distributions and high missing transverse momenta, and are thus not expected to be sensitive in probing the Δ SM.

¹⁴A pair of same-flavour and oppositely charged leptons with di-lepton invariant mass within the 10 GeV window of the Z -boson mass is referred to as on- Z lepton pair. A lepton that does not form

transverse momentum:

- i)* 3ℓ on- Z $E_T^{\text{miss}} < 50$ GeV,
- ii)* 3ℓ on- Z $E_T^{\text{miss}} > 50$ GeV,
- iii)* 3ℓ off- Z $E_T^{\text{miss}} < 50$ GeV,
- iv)* 3ℓ off- Z $E_T^{\text{miss}} > 50$ GeV,
- v)* 4ℓ on- Z $E_T^{\text{miss}} < 50$ GeV,
- vi)* 4ℓ on- Z $E_T^{\text{miss}} > 50$ GeV,
- vii)* 4ℓ off- Z ,

with each $3\ell(4\ell)$ SRs further divided into four(two) bins of the invariant mass of the leptons: 0 GeV– 200 GeV, 200 GeV– 400 GeV, 400 GeV– 600 GeV and > 600 GeV (0 GeV– 400 GeV and > 400 GeV), thereby resulting in 22 SRs in total.

We recast this search to constrain the Δ SM by simulating the processes $pp \rightarrow W^{\pm*} \rightarrow \Delta^0 \Delta^\pm$ and $pp \rightarrow \gamma^*/Z^* \rightarrow \Delta^+ \Delta^-$ with $\Delta^0 \rightarrow W^+W^-$, ZZ and $\Delta^\pm \rightarrow W^\pm Z$, $t\bar{b}$, $c\bar{s}$, $\tau^\pm \nu$ for m_Δ between 120 GeV and 200 GeV using the UFO modules generated from SARAH [114, 115]¹⁵ in MadGraph5_aMC_v3.5.3 [120, 160] with the NNPDF23_nlo_as_0118_qed parton distribution function [121]. The simulated parton-level events are then passed through the regular chain of tools, namely Pythia 8.3 [161] and Delphes 3.5.0 [162], to simulate the effect of subsequent decays of the unstable particles, radiations, showering, fragmentation and hadronisation, various detector effects, and particle-level object reconstruction.

For the selection of various objects, *viz.* photons, leptons (electrons and muons) and jets (including τ -tagged and b -tagged jets), we meticulously follow the said ATLAS search [155]. In particular, we appropriately tune the Delphes card for the ATLAS detector to take into account various object reconstruction, isolation and selection requirements and jet tagging efficiencies. We use the anti- k_T algorithm [163] implemented in FastJet 3.3.4 [164] to reconstruct jets. The missing transverse momentum (with magnitude E_T^{miss}) is estimated from the momentum imbalance in the transverse direction associated with all reconstructed objects in an event. Finally, we apply the event selections and categorise the selected events according to the signal regions in Refs. [155].

While the branching ratio of the dominant Δ^\pm modes depends only on its mass, the partial widths of $\Delta^0 \rightarrow WW, ZZ, bb, \tau\tau$ depend on α in addition (see Sec. 3.3). While Δ^0 exclusively decays to WW for $\alpha \sim 0$, the bb and ZZ modes become relevant for non-zero α . In fact, for $\alpha = \tan^{-1}(4v_\Delta/v_\Phi)$, the rate to WW can even be zero, as can be seen in Fig. 5. However, in this case, the decay to ZZ , which also leads

an on- Z lepton pair with any other lepton in the event is called off- Z .

¹⁵We also build the UFO model files at NLO using FeynRules [116–118]. While it is desirable to perform the simulations at NLO, in order to reduce the computational resources needed for our analysis, we perform them at LO and then naively scale the production cross-section to account for the NLO+NNLL QCD corrections as discussed in Sec. 3.

to a sizable number of leptons, can be sizable. We will therefore consider the two limiting cases of $\text{Br}(\Delta^0 \rightarrow WW) = 1$ and $\text{Br}(\Delta^0 \rightarrow WW) = 0$, where in the latter case non-zero $\text{Br}(\Delta^0 \rightarrow ZZ)$ is considered. We then interpolate the two limiting cases as a function of the triplet mass.

Results

In Fig. 12, we show the upper limits on the visible signal cross-section observed by ATLAS [155] and the Δ SM model predictions for the SRs which give the most relevant constraints. The dashed and solid lines, respectively, indicate the expected and observed limits. The inner green and outer yellow bands around the dashed lines indicate the regions containing 68% and 95% of the distribution of limits expected under the background-only hypothesis. The red-shaded bands indicate the Δ SM model predictions for the corresponding signal cross-section, with the upper (lower) line of each band corresponding to a 100%(0%) branching ratio for $\Delta^0 \rightarrow WW$. One can see that while the predicted effect is, in many cases, close to the observed limits, the Δ SM cannot be excluded with this model-independent multi-lepton search by ATLAS. However, run 3 and high-luminosity data [165] will be able to test the Δ SM in the mass region below 200 GeV.

4.3 Associated production of the triplet-like Higgs and resonant di-photon signatures: $\gamma\gamma + X$

Drell-Yan production of the triplet-like Higgs states via an off-shell W -boson, i.e. $pp \rightarrow W^* \rightarrow \Delta^0 \Delta^\pm$ with $\Delta^0 \rightarrow \gamma\gamma$ leads to final states with a photon pair (di-photon) and additional particles and/or missing transverse momentum from the decay of Δ^\pm . This $\gamma\gamma + X$ signature is shown in Fig. 13. The mass of Δ^0 can be reconstructed from the di-photon invariant mass ($m_{\gamma\gamma}$) distribution.

In the Δ SM model, $\Delta^0 \rightarrow \gamma\gamma$ has a branching ratio of $\sim \mathcal{O}(0.1)\% - \mathcal{O}(1)\%$ (see Fig. 6 and the relevant discussion in Sec. 3.3). Though this decay rate is much lower than the ones for several other channels such as $WW, ZZ, bb, \tau\tau$ (see Fig. 5), the sensitivity of the di-photon final state is enhanced by the clearness of the corresponding detector signal as well as the smaller SM background.

An analysis of $\gamma\gamma + X$ has been performed by ATLAS, targeting the SM Higgs [90]. This search considers 22 SRs categorized by X , the objects produced in association with the di-photon; see Table 3 of Ref. [90] for the definitions of the SR. In addition, ATLAS has released a search for non-resonant di-Higgs production, which includes $\gamma\gamma + \tau$ [91] not covered in the previous analysis. Both these searches provide $m_{\gamma\gamma}$ distributions in the 105 GeV–160 GeV range, thereby covering part of the mass range of our interest for the Δ SM.

Because the ATLAS analyses performed a model-independent analysis of the associated production of the SM Higgs, no channels were combined, and the hypothesis of a BSM Higgs was not considered. However, the sidebands can be used to perform

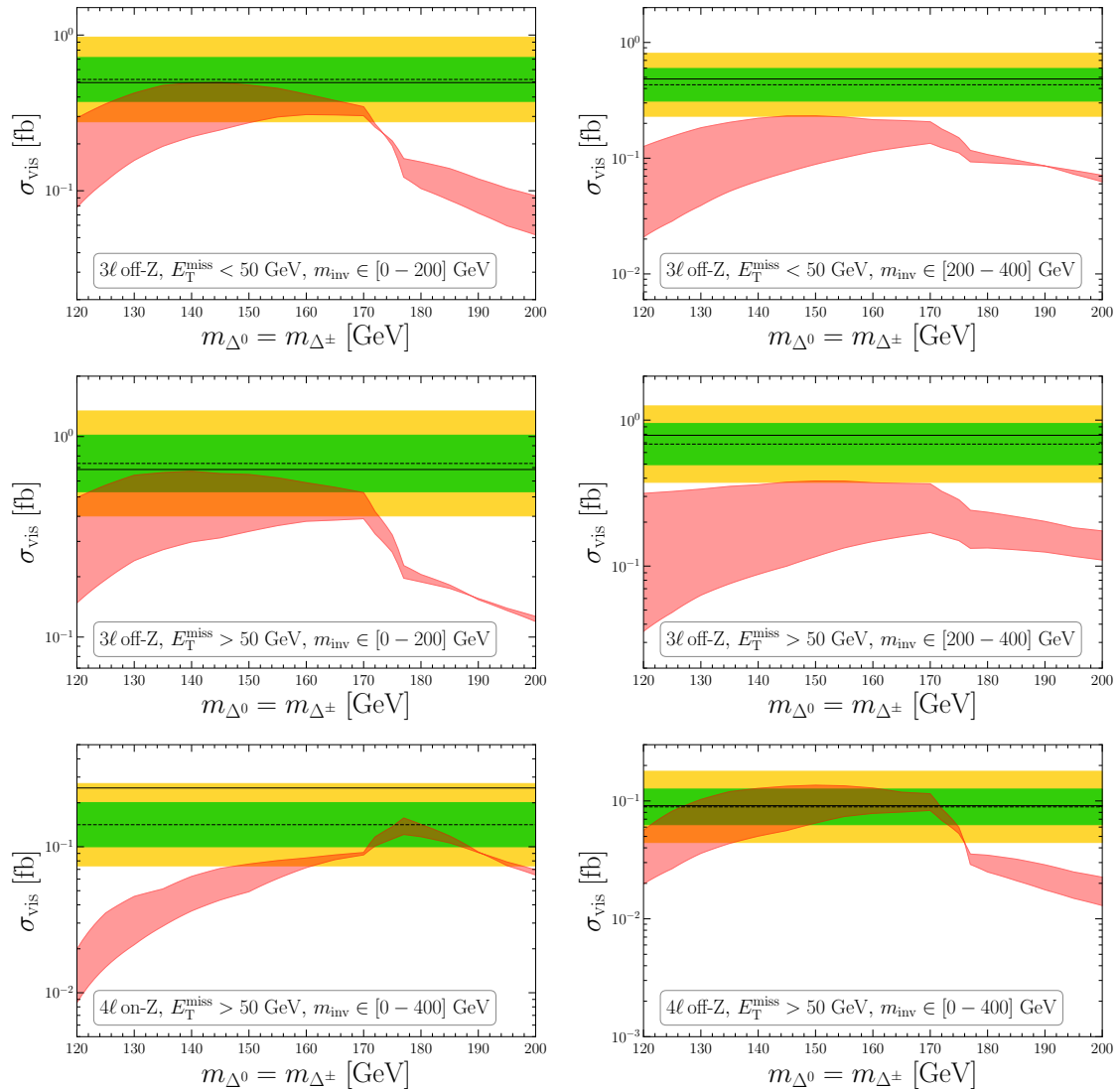


Figure 12. The black solid (dashed) lines show the observed (expected) 95% CL upper limits from ATLAS on the visible cross-section for different signal regions considered in Ref. [155] and the green (yellow) band the expected 1σ (2σ) range. Our model prediction is shown as a red band, where the upper (lower) line of the band is obtained by simulating the processes $pp \rightarrow \Delta^\pm \Delta^\mp$ and $pp \rightarrow \Delta^\pm \Delta^0$ with $\text{Br}(\Delta^0 \rightarrow WW) = 100\%$ (0%) and Δ^\pm decays according to the branching ratios shown in Fig. 8.

a search for BSM Higgses; within the Δ SM, all signal regions are correlated so that they can be combined.

For this, we simulate the process $pp \rightarrow W^{\pm*} \rightarrow (\Delta^0 \rightarrow \gamma\gamma)(\Delta^\pm \rightarrow WZ, tb, cs, \tau\nu)$ for 50 values of m_Δ in the 105 GeV–157 GeV range. As we did for the multi-lepton search in Sec. 4.2, we use the same set of tools to recast this search. Once again, we appropriately tune the delphes card for the ATLAS detector to take into account various object reconstruction, isolation and selection requirements. Following that,

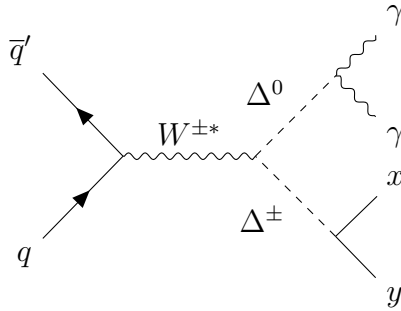


Figure 13. The Drell-Yan production of Δ^0 and Δ^\pm followed by their prompt decays $\Delta^0 \rightarrow \gamma\gamma$ and $\Delta^\pm \rightarrow xy$ ($xy \in WZ, tb, cs, \tau\nu$) leading to $\gamma\gamma + X$ final states.

we apply the event selections and categorise the selected $\gamma\gamma + X$ events into several SRs as in Ref. [90, 91].

Effects in the relevant SRs

Given the dominant decay modes of Δ^\pm (WZ, tb and $\tau\nu$) and their subsequent decays to leptons, quarks and neutrinos, we expect that the SRs targeting leptons (ℓ), taus (τ), multiple jets (j) and E_T^{miss} are the most sensitive ones. Those targeting top quarks are expected to become relevant for larger m_Δ . Among the three SRs related to top quarks, the one targeting hadronically decaying top quarks is not sensitive to the signal of our model for the mass range of our interest because it is targeting hadronically decaying top quarks from $t\bar{t}$ production.¹⁶

Before proceeding, a few comments on SRs are in order. The 1ℓ SR has been considered by both the Ref. [90] and Ref. [91]. Since the latter applies a b -jet veto, this SR is nearly uncorrelated with the ℓb SR considered in Ref. [90]. This leads us to use the 1ℓ SR of Ref. [91]. Furthermore, for both the 1ℓ and $1\tau_{\text{had}}$ SRs of Ref. [91], they use a BDT to further categorise the events into three categories based on the BDT score. Since the corresponding weight files are not available yet, it would be a highly non-trivial task to appropriately implement the same BDTs for a little too gain in sensitivity. Therefore, instead of implementing the BDTs, we take a conservative approach to adding the event yields of all three BDT categories to recover the yields that would have resulted after the event selections (and before the BDTs). Concerning the 3ℓ SR, since ATLAS has observed no event, we treat the entire $m_{\gamma\gamma}$ range as a single bin. Similarly, we do not show the $E_T^{\text{miss}} > 300 \text{ GeV}$ SR since very few events have been observed and it is correlated to the other MET

¹⁶ATLAS uses a boosted decision tree (BDT) for top-quark reconstruction and requires a tight cut of 0.9 on the BDT score. The corresponding signal in the Δ SM model consisting of a bottom quark and an (off-shell) top quark being quite different, the resulting efficiency is expected to be very small, thus rendering this SR irrelevant for the mass range of our interest.

categories.¹⁷ Finally, while scaling by an overall k -factor of 1.15 at the cross-section level accounts for the NLO+NNLL QCD correction in the production of the triplet Higgs states, additional correction accrues from enhanced selection efficiencies. This is particularly important for the SRs targeting high jet activity because of gluon radiation. To estimate this, we simulate the corresponding signal at NLO and find an additional correction factor 1.2 for the $4j$ SR.

After simulating the effect in all signal regions given by ATLAS, taking into account the consideration above, it turns out that the 10 SRs listed in Table 1 are relevant in the Δ SM model for the mass range of our interest. This means that the other SRs lead to such weak constraints on $\text{Br}(\Delta^0 \rightarrow \gamma\gamma)$ that disregarding them in a combined analysis has virtually no impact on the result.

Target	Signal region	Detector level selections	Correlation
High jet activity [90]	$4j$	$n_{\text{jet}} \geq 4, \eta_{\text{jet}} < 2.5$	–
Top [90]	ℓb	$n_{\ell=e,\mu} \geq 1, n_{b\text{-jet}} \geq 1$	–
	t_{lep}	$n_{\ell=e,\mu} = 1, n_{\text{jet}} = n_{b\text{-jet}} = 1$	–
Lepton [90, 91]	2ℓ	$ee, \mu\mu$ or $e\mu$	$< 26\%$ (1ℓ)
	3ℓ	$n_{\ell=e,\mu} \geq 3$	
	1ℓ	$n_{\ell=e,\mu} = 1, n_{\tau_{\text{had}}} = 0, n_{b\text{-jet}} = 0, E_{\text{T}}^{\text{miss}} > 35 \text{ GeV}$ (only for e -channel)	$< 26\%$ (2ℓ)
Tau [91]	$1\tau_{\text{had}}$	$n_{\ell=e,\mu} = 0, n_{\tau_{\text{had}}} = 1, n_{b\text{-jet}} = 0, E_{\text{T}}^{\text{miss}} > 35 \text{ GeV}$	–
$E_{\text{T}}^{\text{miss}}$ [90]	$E_{\text{T}}^{\text{miss}} > 100 \text{ GeV}$	$E_{\text{T}}^{\text{miss}} > 100 \text{ GeV}$	29% ($E_{\text{T}}^{\text{miss}} > 200 \text{ GeV}$)
	$E_{\text{T}}^{\text{miss}} > 200 \text{ GeV}$	$E_{\text{T}}^{\text{miss}} > 200 \text{ GeV}$	29% ($E_{\text{T}}^{\text{miss}} > 100 \text{ GeV}$)
	$E_{\text{T}}^{\text{miss}} > 300 \text{ GeV}$	$E_{\text{T}}^{\text{miss}} > 300 \text{ GeV}$	–

Table 1. The signal regions of the ATLAS analyses [90, 91] which are sensitive to the Drell-Yan production of the scalar triplet within our mass range of interest. n_{ℓ} , n_j , $n_{b\text{-jet}}$, $n_{\tau_{\text{had}}}$ denotes the number of leptons, jets, b -tagged jets and τ -tagged jets, respectively; and η_{jet} stands for the jet rapidity. Also, correlations ($> 5\%$) among overlapping SRs are quoted.

Background (re)fitting

To signals arising from BSM production, as in our case, the background consists of two components: resonant and continuum. The resonant component arises from the SM Higgs boson production and thus manifests itself as a narrow peak in the $m_{\gamma\gamma}$ spectrum. The continuum component, depending on the SRs, arises from the

¹⁷We checked that for our best-fit point for 152 GeV, ≈ 2 events are predicted while ≈ 1 NP event is observed, showing the consistency.

production of two initial/final-state photons, the misidentification of jets and the production of EW bosons and top quarks. The continuum backgrounds are estimated from data by fitting the $m_{\gamma\gamma}$ spectrum in the mass range 105 GeV–160 GeV with an analytic function with free parameters. Note that those estimated by ATLAS in Refs. [90, 91] are obtained assuming there is only a single resonance at 125 GeV, i.e. the SM Higgs. On the contrary, in the Δ SM model, there is another resonance at m_{Δ^0} , i.e. the triplet-like Higgs, albeit with different signal strength. This resonance manifests itself as a narrow peak in the $m_{\gamma\gamma}$ spectrum, much like the one at 125 GeV. Consequently, we need to (re)estimate the continuum background from a (re)fit to the data. ATLAS follows the procedure *spurious-signal test* [166] to select a background function for a given SR from a number of candidate functions such as power-law functions, Bernstein polynomials, and exponential functions (of a polynomial), to ensure small potential bias in the extracted signal yield compared to the experimental precision. However, for the sake of simplicity, we use the following common function for all SRs (except the 3ℓ SR, for which the yields are too small to fit a distribution):

$$\left(1 - \frac{m_{\gamma\gamma}}{\sqrt{s}}\right)^b \left(\frac{m_{\gamma\gamma}}{\sqrt{s}}\right)^{a_0 + a_1 \log(m_{\gamma\gamma}/\sqrt{s})}, \quad (4.3)$$

where a_0 , a_1 and b are the free parameters which are independent across SRs, $\sqrt{s} = 13$ TeV is the LHC run 2 centre-of-mass energy. This function is fitted with the data subtracted by the resonances—SM Higgs at 125 GeV and triplet-like Higgs at m_{Δ^0} —to estimate the (re)fitted continuum background.

Statistical model

The data are interpreted as briefly described below. A likelihood function is built from the number of observed and (re)fitted Δ SM signal-plus-background events. Assuming the bins in the $m_{\gamma\gamma}$ spectrum for a given SR as independent number-counting experiments, the likelihood is modelled as

$$\mathcal{L}_{\text{SR}}(\mu) = \prod_i \text{Pois}(n^i | \mu s^i + b^i) \quad (4.4)$$

where i runs over the 22 bins in the $m_{\gamma\gamma}$ spectrum in the 105 GeV–160 GeV range and μ represents the parameter of interest or signal strength: $\Delta^0 \rightarrow \gamma\gamma$ branching ratio, $\text{Br}(\Delta^0 \rightarrow \gamma\gamma)$ in our case (this choice to be justified shortly). Here, as is typically done for number-counting experiments, the Poisson distribution is used to compare the measured data n with the modelled expectation comprising of a signal yield s and a background yield b . Then, the global likelihood $\mathcal{L}(\mu)$ for the $\gamma\gamma + X$ measurements is obtained as the product of the likelihood functions for the relevant

SRs. Finally, the profile likelihood ratio test statistics [167] is given by

$$\Lambda(\mu) = -2 \log \frac{\mathcal{L}(\mu)}{\mathcal{L}(\hat{\mu})}$$

where $\hat{\mu}$ refers to the value of μ that maximises the likelihood. This test statistics asymptotically follows a χ^2 distribution such that approximate 68% and 95% CL (1σ and 2σ) intervals can be easily constructed by requiring $\Lambda(\mu) = 1$ and $\Lambda(\mu) = 4$, respectively. Note that we allow for an unphysical negative μ to take into account the effect of downward fluctuations of the background.

Results

In Figs. 14 and 15, we show the fit to the di-photon invariant mass distributions for the relevant signal regions listed in Table 1. The data and continuum backgrounds taken from the ATLAS analyses are shown in black (points with error bars) and blue, respectively. Also shown are the 125 GeV SM Higgs signals (magenta) and 152 GeV Δ SM triplet Higgs signals with $\text{Br}(\Delta^0 \rightarrow \gamma\gamma) = 0.7\%$ (green). For brevity, we do not show the (re)fitted continuum backgrounds; the (re)fitted Δ SM signal-plus-backgrounds are shown in red. Note that the Δ SM benchmark chosen here is occasioned by our findings later in this section that there is a strong preference for $\text{Br}(\Delta^0 \rightarrow \gamma\gamma) \approx 0.7\%$ at 152 GeV when all relevant SRs are statistically combined.

Now, we put upper limits on the parameter of interest, $\text{Br}(\Delta^0 \rightarrow \gamma\gamma)$. While this is trivially calculable, as discussed in Sec. 3.3, it crucially depends on the triplet mass m_{Δ^0} , the mixing angle α , the mass-splitting $m_{\Delta^\pm} - m_{\Delta^0}$ (through the $\Delta^0 \Delta^\pm \Delta^\mp$ coupling) and the triplet VEV v_Δ . Hence, rather than varying these parameters, we subsume them within a single observable $\text{Br}(\Delta^0 \rightarrow \gamma\gamma)$, which is of great interest as far as the LHC search program for additional Higgs is concerned. 95% CL upper limits on $\text{Br}(\Delta^0 \rightarrow \gamma\gamma)$ as a function of the triplet Higgs mass m_{Δ^0} for various SRs are shown in Fig. 16. For brevity, we only show the SRs that are most constraining, i.e. provide relevant bounds on $\text{Br}(\Delta^0 \rightarrow \gamma\gamma)$.

We then proceed to find the preferred ranges for $\text{Br}(\Delta^0 \rightarrow \gamma\gamma)$ as a function of m_{Δ^0} for the relevant SRs. The obtained best-fit values, along with the 1σ and 2σ ranges, are shown in Figs. 17 and 18. For reasons mentioned earlier, here, we do not show the corresponding plots for 3ℓ and $E_T^{\text{miss}} > 300$ GeV SRs. Interestingly, all relevant SRs display a preference for a non-zero $\Delta^0 \rightarrow \gamma\gamma$ decay rate around 152 GeV.

Finally, we combine the 10 relevant SRs, including their correlations, to obtain the combined preferred ranges for $\text{Br}(\Delta^0 \rightarrow \gamma\gamma)$ as a function of m_Δ , as shown in Fig. 19.¹⁸ We see a strong preference for a non-zero $\text{Br}(\Delta^0 \rightarrow \gamma\gamma)$ in the 150 GeV–

¹⁸Note that there are moderate correlations among some SRs, in particular, among the E_T^{miss} ones. However, we checked that removing the $E_T^{\text{miss}} > 300$ GeV SR from the fit has a very small impact on the final result.

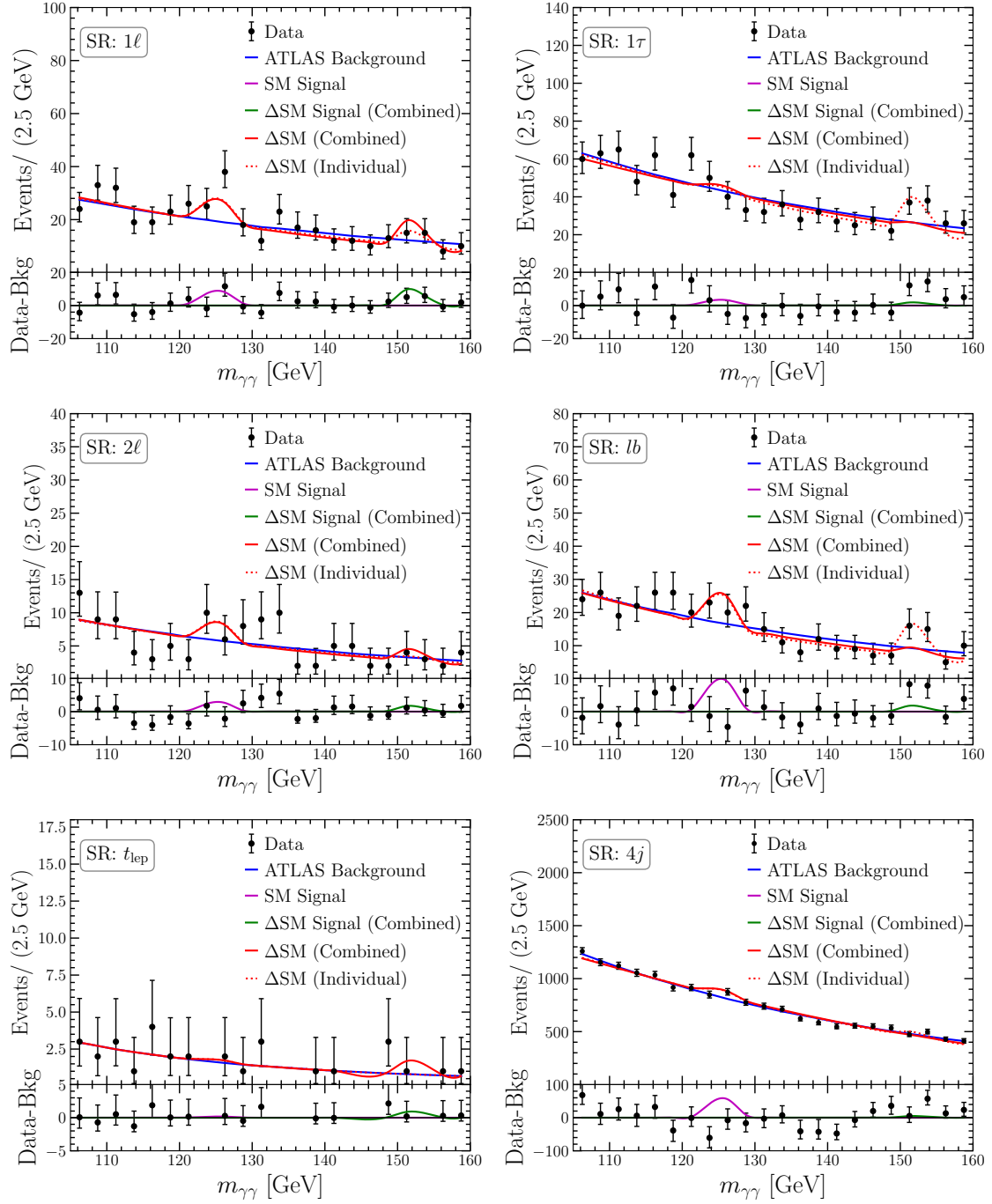


Figure 14. Di-photon invariant mass distributions for the relevant signal regions. The data and corresponding uncertainties (indicated by black points and vertical bars) are shown together with the continuum background (blue line) from the ATLAS analyses and the total Δ SM events (red line). The latter is comprised of the (re)fitted background (not shown for brevity), the SM Higgs signal at 125 GeV (magenta line) and the Δ SM triplet Higgs signal at 152 GeV (green line).

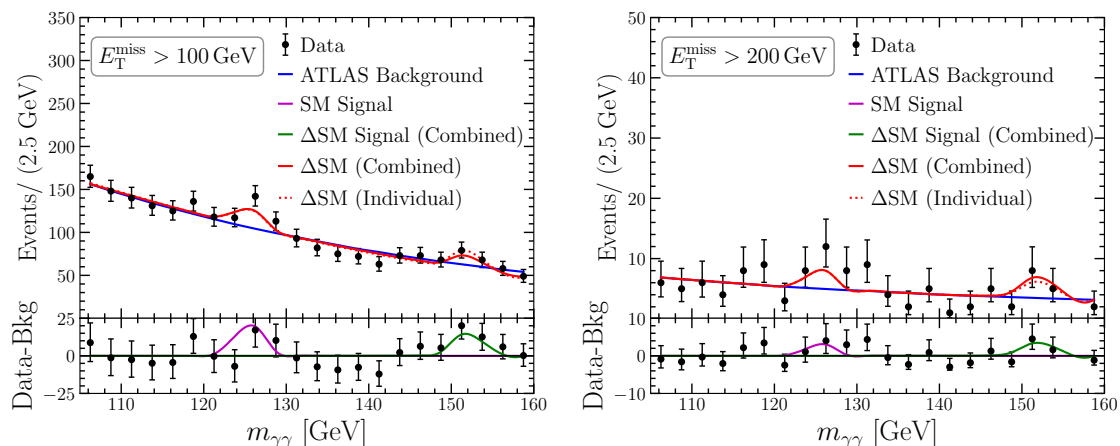


Figure 15. Di-photon invariant mass distributions for the relevant signal regions (continued). The description is the same as of Fig. 14.

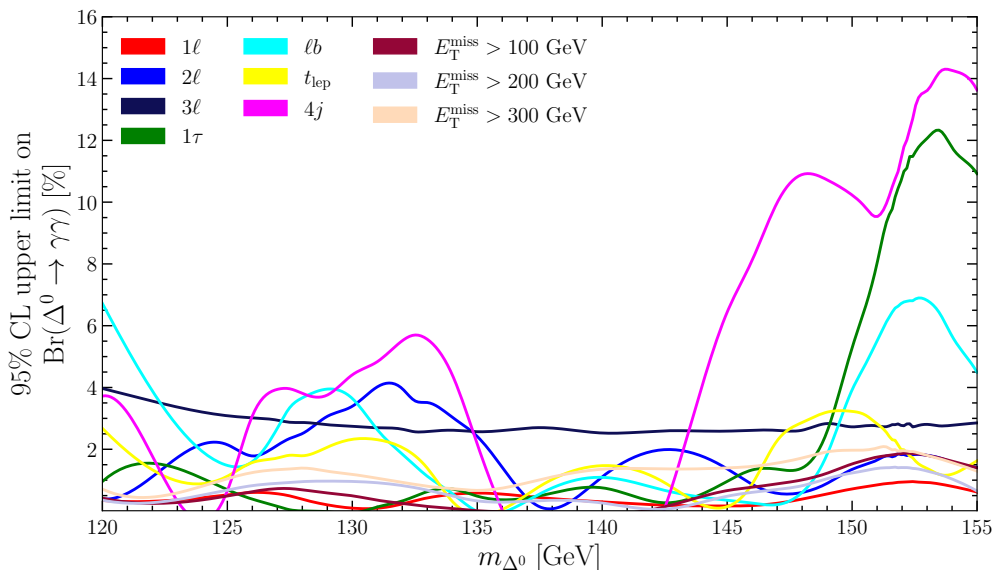


Figure 16. 95% CL upper limits on $\text{Br}(\Delta^0 \rightarrow \gamma\gamma)$ as a function of m_{Δ^0} for various SRs.

155 GeV range. This is most pronounced at 152 GeV with $\text{Br}(\Delta^0 \rightarrow \gamma\gamma) \approx 0.7\%$, and the corresponding significance amounts to 3.9σ .

For the sake of phenomenological interest, we have subsumed the free parameters of the ΔSM model—the triplet mass m_{Δ^0} , the mixing angle α , the mass-splitting $m_{\Delta^\pm} - m_{\Delta^0}$ and the triplet VEV v_Δ —into a single observable $\text{Br}[\Delta^0 \rightarrow \gamma\gamma]$. Before closing this section, we closely look at how the preferred di-photon decay rate can be obtained. For a given m_{Δ^0} and v_Δ , $\text{Br}(\Delta^0 \rightarrow \gamma\gamma)$ depends on α and $m_{\Delta^\pm} - m_{\Delta^0}$. In Fig. 20, we show the preferred regions in the α vs $m_{\Delta^\pm} - m_{\Delta^0}$ plane for $m_{\Delta^0} = 152$ GeV and two values of v_Δ : 4.1 GeV (left) and 2.7 GeV (right), corresponding to the

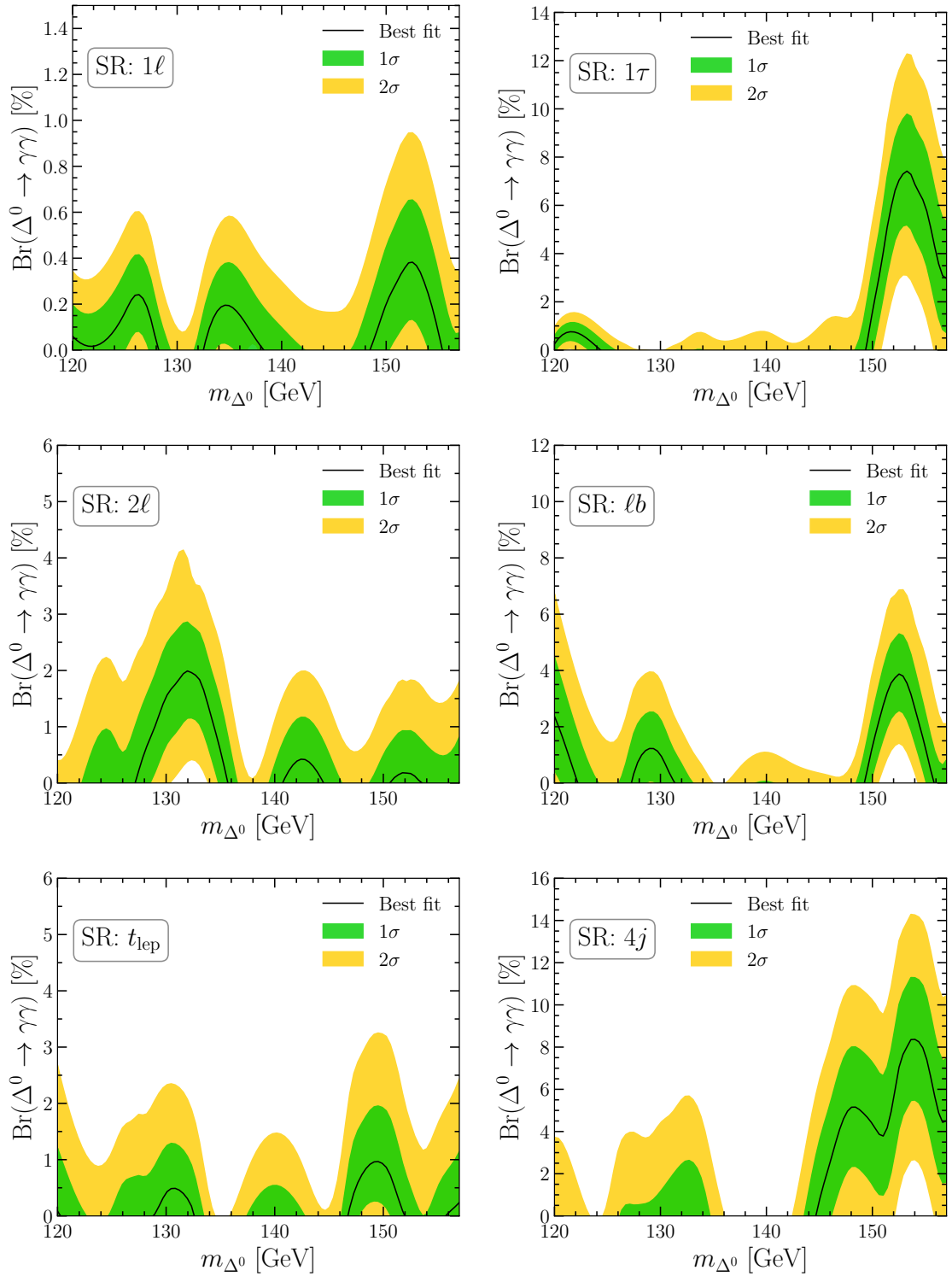


Figure 17. Preferred ranges for $\text{Br}(\Delta^0 \rightarrow \gamma\gamma)$ as a function of m_{Δ^0} for the relevant SRs. Green corresponds to 1σ and yellow to 2σ , and the best fit is shown as a solid black line.

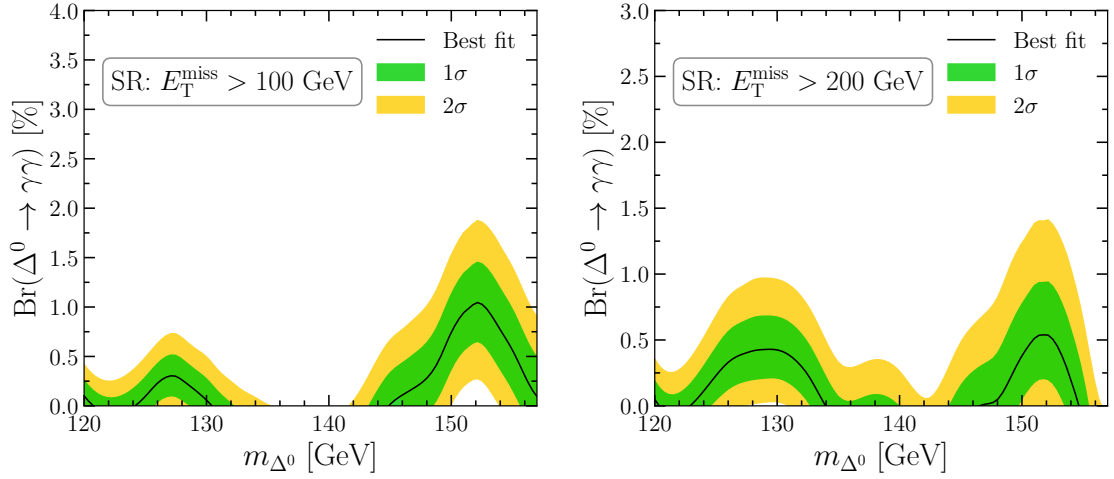


Figure 18. Preferred ranges for $\text{Br}(\Delta^0 \rightarrow \gamma\gamma)$ as a function of m_{Δ^0} for the relevant SRs (continued). Green corresponds to 1σ and yellow to 2σ , and the best fit is shown as a solid black line.

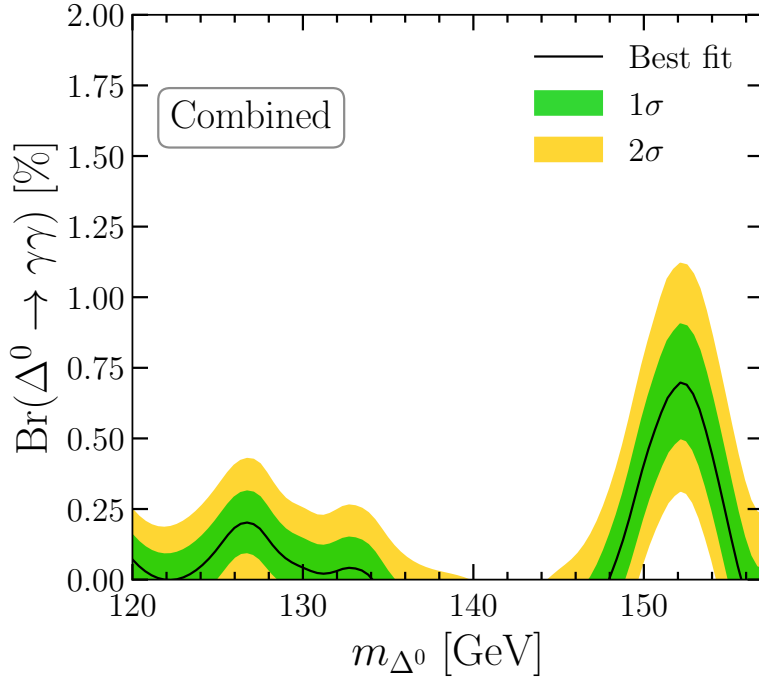


Figure 19. Preferred ranges for $\text{Br}(\Delta^0 \rightarrow \gamma\gamma)$ as a function of m_{Δ^0} for the statistical combination of the relevant SRs.

best-fit values obtained from the world W -mass fit with and without including the CDF-II measurement. The band between the two orange lines satisfies perturbative unitarity, and the region below the blue line leads to a stable vacuum at the EW scale. The green regions are allowed by the SM Higgs to di-photon signal strength [127, 128]

at 1σ (1.02-1.15), 2σ (0.96-1.22) and 3σ (0.90-1.29) levels. The 1σ (0.50–0.90%), 2σ (0.31–1.11%) and 3σ (0.14–1.35%) regions for $\text{Br}(\Delta^0 \rightarrow \gamma\gamma)$ are shown in violet. We see that the 1σ region (and also part of the 2σ region) preferred by the ATLAS $\gamma\gamma + X$ searches are not in accordance with the vacuum stability and perturbative unitarity constraints. This demonstrates that while we have growing evidence for a 152 GeV triplet-like Higgs produced in association with leptons (including τ -leptons), quarks (including b -quarks) and neutrinos, the ΔSM should be superseded by BSM models with additional fields at or above the EW scale so as to restore the stability of the vacuum and perturbativity of the theory.

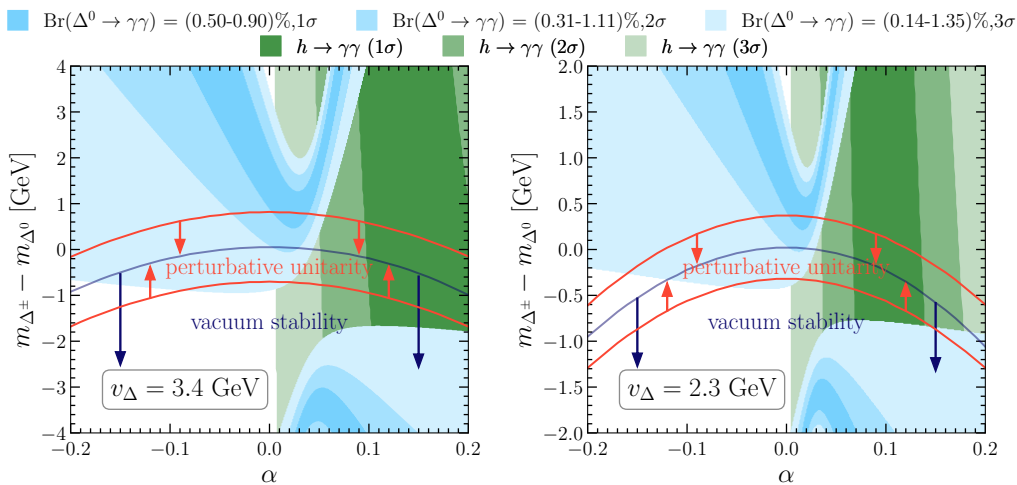


Figure 20. Preferred regions in the α vs $m_{\Delta^\pm} - m_{\Delta^0}$ plane for $m_{\Delta^0} = 152$ GeV and two values of v_Δ : 4.1 GeV (left) and 2.7 GeV (right). The band between the two orange lines satisfies perturbative unitarity, and the region below the blue line leads to a stable vacuum at the EW scale. The green regions are allowed by the SM Higgs to di-photon signal strength at 1σ , 2σ and 3σ levels. The 1σ , 2σ and 3σ regions for $\text{Br}(\Delta^0 \rightarrow \gamma\gamma)$ preferred by the ATLAS $\gamma\gamma + X$ data are shown in violet.

4.4 Higgs to $Z\gamma$ search in the $\ell^+\ell^-\gamma$ final state

Similar to the di-photon mode, Δ^0 can have a branching ratio of about $\mathcal{O}(0.1)\%$ – $\mathcal{O}(1)\%$ (see Fig. 7 and the relevant discussion in Sec. 3.3). Experimentally, the final state resulting from the leptonic decay of Z ($Z \rightarrow \ell^+\ell^-$ with $\ell = e, \mu$) is the most accessible since the leptons are highly distinctive. CMS has recently performed such a pertinent search with the full run 2 data in Ref. [130]. This search categorises the events into three broad mutually exclusive SRs: Lepton-tagged, Dijet, and Untagged, further categorising the latter two into 3 and 4 SRs. We meticulously recast this search in the context of the ΔSM and find that only the Lepton-tagged SR is relevant. In Fig. 21, we show the preferred ranges for $\text{Br}(\Delta^0 \rightarrow Z\gamma)$ as a function of m_{Δ^0} .

Though the current bounds are not competitive with di-photon searches, they are expected to become relevant with high-luminosity LHC data [165].

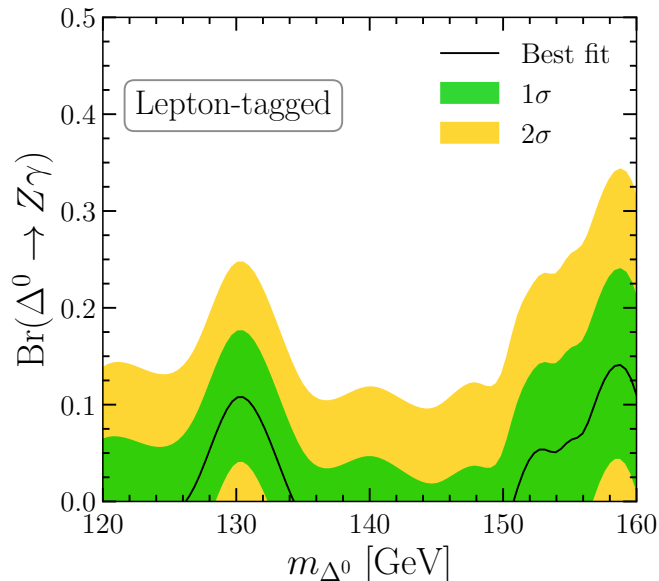


Figure 21. Preferred ranges for $\text{Br}(\Delta^0 \rightarrow Z\gamma)$ as a function of m_{Δ^0} . Green corresponds to 1σ and yellow to 2σ , and the best fit is shown as a solid black line.

5 Summary and Outlook

Though the ongoing LHC search program for new particles has not led to any discovery yet, it has, nonetheless, unveiled several hints for new particles in the form of “anomalies” [10]. This includes the multi-lepton anomalies [70, 76] which points towards the existence of a new Higgs with a mass of 150 ± 5 GeV which dominantly decays to WW [69]. Furthermore, the re-analyses of the sidebands of the ATLAS and CMS Higgs boson searches indicate the presence of a new narrow resonance with a mass around 152 GeV produced in association with leptons, quarks, and neutrinos [77, 78].

In this context, it has been shown that the $\gamma\gamma + X$ excesses are consistent with the Drell-Yan production of a 152 GeV Higgs from a scalar triplet with $Y = 0$, with a significance of $\approx 4\sigma$ [66, 88], which predicts a positive-definite shift in the W mass, in agreement with the global fit. Furthermore, its neutral component decays dominantly to WW , as suggested by the multi-lepton anomalies.

Motivated by this, we have detailed the $Y = 0$ Higgs triplet model and its phenomenology in this work. In particular, we have studied the tree-level perturbative unitarity and bounded-from-below constraints on the scalar potential. Further, we have discussed various possible vacua configurations and the stability of the neutral

ones against the charge-breaking ones, which is discussed in Appendix C. We showed that the absence of tachyonic modes in the Higgs sector suffices to ensure that the desired EW vacuum corresponds to the global minimum of the potential. Combined, these constraints delineate the theoretically allowed parameter space within the perturbative regime and, together with the constraints from the ρ parameter, drive the triplet-like neutral and charged Higgs states to be quasi-mass-degenerate.

We have discussed the production and decays of the Higgs states, including the $h \rightarrow \gamma\gamma$, $h \rightarrow Z\gamma$ and $h \rightarrow ZZ^*$ decays, which put non-trivial constraints on the model parameter space. Furthermore, we have detailed their phenomenology at the LHC based on three types of final states: stau-like signature, multi-lepton and $\gamma\gamma+X$ final states. The findings are summarised below.

- i)* Low-mass ($\lesssim 120$ GeV) triplet-like charged Higgs dominantly decays to $\tau\nu$. Therefore, the process $pp \rightarrow \Delta^+\Delta^-$ leads to final states involving a pair of τ -leptons and missing transverse momentum, which is akin to the collider signature of stau. Our reinterpretation of the corresponding CMS search [150] excludes triplet-like charged Higgs with a mass below 110 GeV at 95% CL.
- ii)* For triplet-like Higgs bosons with higher masses ($\gtrsim 120$ GeV) the dominant decays modes are $\Delta^\pm \rightarrow W^\pm Z, t\bar{b}$ and $\Delta^0 \rightarrow W^+W^-, ZZ$. Therefore, their Drell-Yan production can lead to final states with multiple charged leptons from the leptonic decays of W and Z . To probe the Δ SM, we recast a recent model-independent analysis of ATLAS [155] involving three and four leptons in the final state. Our analysis shows that for some SRs, the predicted effect is close to the observed limit of ATLAS, but Δ SM cannot be excluded from this search. However, run 3 and high-luminosity LHC data will be able to test the signatures of the Δ SM in multi-lepton final states.
- iii)* The associated production of the triplet-like Higgses and their prompt decays to di-photon lead to $\gamma\gamma + X$ final states. We have performed two such pertinent searches by ATLAS. We have performed a (re)fit to the data to determine the continuum background and a likelihood-based statistical interpretation to find that, out of the 25 signal regions considered, 10 of them put stringent limits on the triplet-like Higgs, particularly on its di-photon branching ratio $\text{Br}(\Delta^0 \rightarrow \gamma\gamma)$. Interestingly, all relevant signal regions show a weakening of the limits around 125 GeV–130 GeV and 152 GeV. More importantly, there is a strong preference for a non-zero di-photon decay rate in the 150 GeV–155 GeV range. When all relevant SRs are statistically combined, this is most pronounced at 152 GeV with the corresponding branching ratio of about 0.7% and the corresponding significance of about 3.9σ . While such a sizable branching ratio to di-photons is easily achievable in the Δ SM, part of this model parameter space consistent with the di-photon signal strength of the SM Higgs is in tension with the vacuum stability and perturbative unitarity.

The last point, i.e. the preferred range for the di-photon decay rate is in tension with the vacuum stability and perturbative unitarity, demonstrates that while we have growing evidence for a 152 GeV Higgs produced in association with leptons, quarks and neutrinos, the Δ SM is not expected to be the final theory superseding the SM. In fact, with additional fields at or above the EW scale, the problem of the large di-photon rate in unstable field configurations can be solved in (at least) three non-exclusive ways. Additional field(s) can

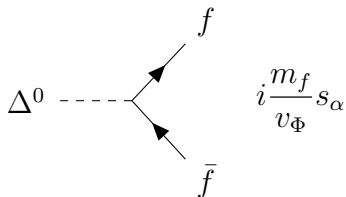
- i)* modify the (effective) scalar potential such that the vacuum stability is restored at larger field values,
- ii)* lead to loop contributions to $\Delta^0 \rightarrow \gamma\gamma$,
- iii)* allow for a larger VEV of the triplet by cancelling its effect in the ρ parameter as in the Georgi-Machacek model [168], thereby enlarging the region with the stable EW vacuum.

(*i*) and (*ii*) are possible, e.g. by introducing additional charged Higgs bosons; an interesting UV-realisation of this is the Δ 2HDMS: the Δ SM extended with a second Higgs doublet and a singlet [75]. In addition to explaining the di-photon excess in associated production [89] this model can address the significant tensions in differential top quark distributions [169] as shown in Ref. [74] and lead to baryogenesis via a two-step phase transition [170].

In summary, the Δ SM, analysed in detail in this article, represents a step towards the establishment of a model that can simultaneously explain the multi-lepton anomalies and the narrow resonance in associated production with a mass of 152 GeV. However, more data and improved SM predictions are necessary to arrive at the conclusive model superseding the SM.

A Feynman rules for the Δ SM

Here, we provide the Feynman rules for vertices involving the triplet fields. All momenta are considered to be incoming. We take the positively charged components of the triplets as particles and the negatively charged ones as antiparticles. Consequently, particle flow arrows point in the direction of particle momentum, while they point opposite to the momentum direction for antiparticles. We use the shorthand notations $s_\beta = \sin \beta$ and $c_\beta = \cos \beta$.



$$\Delta^\pm \text{ --- } \begin{array}{l} \nearrow \bar{\nu}, \bar{\ell} \\ \searrow \ell, \nu \end{array} \quad i \frac{\sqrt{2} m_\ell}{v_\Phi} s_\beta P_{R,L}$$

$$\Delta^\pm \text{ --- } \begin{array}{l} \nearrow \bar{u}_i, \bar{d}_i \\ \searrow d_j, u_j \end{array} \quad -i \frac{\sqrt{2}}{v_\Phi} s_\beta V_{u_i, d_j} (m_{u_i} P_L - m_{d_j} P_R), \quad i \frac{\sqrt{2}}{v_\Phi} s_\beta V_{u_j, d_i}^* (m_{d_i} P_L - m_{u_j} P_R)$$

$$\Delta^0 \text{ --- } \begin{array}{l} W_\mu^- \\ \text{---} \\ W_\nu^+ \end{array} \quad -\frac{i}{2} g^2 (v_\Phi s_\alpha - 4v_\Delta c_\alpha) g_{\mu\nu}$$

$$\Delta^0 \text{ --- } \begin{array}{l} Z_\mu \\ \text{---} \\ Z_\nu \end{array} \quad -\frac{i}{2} \frac{g^2}{c_w^2} v_\Phi s_\alpha g_{\mu\nu}$$

$$\Delta^\pm \text{ --- } \begin{array}{l} W_\mu^\mp \\ \text{---} \\ Z_\nu \end{array} \quad -\frac{i}{2} \frac{g^2}{c_w} (2v_\Delta c_w^2 c_\beta - v_\Phi s_w^2 s_\beta) g_{\mu\nu}$$

$$\Delta^\pm \text{ --- } \begin{array}{l} W_\nu^\mp \\ \text{---} \\ \gamma_\mu \end{array} \quad -\frac{i}{2} g^2 s_w (2v_\Delta c_\beta + v_\Phi s_\beta) g_{\mu\nu}$$

$$\Delta^\pm \text{ --- } \begin{array}{l} W_\mu^\mp \\ \text{---} \\ \Delta^0 \end{array} \quad \mp \frac{i}{2} g (s_\alpha s_\beta - 2c_\alpha c_\beta) (p_\mu^{\Delta^0} - p_\mu^{\Delta^\pm})$$

$$\begin{array}{c}
W_\mu^\mp \\
\diagup \\
\Delta^\pm \text{---} \\
\diagdown \\
h
\end{array}
\quad \mp \frac{i}{2} g (2s_\alpha c_\beta + c_\alpha s_\beta) (-p_\mu^h + p_\mu^{\Delta^\pm})$$

$$\begin{array}{c}
\Delta^- \\
\diagup \\
\Delta^+ \text{---} \\
\diagdown \\
\gamma_\mu
\end{array}
\quad -ie (p_\mu^{\Delta^-} - p_\mu^{\Delta^+})$$

$$\begin{array}{c}
\Delta^- \\
\diagup \\
\Delta^+ \text{---} \\
\diagdown \\
Z_\mu
\end{array}
\quad -\frac{i}{2} \frac{g}{c_w} (c_\beta^2 + c_{2w}) (p_\mu^{\Delta^-} - p_\mu^{\Delta^+})$$

$$\begin{array}{c}
W_\mu^- \\
\diagup \\
\Delta^0 \text{---} \\
\diagdown \\
\Delta^0 \\
W_\nu^+
\end{array}
\quad \frac{i}{2} g^2 (1 + 3c_\alpha^2) g_{\mu\nu}$$

$$\begin{array}{c}
Z_\mu \\
\diagup \\
\Delta^0 \text{---} \\
\diagdown \\
\Delta^0 \\
Z_\nu
\end{array}
\quad \frac{i}{2} \frac{g^2}{c_w^2} s_\alpha^2 g_{\mu\nu}$$

$$\begin{array}{c}
W_\mu^\mp \\
\diagup \\
\Delta^\pm \text{---} \\
\diagdown \\
\Delta^0 \\
Z_\nu
\end{array}
\quad -\frac{i}{2} \frac{g^2}{c_w} (2c_w^2 c_\alpha c_\beta + s_w^2 s_\alpha s_\beta) g_{\mu\nu}$$

$$\begin{array}{c}
W_\nu^\mp \\
\diagup \\
\Delta^\pm \text{---} \\
\diagdown \\
\Delta^0 \\
\gamma_\mu
\end{array}
\quad -\frac{i}{2} g^2 s_w (2c_\alpha c_\beta - s_\alpha s_\beta) g_{\mu\nu}$$

$$-2ig^2 c_\beta^2 g_{\mu\nu}$$

$$\frac{i}{2} g^2 (1 + c_\beta^2) g_{\mu\nu}$$

$$\frac{i}{2} \frac{g^2}{c_w^2} (4c_\beta^2 c_w^4 + s_\beta^2 c_{2w}^2) g_{\mu\nu}$$

$$2ie^2 g_{\mu\nu}$$

$$i \frac{eg}{c_w} (c_\beta^2 + c_{2w}) g_{\mu\nu}$$

$$-\frac{3}{2} i [-Ac_\alpha s_\alpha^2 - 2c_\alpha^2 s_\alpha v_\Phi \lambda_{\Phi\Delta} + c_\alpha^3 \lambda_\Delta v_\Delta + s_\alpha s_{2\alpha} v_\Delta \lambda_{\Phi\Delta} - \lambda_\Phi s_\alpha^3 v_\Phi]$$

$$-\frac{1}{8} i [2s_\alpha (3c_{2\alpha} (A + v_\Delta (\lambda_\Delta - 2\lambda_{\Phi\Delta})) + A - 2v_\Delta \lambda_{\Phi\Delta} + 3\lambda_\Delta v_\Delta) - 3c_{3\alpha} v_\Phi (\lambda_\Phi - 2\lambda_{\Delta\Phi}) + c_\alpha v_\Phi (2\lambda_{\Phi\Delta} + 3\lambda_\Phi)]$$

$$\begin{array}{c}
h \\
\diagup \quad \diagdown \\
\Delta^0 \text{ ---} \\
\diagdown \quad \diagup \\
h
\end{array}
\quad \frac{1}{8}i[c_\alpha (A - 2v_\Delta \lambda_{\Phi\Delta} - 3\lambda_\Delta v_\Delta) + 3c_{3\alpha} (A - 2v_\Delta \lambda_{\Phi\Delta} + \lambda_\Delta v_\Delta) + 3s_{3\alpha} v_\Phi (\lambda_\Phi - 2\lambda_{\Delta\Phi}) + s_\alpha v_\Phi (2\lambda_{\Phi\Delta} + 3\lambda_\Phi)]$$

$$\begin{array}{c}
\Delta^- \\
\diagup \quad \diagdown \\
h \text{ ---} \\
\diagdown \quad \diagup \\
\Delta^+
\end{array}
\quad -\frac{1}{2}i[-2Ac_\alpha c_\beta s_\beta + s_\beta^2 (s_\alpha (A + 2v_\Delta \lambda_{\Delta\Phi}) + c_\alpha \lambda_\Phi v_\Phi) + c_\beta^2 (2c_\alpha v_\Phi \lambda_{\Phi\Delta} + \lambda_\Delta s_\alpha v_\Delta)]$$

$$\begin{array}{c}
\Delta^- \\
\diagup \quad \diagdown \\
\Delta^0 \text{ ---} \\
\diagdown \quad \diagup \\
\Delta^+
\end{array}
\quad -\frac{1}{2}i[s_\alpha (As_{2\beta} - 2c_\beta^2 v_\Phi \lambda_{\Phi\Delta} - \lambda_\Phi s_\beta^2 v_\Phi) + c_\alpha (s_\beta^2 (A + 2v_\Delta \lambda_{\Phi\Delta}) + c_\beta^2 \lambda_\Delta v_\Delta)]$$

$$\begin{array}{c}
\Delta^0 \quad \Delta^0 \\
\diagdown \quad \diagup \\
\Delta^0 \quad \Delta^0
\end{array}
\quad -\frac{3}{2}i (c_\alpha^4 \lambda_\Delta + s_{2\alpha}^2 \lambda_{\Phi\Delta} + \lambda_\Phi s_\alpha^4)$$

$$\begin{array}{c}
\Delta^0 \quad \Delta^0 \\
\diagdown \quad \diagup \\
\Delta^0 \quad h
\end{array}
\quad -\frac{3}{8}is_{2\alpha}[c_{2\alpha} (-4\lambda_{\Phi\Delta} + \lambda_\Delta + \lambda_\Phi) + \lambda_\Delta - \lambda_\Phi]$$

$$\begin{array}{c}
\Delta^0 \quad h \\
\diagdown \quad \diagup \\
\Delta^0 \quad h
\end{array}
\quad -\frac{1}{16}i[-3c_{4\alpha} (-4\lambda_{\Phi\Delta} + \lambda_\Delta + \lambda_\Phi) + 3(\lambda_\Delta + \lambda_\Phi) + 4\lambda_{\Phi\Delta}]$$

$$\begin{array}{c}
\Delta^0 \quad h \\
\diagdown \quad \diagup \\
h \quad h
\end{array}
\quad \frac{3}{8}is_{2\alpha}[c_{2\alpha} (-4\lambda_{\Phi\Delta} + \lambda_\Delta + \lambda_\Phi) - \lambda_\Delta + \lambda_\Phi]$$

$$\begin{array}{ccc}
\Delta^0 & & \Delta^- \\
& \diagdown & / \\
& & \times \\
& / & \diagdown \\
\Delta^0 & & \Delta^+
\end{array}
\quad -\frac{1}{2}i[c_\alpha^2(c_\beta^2\lambda_\Delta + 2s_\beta^2\lambda_{\Phi\Delta}) + s_\alpha^2(2c_\beta^2\lambda_{\Phi\Delta} + \lambda_\Phi s_\beta^2)]$$

$$\begin{array}{ccc}
h & & \Delta^- \\
& \diagdown & / \\
& & \times \\
& / & \diagdown \\
h & & \Delta^+
\end{array}
\quad -\frac{1}{2}i[c_\alpha^2(2c_\beta^2\lambda_{\Phi\Delta} + \lambda_\Phi s_\beta^2) + s_\alpha^2(c_\beta^2\lambda_\Delta + 2s_\beta^2\lambda_{\Phi\Delta})]$$

$$\begin{array}{ccc}
\Delta^0 & & \Delta^- \\
& \diagdown & / \\
& & \times \\
& / & \diagdown \\
h & & \Delta^+
\end{array}
\quad -\frac{1}{8}is_{2\alpha}[c_{2\beta}(-4\lambda_{\Phi\Delta} + \lambda_\Delta + \lambda_\Phi) + \lambda_\Delta - \lambda_\Phi]$$

$$\begin{array}{ccc}
\Delta^+ & & \Delta^- \\
& \diagdown & / \\
& & \times \\
& / & \diagdown \\
\Delta^- & & \Delta^+
\end{array}
\quad -i[c_\beta^4\lambda_\Delta + s_{2\beta}^2\lambda_{\Phi\Delta} + \lambda_\Phi s_\beta^4]$$

B Loop functions

In this appendix, we collect all the loop functions or form factors used in the Higgs decays in Sec. 3.2 and Sec. 3.3. The ones relevant for the loop-induced Higgs decays are

$$\beta_{\gamma\gamma}^0(x) = -x[1 - xf(x)],$$

$$\beta_{\gamma\gamma}^{1/2}(x) = 2x[1 + (1-x)f(x)],$$

$$\beta_{\gamma\gamma}^1(x) = -[2 + 3x + 3x(2-x)f(x)],$$

$$\beta_{Z\gamma}^0(x, y) = \frac{\cos 2\theta_w}{\cos \theta_w} I_1(x, y),$$

$$\beta_{Z\gamma}^{1/2}(x, y) = I_1(x, y) - I_2(x, y),$$

$$\beta_{Z\gamma}^1(x, y) = \cos \theta_w \left[\left\{ \left(1 + \frac{2}{x}\right) \tan^2 \theta_w - \left(5 + \frac{2}{x}\right) \right\} I_1(x, y) + 4(3 - \tan^2 \theta_w) I_2(x, y) \right],$$

with the functions $f(x), j(x), I_1(x, y)$ and $I_2(x, y)$ defined as

$$\begin{aligned}
f(x) &= \begin{cases} \left[\sin^{-1}(\sqrt{1/x}) \right]^2 & x \geq 1 \\ -\frac{1}{4} \left[\log \frac{1+\sqrt{1-x}}{1-\sqrt{1-x}} - i\pi \right]^2 & x < 1 \end{cases} \\
j(x) &= \begin{cases} \sqrt{x-1} \sin^{-1}(\sqrt{1/x}) & x \geq 1 \\ \frac{1}{2} \sqrt{1-x} \left[\log \frac{1+\sqrt{1-x}}{1-\sqrt{1-x}} - i\pi \right] & x < 1 \end{cases} \\
I_1(x, y) &= \frac{xy}{2(x-y)} + \frac{x^2 y^2}{2(x-y)^2} [f(x) - f(y)] + \frac{x^2 y}{(x-y)^2} [j(x) - j(y)], \\
I_2(x, y) &= -\frac{xy}{2(x-y)} [f(x) - f(y)],
\end{aligned}$$

and the ones relevant for the tree-level Higgs decays are

$$\begin{aligned}
\beta(x, y) &= (1-x-y)^2 - 4xy, \\
\beta_{ff'}(x, y) &= [(x+y)(1-x-y) - 4xy] \times \sqrt{\beta(x, y)}, \\
\beta_S(x) &= (x-1) \left(2 - \frac{1}{2} \log x \right) + \frac{1-5x}{\sqrt{4x-1}} \left[\tan^{-1} \frac{2x-1}{\sqrt{4x-1}} - \tan^{-1} \frac{1}{\sqrt{4x-1}} \right], \\
\beta_V(x) &= (1-4x+12x^2) \times \sqrt{\beta(x, x)}, \\
\beta'_V(x) &= \frac{3(1-8x+20x^2)}{\sqrt{4x-1}} \cos^{-1} \frac{3x-1}{2x\sqrt{x}} - \frac{(1-x)}{2x} (2-13x+47x^2) - \frac{3}{2}(1-6x+4x^2) \log x, \\
\beta_t(x, y) &= \frac{y^2}{x^3} (4xy+3x-4y) \log \frac{y(x-1)}{x-y} + (3x^2-4x-3y^2+1) \log \frac{x-1}{x-y} - \frac{5}{2} \\
&\quad + \frac{1-y}{x^2} (3x^3-xy-2xy^2+4y^2) + y \left(4 - \frac{3}{2}y \right), \\
G(x, y) &= \frac{1}{12y} \left[2(-1+x)^3 - 9(-1+x^2)y + 6(-1+x)y^2 - 6(1+x-y)y\sqrt{-\beta(x, y)} \times \right. \\
&\quad \left. \left\{ \tan^{-1} \left(\frac{1-x+y}{\sqrt{-\beta(x, y)}} \right) + \tan^{-1} \left(\frac{1-x-y}{\sqrt{-\beta(x, y)}} \right) \right\} - 3(1+(x-y)^2-2y)y \log x \right], \\
H(x, y) &= \frac{1}{4x\sqrt{-\beta(x, y)}} \left\{ \tan^{-1} \left(\frac{1-x+y}{\sqrt{-\beta(x, y)}} \right) + \tan^{-1} \left(\frac{1-x-y}{\sqrt{-\beta(x, y)}} \right) \right\} \left\{ -3x^3 + (9y+7)x^2 \right. \\
&\quad \left. - 5(1-y)^2x + (1-y)^3 \right\} + \frac{1}{24xy} \left\{ (-1+x)(2+2x^2+6y^2-4x-9y+39xy) \right. \\
&\quad \left. - 3y(1-3x^2+y^2-4x-2y+6xy) \log x \right\},
\end{aligned}$$

C Stability and charge-breaking minima

The scalar potential in Eq. (2.8), in principle, can have several stationary points—both electric charge-conserving and charge-breaking. In this section, we discuss all possible stationary points and obtain the necessary conditions for the desired EW vacuum to be the global minimum of the model by calculating the differences in the potential depths between the desired EW vacuum and others, some of which might not be phenomenologically viable. It might be argued that absolute stability of the vacuum is not a necessary requirement since the vacuum could be meta-stable, i.e. have, a lifetime longer than the age of the Universe. While the latter is certainly an interesting possibility, it would require a detailed calculation of the tunnelling time of the vacuum into the global minimum, which is beyond the scope of this work. Therefore, we restrict to the stronger requirement that the vacuum is at the global minimum.

Concerning the gauge choice, note that we can always absorb three real scalar component fields via a suitable gauge choice (such as a rotation in field space). For definiteness, we choose the SM unitary gauge, wherein the doublet is reduced to a neutral, real component. As a consequence, the doublet VEV is, without loss of generality, always real and neutral. Further, the triplet being real (see Eq. (2.2) and the text thereafter), the corresponding VEVs are also real.

The Δ SM can have several stationary points as listed in Table 2. Of these, three are charge-conserving minima: N_1 , N_2 and N_3 , referred to as *normal minima*, wherein the neutral components of the scalar fields get VEVs. On the contrary, there are two possible charge-breaking (CB) minima. Such a scenario exists when electric charge-carrying VEVs appear after spontaneous symmetry breaking. The occurrence of CB vacuum results in a non-zero photon mass, which is incompatible with electromagnetic observations.

N1	$\langle\Phi^0\rangle = \frac{1}{\sqrt{2}}v_\Phi$	$\langle\Delta^0\rangle = v_\Delta$	$\langle\Delta^\pm\rangle = 0$
N2	$\langle\Phi^0\rangle = \frac{1}{\sqrt{2}}v_\Phi$	$\langle\Delta^0\rangle = 0$	$\langle\Delta^\pm\rangle = 0$
N3	$\langle\Phi^0\rangle = 0$	$\langle\Delta^0\rangle = v_\Delta$	$\langle\Delta^\pm\rangle = 0$
CB1	$\langle\Phi^0\rangle = \frac{1}{\sqrt{2}}v$	$\langle\Delta^0\rangle = v_0$	$\langle\Delta^\pm\rangle = v_1$
CB2	$\langle\Phi^0\rangle = \frac{1}{\sqrt{2}}v$	$\langle\Delta^0\rangle = 0$	$\langle\Delta^\pm\rangle = v_1$

Table 2. Possible stationary points in the Δ SM model.

N1 stationary point

The *N1* stationary point corresponds to the vacuum structure where both Φ^0 and Δ^0 get VEVs:

$$\langle \Phi \rangle_{N1} = \frac{1}{\sqrt{2}} \begin{pmatrix} 0 \\ v_\Phi \end{pmatrix}, \quad \langle \Delta \rangle_{N1} = \frac{1}{2} \begin{pmatrix} v_\Delta & 0 \\ 0 & -v_\Delta \end{pmatrix}, \quad (\text{C.1})$$

This vacuum structure has been detailed in Section 2.

N2 stationary point

The *N2* stationary point corresponds to the vacuum structure where only Φ^0 gets VEV:

$$\langle \Phi \rangle_{N2} = \frac{1}{\sqrt{2}} \begin{pmatrix} 0 \\ v_\Phi \end{pmatrix}, \quad \langle \Delta \rangle_{N2} = \frac{1}{2} \begin{pmatrix} 0 & 0 \\ 0 & 0 \end{pmatrix}, \quad (\text{C.2})$$

The minimization condition for this vacuum configuration is

$$\mu_\Phi^2 = \frac{1}{4} v_\Phi^2 \lambda_\Phi. \quad (\text{C.3})$$

To get the correct electroweak symmetry breaking for this vacuum configuration, we need $v_\Phi = 246$ GeV. Also, to get *N2* extremum, we require $A = 0$, thereby restoring the global $O(4)_H \times O(3)_\Delta$ symmetry of the potential in Eq. (2.8). The consequence is the degenerate mass spectrum for the triplet scalars: $m_{\Delta^0} = m_{\Delta^\pm}$. The scalar masses are given by,

$$m_h^2 = \frac{\lambda_\Phi v_\Phi^2}{2}, \quad (\text{C.4})$$

$$m_{\Delta^0}^2 = m_{\Delta^\pm}^2 = \frac{\lambda_{\Phi\Delta} v_\Phi^2}{2} - \mu_\Delta^2. \quad (\text{C.5})$$

N3 stationary point

The *N3* stationary point corresponds to the vacuum structure where only Δ^0 gets VEV:

$$\langle \Phi \rangle_{N3} = \frac{1}{\sqrt{2}} \begin{pmatrix} 0 \\ 0 \end{pmatrix}, \quad \langle \Delta \rangle_{N3} = \frac{1}{2} \begin{pmatrix} v_\Delta & 0 \\ 0 & -v_\Delta \end{pmatrix}, \quad (\text{C.6})$$

As the absence of a doublet VEV would imply massless fermions, this extremum is in disagreement with observations. Therefore, we do not discuss this further.

CB1 stationary point

In the CB1 case, both the neutral and charged components of the triplet scalar, Δ^0 and Δ^\pm get VEVs:

$$\langle \Phi \rangle = \frac{1}{\sqrt{2}} \begin{pmatrix} 0 \\ v \end{pmatrix}, \quad \langle \Delta \rangle = \frac{1}{2} \begin{pmatrix} v_0 & v_1 \\ v_1 & -v_0 \end{pmatrix}. \quad (\text{C.7})$$

This configuration is the most generic CB vacuum. The minimization condition for this vacuum configuration is

$$\mu_{\Phi}^2 = \frac{v^2}{4} \lambda_{\Phi} + \left(\frac{v_0^2}{2} + v_1^2 \right) \lambda_{\Phi\Delta} \quad (\text{C.8})$$

$$\mu_{\Delta}^2 = \left(\frac{v_0^2}{4} + \frac{v_1^2}{2} \right) \lambda_{\Delta} + \frac{v^2}{2} \lambda_{\Phi\Delta} \quad (\text{C.9})$$

$$A = 0 \quad (\text{C.10})$$

CB2 stationary point

In the CB2 case, only the charged component of the triplet scalar, Δ^{\pm} gets VEV:

$$\langle \Phi \rangle = \frac{1}{\sqrt{2}} \begin{pmatrix} 0 \\ v \end{pmatrix}, \quad \langle \Delta \rangle = \frac{1}{2} \begin{pmatrix} 0 & v_1 \\ v_1 & 0 \end{pmatrix} \quad (\text{C.11})$$

The minimization condition for this vacuum configuration is

$$\mu_{\Phi}^2 = \frac{v^2}{4} \lambda_{\Phi} + v_1^2 \lambda_{\Phi\Delta} \quad (\text{C.12})$$

$$\mu_{\Delta}^2 = \frac{v_1^2}{2} \lambda_{\Delta} + \frac{v^2}{2} \lambda_{\Phi\Delta} \quad (\text{C.13})$$

Condition for global minima

In this section, we will examine the stability of the *normal minima*, in particular, the *N1* stationary point, which we assume to be the desired global minimum of the model. To this end, assuming that *N1* or *N2* coexists with the *CB* minima in some region of the model parameter space, we calculate the differences in potential depth between the co-existing minima. For *N1* to be the global minimum, it is crucial that the potential depth at *N1* is lower than those of the co-existing minima.

To calculate the difference in potential depth between two co-existing minima, we follow the bilinear formalism detailed in Refs. [171, 172], see Refs. [173–175] for recent works. Note that the potential V in Eq. (2.8) is the sum of three homogeneous functions of order 2, 3 and 4 in the fields Φ and Δ :

$$V = V_2 + V_3 + V_4. \quad (\text{C.14})$$

Consequently, up to V_3 , V can be expressed as a quadratic polynomial on the vector X constructed from the bilinears $x_1 = |\Phi|^2$, $x_2 = |\Delta^0|^2/2$ and $x_3 = |\Delta^{\pm}|^2/2$. Therefore, we have

$$V = \underbrace{M^T X}_{V_2} + \underbrace{A \Phi^\dagger \Delta \Phi}_{V_3} + \underbrace{\frac{1}{2} X^T \Lambda X}_{V_4}, \quad (\text{C.15})$$

where

$$X = \begin{pmatrix} x_1 \\ x_2 \\ x_3 \end{pmatrix}, \quad M = \begin{pmatrix} -\mu_\Phi^2 \\ -\mu_\Delta^2 \\ -2\mu_\Delta^2 \end{pmatrix}, \quad \Lambda = \begin{pmatrix} \frac{\lambda_\Phi}{2} & \lambda_{\Phi\Delta} & 2\lambda_{\Phi\Delta} \\ \lambda_{\Phi\Delta} & \frac{\lambda_\Delta}{2} & \lambda_\Delta \\ 2\lambda_{\Phi\Delta} & \lambda_\Delta & 2\lambda_\Delta \end{pmatrix} \quad (\text{C.16})$$

At any stationary point SP , the potential V must follow the minimisation conditions, *i.e.* $\frac{\partial V}{\partial \phi_i} = 0$ with ϕ_i denoting real scalar degree of freedoms of the model. Thus, we have

$$\sum_i \phi_i \frac{\partial V}{\partial \phi_i} \Big|_{SP} = 0 \quad \Rightarrow \quad 2(V_2)_{SP} + 3(V_3)_{SP} + 4(V_4)_{SP} = 0, \quad (\text{C.17})$$

where the latter follows from Euler's homogeneous function theorem. Therefore, the value of V evaluated at SP is

$$V_{SP} = \frac{1}{2}(V_2)_{SP} + \frac{1}{4}(V_4)_{SP}. \quad (\text{C.18})$$

Now, we define the gradient of $V_2 + V_4$ along X : $V' = M + \Lambda X$ and compute the product of V' evaluated at a stationary point with X evaluated at a different stationary point:

$$X_{SP1}^T V'_{SP2} = 2V_{SP1} - \frac{1}{2}(V_3)_{SP1} + X_{SP1}^T \Lambda X_{SP2}, \quad (\text{C.19})$$

$$X_{SP2}^T V'_{SP1} = 2V_{SP2} - \frac{1}{2}(V_3)_{SP2} + X_{SP2}^T \Lambda X_{SP1} \quad (\text{C.20})$$

Finally, subtracting these two equations, we get

$$V_{SP2} - V_{SP1} = \frac{1}{2} (X_{SP2}^T V'_{SP1} - X_{SP1}^T V'_{SP2}) + \frac{1}{4} ((V_3)_{SP2} - (V_3)_{SP1}). \quad (\text{C.21})$$

In what follows, we present the bilinear vector X for all possible stationary points and the differences in potential depth between the co-existing minima using Eq. (C.21).

$$X_{N1} = \frac{1}{2} \begin{pmatrix} v_\Phi^2 \\ v_\Delta^2 \\ 0 \end{pmatrix}, \quad X_{N2} = \frac{1}{2} \begin{pmatrix} v_\Phi^2 \\ 0 \\ 0 \end{pmatrix}, \quad X_{CB1} = \frac{1}{2} \begin{pmatrix} v^2 \\ v_1^2 \\ v_2^2 \end{pmatrix}, \quad X_{CB2} = \frac{1}{2} \begin{pmatrix} v^2 \\ 0 \\ v_2^2 \end{pmatrix}, \quad (\text{C.22})$$

$$V_{CB1} - V_{N1} = \frac{(v_\Delta^2 + 2v_1^2 + 4v_2^2)v_\Phi^2 + 4v_\Delta^2 v^2}{8(4v_\Delta^2 + v_\Phi^2)} m_{\Delta^\pm}^2, \quad (\text{C.23})$$

$$V_{CB2} - V_{N1} = \frac{4v_2^2 v_\Phi^2 + v_\Delta^2 (v_\Phi^2 + 4v^2)}{8(4v_\Delta^2 + v_\Phi^2)} m_{\Delta^\pm}^2, \quad (\text{C.24})$$

$$V_{N2} - V_{N1} = \frac{v_\Delta^2}{2} m_h^2, \quad (\text{C.25})$$

$$V_{CB1} - V_{N2} = \frac{v_1^2 + v_2^2}{4} m_{\Delta^0}^2, \quad (\text{C.26})$$

$$V_{CB2} - V_{N2} = \frac{v_2^2}{2} m_{\Delta^0}^2, \quad (\text{C.27})$$

where m_h , m_{Δ^0} and m_{Δ^\pm} in Eq. (C.23), Eq. (C.24) and Eq. (C.25) are the physical masses evaluated at the N_1 stationary point, whereas those in Eq. (C.26) and (C.27) are evaluated at the N_2 stationary point. Therefore, as it turns out, the desired EW vacuum N_1 is indeed the global minimum of the model for $v_\Delta > 0$ as long as the scalars are not tachyonic, *i.e.* $m_h^2 > 0$, $m_{\Delta^0}^2 > 0$ and $m_{\Delta^\pm}^2 > 0$. While for $v_\Delta = 0$, the normal minimum N_2 is the global minimum.

Acknowledgments

S.A. acknowledges partial support from the National Natural Science Foundation of China under grant No. 11835013. The work of A.C. is supported by a professorship grant from the Swiss National Science Foundation (No. PP00P21_76884). S.P.M. acknowledges using the SAMKHYA: High-Performance Computing Facility provided by the Institute of Physics, Bhubaneswar.

References

- [1] **Particle Data Group** Collaboration, R. L. Workman *et al.*, “Review of Particle Physics,” *PTEP* **2022** (2022) 083C01.
- [2] **HFLAV** Collaboration, Y. S. Amhis *et al.*, “Averages of b -hadron, c -hadron, and τ -lepton properties as of 2018,” *Eur. Phys. J. C* **81** no. 3, (2021) 226, [arXiv:1909.12524 \[hep-ex\]](#).
- [3] **ALEPH, DELPHI, L3, OPAL, SLD, LEP Electroweak Working Group, SLD Electroweak Group, SLD Heavy Flavour Group** Collaboration, S. Schael *et al.*, “Precision electroweak measurements on the Z resonance,” *Phys. Rept.* **427** (2006) 257–454, [arXiv:hep-ex/0509008](#).
- [4] P. W. Higgs, “Broken symmetries, massless particles and gauge fields,” *Phys. Lett.* **12** (1964) 132–133.
- [5] F. Englert and R. Brout, “Broken Symmetry and the Mass of Gauge Vector Mesons,” *Phys. Rev. Lett.* **13** (1964) 321–323.
- [6] P. W. Higgs, “Broken Symmetries and the Masses of Gauge Bosons,” *Phys. Rev. Lett.* **13** (1964) 508–509.
- [7] G. S. Guralnik, C. R. Hagen, and T. W. B. Kibble, “Global Conservation Laws and Massless Particles,” *Phys. Rev. Lett.* **13** (1964) 585–587.

- [8] **ATLAS** Collaboration, G. Aad et al., “Observation of a new particle in the search for the Standard Model Higgs boson with the ATLAS detector at the LHC,” *Phys. Lett. B* **716** (2012) 1–29, [arXiv:1207.7214 \[hep-ex\]](#).
- [9] **CMS** Collaboration, S. Chatrchyan et al., “Observation of a New Boson at a Mass of 125 GeV with the CMS Experiment at the LHC,” *Phys. Lett. B* **716** (2012) 30–61, [arXiv:1207.7235 \[hep-ex\]](#).
- [10] A. Crivellin and B. Mellado, “Anomalies in particle physics and their implications for physics beyond the standard model,” *Nature Rev. Phys.* **6** no. 5, (2024) 294–309, [arXiv:2309.03870 \[hep-ph\]](#).
- [11] **CMS** Collaboration, S. Chatrchyan et al., “Study of the Mass and Spin-Parity of the Higgs Boson Candidate Via Its Decays to Z Boson Pairs,” *Phys. Rev. Lett.* **110** no. 8, (2013) 081803, [arXiv:1212.6639 \[hep-ex\]](#).
- [12] **ATLAS** Collaboration, G. Aad et al., “Evidence for the spin-0 nature of the Higgs boson using ATLAS data,” *Phys. Lett. B* **726** (2013) 120–144, [arXiv:1307.1432 \[hep-ex\]](#).
- [13] **ATLAS, CMS** Collaboration, G. Aad et al., “Measurements of the Higgs boson production and decay rates and constraints on its couplings from a combined ATLAS and CMS analysis of the LHC pp collision data at $\sqrt{s} = 7$ and 8 TeV,” *JHEP* **08** (2016) 045, [arXiv:1606.02266 \[hep-ex\]](#).
- [14] **ATLAS, CMS** Collaboration, J. M. Langford, “Combination of Higgs measurements from ATLAS and CMS : couplings and κ -framework,” *PoS LHCP2020* (2021) 136.
- [15] **ATLAS** Collaboration, “Combined measurements of Higgs boson production and decay using up to 139 fb^{-1} of proton-proton collision data at $\sqrt{s} = 13$ TeV collected with the ATLAS experiment,”.
- [16] V. Silveira and A. Zee, “SCALAR PHANTOMS,” *Phys. Lett. B* **161** (1985) 136–140.
- [17] M. Pietroni, “The Electroweak phase transition in a nonminimal supersymmetric model,” *Nucl. Phys. B* **402** (1993) 27–45, [arXiv:hep-ph/9207227](#).
- [18] J. McDonald, “Gauge singlet scalars as cold dark matter,” *Phys. Rev. D* **50** (1994) 3637–3649, [arXiv:hep-ph/0702143](#).
- [19] T. D. Lee, “A Theory of Spontaneous T Violation,” *Phys. Rev. D* **8** (1973) 1226–1239.
- [20] H. E. Haber and G. L. Kane, “The Search for Supersymmetry: Probing Physics Beyond the Standard Model,” *Phys. Rept.* **117** (1985) 75–263.
- [21] J. E. Kim, “Light Pseudoscalars, Particle Physics and Cosmology,” *Phys. Rept.* **150** (1987) 1–177.
- [22] R. D. Peccei and H. R. Quinn, “ CP Conservation in the Presence of Instantons,” *Phys. Rev. Lett.* **38** (1977) 1440–1443.

- [23] N. Turok and J. Zadrozny, “Electroweak baryogenesis in the two doublet model,” *Nucl. Phys. B* **358** (1991) 471–493.
- [24] W. Konetschny and W. Kummer, “Nonconservation of Total Lepton Number with Scalar Bosons,” *Phys. Lett. B* **70** (1977) 433–435.
- [25] T. P. Cheng and L.-F. Li, “Neutrino Masses, Mixings and Oscillations in $SU(2) \times U(1)$ Models of Electroweak Interactions,” *Phys. Rev. D* **22** (1980) 2860.
- [26] G. Lazarides, Q. Shafi, and C. Wetterich, “Proton Lifetime and Fermion Masses in an $SO(10)$ Model,” *Nucl. Phys. B* **181** (1981) 287–300.
- [27] J. Schechter and J. W. F. Valle, “Neutrino Masses in $SU(2) \times U(1)$ Theories,” *Phys. Rev. D* **22** (1980) 2227.
- [28] M. Magg and C. Wetterich, “Neutrino Mass Problem and Gauge Hierarchy,” *Phys. Lett. B* **94** (1980) 61–64.
- [29] R. N. Mohapatra and G. Senjanovic, “Neutrino Masses and Mixings in Gauge Models with Spontaneous Parity Violation,” *Phys. Rev. D* **23** (1981) 165.
- [30] CDF Collaboration, T. Aaltonen et al., “High-precision measurement of the W boson mass with the CDF II detector,” *Science* **376** no. 6589, (2022) 170–176.
- [31] J. Butterworth, J. Heeck, S. H. Jeon, O. Mattelaer, and R. Ruiz, “Testing the scalar triplet solution to CDF’s heavy W problem at the LHC,” *Phys. Rev. D* **107** no. 7, (2023) 075020, [arXiv:2210.13496 \[hep-ph\]](#).
- [32] J. Heeck, “ W -boson mass in the triplet seesaw model,” *Phys. Rev. D* **106** no. 1, (2022) 015004, [arXiv:2204.10274 \[hep-ph\]](#).
- [33] A. Strumia, “Interpreting electroweak precision data including the W -mass CDF anomaly,” *JHEP* **08** (2022) 248, [arXiv:2204.04191 \[hep-ph\]](#).
- [34] I. Dorsner and I. Mocioiu, “Predictions from type II see-saw mechanism in $SU(5)$,” *Nucl. Phys. B* **796** (2008) 123–136, [arXiv:0708.3332 \[hep-ph\]](#).
- [35] P. Fileviez Perez, H. H. Patel, and A. D. Plascencia, “On the W mass and new Higgs bosons,” *Phys. Lett. B* **833** (2022) 137371, [arXiv:2204.07144 \[hep-ph\]](#).
- [36] Y. Cheng, X.-G. He, F. Huang, J. Sun, and Z.-P. Xing, “Electroweak precision tests for triplet scalars,” *Nucl. Phys. B* **989** (2023) 116118, [arXiv:2208.06760 \[hep-ph\]](#).
- [37] T. G. Rizzo, “Kinetic mixing, dark Higgs triplets, and M_W ,” *Phys. Rev. D* **106** no. 3, (2022) 035024, [arXiv:2206.09814 \[hep-ph\]](#).
- [38] J.-W. Wang, X.-J. Bi, P.-F. Yin, and Z.-H. Yu, “Electroweak dark matter model accounting for the CDF W -mass anomaly,” *Phys. Rev. D* **106** no. 5, (2022) 055001, [arXiv:2205.00783 \[hep-ph\]](#).
- [39] M. Chabab, M. C. Peyranère, and L. Rahili, “Probing the Higgs sector of $Y = 0$ Higgs Triplet Model at LHC,” *Eur. Phys. J. C* **78** no. 10, (2018) 873, [arXiv:1805.00286 \[hep-ph\]](#).

- [40] Y. Shimizu and S. Takeshita, “ W boson mass and grand unification via the type-II seesaw-like mechanism,” *Nucl. Phys. B* **994** (2023) 116290, [arXiv:2303.11070 \[hep-ph\]](#).
- [41] A. Crivellin, M. Kirk, and A. Thapa, “Minimal model for the W -boson mass, $(g - 2)_\mu$, $h \rightarrow \mu^+ \mu^-$ and quark-mixing-matrix unitarity,” *Phys. Rev. D* **108** no. 3, (2023) L031702, [arXiv:2305.03081 \[hep-ph\]](#).
- [42] T. A. Chowdhury, J. Heeck, A. Thapa, and S. Saad, “ W boson mass shift and muon magnetic moment in the Zee model,” *Phys. Rev. D* **106** no. 3, (2022) 035004, [arXiv:2204.08390 \[hep-ph\]](#).
- [43] R. Decruz and A. Thapa, “ W boson mass shift, dark matter, and $(g - 2)_\ell$ in a scotogenic-Zee model,” *Phys. Rev. D* **107** no. 1, (2023) 015002, [arXiv:2205.02217 \[hep-ph\]](#).
- [44] K. S. Babu, S. Jana, and V. P. K., “Correlating W -Boson Mass Shift with Muon $(g - 2)$ in the Two Higgs Doublet Model,” *Phys. Rev. Lett.* **129** no. 12, (2022) 121803, [arXiv:2204.05303 \[hep-ph\]](#).
- [45] G. Arcadi and A. Djouadi, “2HD+a light pseudoscalar model for a combined explanation of the possible excesses in the CDF M_W measurement and $(g - 2)_\mu$ with dark matter,” *Phys. Rev. D* **106** no. 9, (2022) 095008, [arXiv:2204.08406 \[hep-ph\]](#).
- [46] J. Kim, S. Lee, P. Sanyal, and J. Song, “CDF W -boson mass and muon $(g - 2)$ in a type-X two-Higgs-doublet model with a Higgs-phobic light pseudoscalar,” *Phys. Rev. D* **106** no. 3, (2022) 035002, [arXiv:2205.01701 \[hep-ph\]](#).
- [47] J. Kim, “Compatibility of muon $g - 2$, W mass anomaly in type-X 2HDM,” *Phys. Lett. B* **832** (2022) 137220, [arXiv:2205.01437 \[hep-ph\]](#).
- [48] N. Chakrabarty, “Muon $g - 2$ and W -mass anomalies explained and the electroweak vacuum stabilized by extending the minimal type-II seesaw model,” *Phys. Rev. D* **108** no. 7, (2023) 075024, [arXiv:2206.11771 \[hep-ph\]](#).
- [49] T. A. Chowdhury, K. Ezzat, S. Khalil, E. Ma, and D. Nanda, “Higgs quadruplet impact on W mass shift, dark matter, and LHC signatures,” *Phys. Rev. D* **109** no. 7, (2024) 075039, [arXiv:2312.11833 \[hep-ph\]](#).
- [50] T.-K. Chen, C.-W. Chiang, and K. Yagyu, “Explanation of the W mass shift at CDF II in the extended Georgi-Machacek model,” *Phys. Rev. D* **106** no. 5, (2022) 055035, [arXiv:2204.12898 \[hep-ph\]](#).
- [51] S. Kanemura and K. Yagyu, “Implication of the W boson mass anomaly at CDF II in the Higgs triplet model with a mass difference,” *Phys. Lett. B* **831** (2022) 137217, [arXiv:2204.07511 \[hep-ph\]](#).
- [52] S. Ashanujjaman, K. Ghosh, and R. Sahu, “Low-mass doubly charged Higgs bosons at the LHC,” *Phys. Rev. D* **107** no. 1, (2023) 015018, [arXiv:2211.00632 \[hep-ph\]](#).

- [53] D. A. Ross and M. J. G. Veltman, “Neutral Currents in Neutrino Experiments,” *Nucl. Phys. B* **95** (1975) 135–147.
- [54] J. F. Gunion, R. Vega, and J. Wudka, “Higgs triplets in the standard model,” *Phys. Rev. D* **42** (1990) 1673–1691.
- [55] T. Blank and W. Hollik, “Precision observables in $SU(2) \times U(1)$ models with an additional Higgs triplet,” *Nucl. Phys. B* **514** (1998) 113–134, [arXiv:hep-ph/9703392](#).
- [56] J. R. Forshaw, A. Sabio Vera, and B. E. White, “Mass bounds in a model with a triplet Higgs,” *JHEP* **06** (2003) 059, [arXiv:hep-ph/0302256](#).
- [57] P. H. Chankowski, S. Pokorski, and J. Wagner, “(Non)decoupling of the Higgs triplet effects,” *Eur. Phys. J. C* **50** (2007) 919–933, [arXiv:hep-ph/0605302](#).
- [58] M.-C. Chen, S. Dawson, and T. Krupovnickas, “Higgs triplets and limits from precision measurements,” *Phys. Rev. D* **74** (2006) 035001, [arXiv:hep-ph/0604102](#).
- [59] R. S. Chivukula, N. D. Christensen, and E. H. Simmons, “Low-energy effective theory, unitarity, and non-decoupling behavior in a model with heavy Higgs-triplet fields,” *Phys. Rev. D* **77** (2008) 035001, [arXiv:0712.0546 \[hep-ph\]](#).
- [60] P. Bandyopadhyay and A. Costantini, “Obscure Higgs boson at Colliders,” *Phys. Rev. D* **103** no. 1, (2021) 015025, [arXiv:2010.02597 \[hep-ph\]](#).
- [61] G. Lazarides, R. Maji, R. Roshan, and Q. Shafi, “Heavier W boson, dark matter, and gravitational waves from strings in an $SO(10)$ axion model,” *Phys. Rev. D* **106** no. 5, (2022) 055009, [arXiv:2205.04824 \[hep-ph\]](#).
- [62] J. Butterworth, H. Debnath, P. Fileviez Perez, and F. Mitchell, “Custodial symmetry breaking and Higgs boson signatures at the LHC,” *Phys. Rev. D* **109** no. 9, (2024) 095014, [arXiv:2309.10027 \[hep-ph\]](#).
- [63] G. Senjanović and M. Zantedeschi, “ $SU(5)$ grand unification and W -boson mass,” *Phys. Lett. B* **837** (2023) 137653, [arXiv:2205.05022 \[hep-ph\]](#).
- [64] A. Crivellin, M. Kirk, and A. Thapa, “Minimal model for the W -boson mass, $(g-2)_\mu$, $h \rightarrow \mu^+ \mu^-$ and quark-mixing-matrix unitarity,” *Phys. Rev. D* **108** no. 3, (2023) L031702, [arXiv:2305.03081 \[hep-ph\]](#).
- [65] T.-K. Chen, C.-W. Chiang, and K. Yagyu, “ CP violation in a model with Higgs triplets,” *JHEP* **06** (2023) 069, [arXiv:2303.09294 \[hep-ph\]](#). [Erratum: *JHEP* 07, 169 (2023)].
- [66] S. Ashanujjaman, S. Banik, G. Coloretti, A. Crivellin, B. Mellado, and A.-T. Mulaudzi, “ $SU(2)_L$ triplet scalar as the origin of the 95 GeV excess?,” *Phys. Rev. D* **108** no. 9, (2023) L091704, [arXiv:2306.15722 \[hep-ph\]](#).
- [67] G. Degrandi and P. Slavich, “On the two-loop BSM corrections to $h \rightarrow \gamma\gamma$ in a triplet extension of the SM,” [arXiv:2407.18185 \[hep-ph\]](#).
- [68] S. von Buddenbrock, N. Chakrabarty, A. S. Cornell, D. Kar, M. Kumar, T. Mandal,

- B. Mellado, B. Mukhopadhyaya, R. G. Reed, and X. Ruan, “Phenomenological signatures of additional scalar bosons at the LHC,” *Eur. Phys. J. C* **76** no. 10, (2016) 580, [arXiv:1606.01674 \[hep-ph\]](#).
- [69] S. von Buddenbrock, A. S. Cornell, A. Fadol, M. Kumar, B. Mellado, and X. Ruan, “Multi-lepton signatures of additional scalar bosons beyond the Standard Model at the LHC,” *J. Phys. G* **45** no. 11, (2018) 115003, [arXiv:1711.07874 \[hep-ph\]](#).
- [70] S. Buddenbrock, A. S. Cornell, Y. Fang, A. Fadol Mohammed, M. Kumar, B. Mellado, and K. G. Tomiwa, “The emergence of multi-lepton anomalies at the LHC and their compatibility with new physics at the EW scale,” *JHEP* **10** (2019) 157, [arXiv:1901.05300 \[hep-ph\]](#).
- [71] S. von Buddenbrock, R. Ruiz, and B. Mellado, “Anatomy of inclusive $t\bar{t}W$ production at hadron colliders,” *Phys. Lett. B* **811** (2020) 135964, [arXiv:2009.00032 \[hep-ph\]](#).
- [72] Y. Hernandez, M. Kumar, A. S. Cornell, S.-E. Dahbi, Y. Fang, B. Lieberman, B. Mellado, K. Monnagotla, X. Ruan, and S. Xin, “The anomalous production of multi-lepton and its impact on the measurement of Wh production at the LHC,” *Eur. Phys. J. C* **81** no. 4, (2021) 365, [arXiv:1912.00699 \[hep-ph\]](#).
- [73] G. Coloretti, A. Crivellin, S. Bhattacharya, and B. Mellado, “Searching for low-mass resonances decaying into W bosons,” *Phys. Rev. D* **108** no. 3, (2023) 035026, [arXiv:2302.07276 \[hep-ph\]](#).
- [74] S. Banik, G. Coloretti, A. Crivellin, and B. Mellado, “Uncovering New Higgses in the LHC Analyses of Differential $t\bar{t}$ Cross Sections,” [arXiv:2308.07953 \[hep-ph\]](#).
- [75] G. Coloretti, A. Crivellin, and B. Mellado, “Combined explanation of LHC multilepton, diphoton, and top-quark excesses,” *Phys. Rev. D* **110** no. 7, (2024) 073001, [arXiv:2312.17314 \[hep-ph\]](#).
- [76] O. Fischer et al., “Unveiling hidden physics at the LHC,” *Eur. Phys. J. C* **82** no. 8, (2022) 665, [arXiv:2109.06065 \[hep-ph\]](#).
- [77] A. Crivellin, Y. Fang, O. Fischer, S. Bhattacharya, M. Kumar, E. Malwa, B. Mellado, N. Rapheeha, X. Ruan, and Q. Sha, “Accumulating evidence for the associated production of a new Higgs boson at the LHC,” *Phys. Rev. D* **108** no. 11, (2023) 115031, [arXiv:2109.02650 \[hep-ph\]](#).
- [78] S. Bhattacharya, G. Coloretti, A. Crivellin, S.-E. Dahbi, Y. Fang, M. Kumar, and B. Mellado, “Growing Excesses of New Scalars at the Electroweak Scale,” [arXiv:2306.17209 \[hep-ph\]](#).
- [79] CMS Collaboration, A. M. Sirunyan et al., “Measurements of Higgs boson production cross sections and couplings in the diphoton decay channel at $\sqrt{s} = 13$ TeV,” *JHEP* **07** (2021) 027, [arXiv:2103.06956 \[hep-ex\]](#).
- [80] ATLAS Collaboration, “Measurement of the properties of Higgs boson production

at $\sqrt{s} = 13$ TeV in the $H \rightarrow \gamma\gamma$ channel using 139 fb^{-1} of pp collision data with the ATLAS experiment.”.

- [81] **ATLAS** Collaboration, G. Aad *et al.*, “ CP Properties of Higgs Boson Interactions with Top Quarks in the $t\bar{t}H$ and tH Processes Using $H \rightarrow \gamma\gamma$ with the ATLAS Detector,” *Phys. Rev. Lett.* **125** no. 6, (2020) 061802, [arXiv:2004.04545 \[hep-ex\]](#).
- [82] **CMS** Collaboration, A. M. Sirunyan *et al.*, “Measurements of $t\bar{t}H$ Production and the CP Structure of the Yukawa Interaction between the Higgs Boson and Top Quark in the Diphoton Decay Channel,” *Phys. Rev. Lett.* **125** no. 6, (2020) 061801, [arXiv:2003.10866 \[hep-ex\]](#).
- [83] **ATLAS** Collaboration, G. Aad *et al.*, “Search for dark matter in events with missing transverse momentum and a Higgs boson decaying into two photons in pp collisions at $\sqrt{s} = 13$ TeV with the ATLAS detector,” *JHEP* **10** (2021) 013, [arXiv:2104.13240 \[hep-ex\]](#).
- [84] **CMS** Collaboration, A. M. Sirunyan *et al.*, “Search for dark matter produced in association with a Higgs boson decaying to $\gamma\gamma$ or $\tau^+\tau^-$ at $\sqrt{s} = 13$ TeV,” *JHEP* **09** (2018) 046, [arXiv:1806.04771 \[hep-ex\]](#).
- [85] **CMS** Collaboration, A. M. Sirunyan *et al.*, “Search for the decay of a Higgs boson in the $\ell\ell\gamma$ channel in proton-proton collisions at $\sqrt{s} = 13$ TeV,” *JHEP* **11** (2018) 152, [arXiv:1806.05996 \[hep-ex\]](#).
- [86] **ATLAS** Collaboration, G. Aad *et al.*, “Measurements of WH and ZH production in the $H \rightarrow b\bar{b}$ decay channel in pp collisions at 13 TeV with the ATLAS detector,” *Eur. Phys. J. C* **81** no. 2, (2021) 178, [arXiv:2007.02873 \[hep-ex\]](#).
- [87] S. Ashanujjaman, S. Banik, G. Coloretti, A. Crivellin, S. P. Maharathy, and B. Mellado, “Explaining the $\gamma\gamma + X$ Excesses at ≈ 151.5 GeV via the Drell-Yan Production of a Higgs Triplet,” [arXiv:2402.00101 \[hep-ph\]](#).
- [88] A. Crivellin, S. Ashanujjaman, S. Banik, G. Coloretti, S. P. Maharathy, and B. Mellado, “Growing Evidence for a Higgs Triplet,” [arXiv:2404.14492 \[hep-ph\]](#).
- [89] S. Banik and A. Crivellin, “Explanation of the excesses in associated di-photon production at 152 GeV in 2HDM,” *JHEP* **10** (2024) 203, [arXiv:2407.06267 \[hep-ph\]](#).
- [90] **ATLAS** Collaboration, G. Aad *et al.*, “Model-independent search for the presence of new physics in events including $H \rightarrow \gamma\gamma$ with $\sqrt{s} = 13$ TeV pp data recorded by the ATLAS detector at the LHC,” *JHEP* **07** (2023) 176, [arXiv:2301.10486 \[hep-ex\]](#).
- [91] **ATLAS** Collaboration, G. Aad *et al.*, “Search for non-resonant Higgs boson pair production in final states with leptons, taus, and photons in pp collisions at $\sqrt{s} = 13$ TeV with the ATLAS detector,” *JHEP* **08** (2024) 164, [arXiv:2405.20040 \[hep-ex\]](#).

- [92] **CMS** Collaboration, A. M. Sirunyan *et al.*, “Search for a standard model-like Higgs boson in the mass range between 70 and 110 GeV in the diphoton final state in proton-proton collisions at $\sqrt{s} = 8$ and 13 TeV,” *Phys. Lett. B* **793** (2019) 320–347, [arXiv:1811.08459 \[hep-ex\]](#).
- [93] **CMS** Collaboration, “Search for a standard model-like Higgs boson in the mass range between 70 and 110 GeV in the diphoton final state in proton-proton collisions at $\sqrt{s} = 13$ TeV,”.
- [94] **CMS** Collaboration, A. Tumasyan *et al.*, “Searches for additional Higgs bosons and for vector leptoquarks in $\tau\tau$ final states in proton-proton collisions at $\sqrt{s} = 13$ TeV,” *JHEP* **07** (2023) 073, [arXiv:2208.02717 \[hep-ex\]](#).
- [95] **ATLAS** Collaboration, “Search for resonances in the 65 to 110 GeV diphoton invariant mass range using 80 fb⁻¹ of pp collisions collected at $\sqrt{s} = 13$ TeV with the ATLAS detector,”.
- [96] **ATLAS** Collaboration, G. Aad *et al.*, “Measurements of Higgs boson production cross-sections in the $H \rightarrow \tau^+\tau^-$ decay channel in pp collisions at $\sqrt{s} = 13$ TeV with the ATLAS detector,” *JHEP* **08** (2022) 175, [arXiv:2201.08269 \[hep-ex\]](#).
- [97] **LEP Working Group for Higgs boson searches, ALEPH, DELPHI, L3, OPAL** Collaboration, R. Barate *et al.*, “Search for the standard model Higgs boson at LEP,” *Phys. Lett. B* **565** (2003) 61–75, [arXiv:hep-ex/0306033](#).
- [98] T.-K. Chen, C.-W. Chiang, S. Heinemeyer, and G. Weiglein, “95 GeV Higgs boson in the Georgi-Machacek model,” *Phys. Rev. D* **109** no. 7, (2024) 075043, [arXiv:2312.13239 \[hep-ph\]](#).
- [99] D. López-Val and T. Robens, “ Δr and the W -boson mass in the singlet extension of the standard model,” *Phys. Rev. D* **90** (2014) 114018, [arXiv:1406.1043 \[hep-ph\]](#).
- [100] G. ’t Hooft, “Naturalness, chiral symmetry, and spontaneous chiral symmetry breaking,” *NATO Sci. Ser. B* **59** (1980) 135–157.
- [101] M. Cirelli, N. Fornengo, and A. Strumia, “Minimal dark matter,” *Nucl. Phys. B* **753** (2006) 178–194, [arXiv:hep-ph/0512090](#).
- [102] P. Fileviez Perez, H. H. Patel, M. J. Ramsey-Musolf, and K. Wang, “Triplet Scalars and Dark Matter at the LHC,” *Phys. Rev. D* **79** (2009) 055024, [arXiv:0811.3957 \[hep-ph\]](#).
- [103] S. Kanemura and K. Yagyu, “Radiative corrections to electroweak parameters in the Higgs triplet model and implication with the recent Higgs boson searches,” *Phys. Rev. D* **85** (2012) 115009, [arXiv:1201.6287 \[hep-ph\]](#).
- [104] P. B. Pal, “What is the equivalence theorem really?,” [arXiv:hep-ph/9405362](#).
- [105] J. Horejsi, “Electroweak interactions and high-energy limit: An Introduction to equivalence theorem,” *Czech. J. Phys.* **47** (1997) 951–977, [arXiv:hep-ph/9603321](#).
- [106] J. E. Camargo-Molina, B. Garbrecht, B. O’Leary, W. Porod, and F. Staub, “Constraining the Natural MSSM through tunneling to color-breaking vacua at zero

- and non-zero temperature,” *Phys. Lett. B* **737** (2014) 156–161, [arXiv:1405.7376 \[hep-ph\]](#).
- [107] J. E. Camargo-Molina, B. O’Leary, W. Porod, and F. Staub, “**Vevacious**: A Tool For Finding The Global Minima Of One-Loop Effective Potentials With Many Scalars,” *Eur. Phys. J. C* **73** no. 10, (2013) 2588, [arXiv:1307.1477 \[hep-ph\]](#).
- [108] W. Porod, “SPHeno, a program for calculating supersymmetric spectra, SUSY particle decays and SUSY particle production at e^+e^- colliders,” *Comput. Phys. Commun.* **153** (2003) 275–315, [arXiv:hep-ph/0301101](#).
- [109] W. Porod and F. Staub, “SPHeno 3.1: Extensions including flavour, CP -phases and models beyond the MSSM,” *Comput. Phys. Commun.* **183** (2012) 2458–2469, [arXiv:1104.1573 \[hep-ph\]](#).
- [110] M. D. Goodsell and A. Joury, “BSMArt: Simple and fast parameter space scans,” *Comput. Phys. Commun.* **297** (2024) 109057, [arXiv:2301.01154 \[hep-ph\]](#).
- [111] H. E. Logan, “Lectures on perturbative unitarity and decoupling in Higgs physics,” [arXiv:2207.01064 \[hep-ph\]](#).
- [112] C. Anastasiou, C. Duhr, F. Dulat, E. Furlan, T. Gehrmann, F. Herzog, A. Lazopoulos, and B. Mistlberger, “High precision determination of the gluon fusion Higgs boson cross-section at the LHC,” *JHEP* **05** (2016) 058, [arXiv:1602.00695 \[hep-ph\]](#).
- [113] **LHC Higgs Cross Section Working Group** Collaboration, J. R. Andersen et al., “Handbook of LHC Higgs Cross Sections: 3. Higgs Properties,” [arXiv:1307.1347 \[hep-ph\]](#).
- [114] F. Staub, “SARAH 4 : A tool for (not only SUSY) model builders,” *Comput. Phys. Commun.* **185** (2014) 1773–1790, [arXiv:1309.7223 \[hep-ph\]](#).
- [115] F. Staub, “Exploring new models in all detail with SARAH,” *Adv. High Energy Phys.* **2015** (2015) 840780, [arXiv:1503.04200 \[hep-ph\]](#).
- [116] C. Degrande, C. Duhr, B. Fuks, D. Grellscheid, O. Mattelaer, and T. Reiter, “UFO - The Universal FeynRules Output,” *Comput. Phys. Commun.* **183** (2012) 1201–1214, [arXiv:1108.2040 \[hep-ph\]](#).
- [117] A. Alloul, N. D. Christensen, C. Degrande, C. Duhr, and B. Fuks, “FeynRules 2.0 - A complete toolbox for tree-level phenomenology,” *Comput. Phys. Commun.* **185** (2014) 2250–2300, [arXiv:1310.1921 \[hep-ph\]](#).
- [118] C. Degrande, “Automatic evaluation of UV and R2 terms for beyond the Standard Model Lagrangians: a proof-of-principle,” *Comput. Phys. Commun.* **197** (2015) 239–262, [arXiv:1406.3030 \[hep-ph\]](#).
- [119] J. Alwall, M. Herquet, F. Maltoni, O. Mattelaer, and T. Stelzer, “MadGraph 5 : Going Beyond,” *JHEP* **06** (2011) 128, [arXiv:1106.0522 \[hep-ph\]](#).
- [120] J. Alwall, R. Frederix, S. Frixione, V. Hirschi, F. Maltoni, O. Mattelaer, H. S. Shao, T. Stelzer, P. Torrielli, and M. Zaro, “The automated computation of tree-level and

- next-to-leading order differential cross sections, and their matching to parton shower simulations,” *JHEP* **07** (2014) 079, [arXiv:1405.0301 \[hep-ph\]](#).
- [121] **NNPDF** Collaboration, R. D. Ball, V. Bertone, S. Carrazza, L. Del Debbio, S. Forte, A. Guffanti, N. P. Hartland, and J. Rojo, “Parton distributions with QED corrections,” *Nucl. Phys. B* **877** (2013) 290–320, [arXiv:1308.0598 \[hep-ph\]](#).
- [122] R. Ruiz, “QCD Corrections to Pair Production of Type III Seesaw Leptons at Hadron Colliders,” *JHEP* **12** (2015) 165, [arXiv:1509.05416 \[hep-ph\]](#).
- [123] A. A. H., B. Fuks, H.-S. Shao, and Y. Simon, “Precision predictions for exotic lepton production at the Large Hadron Collider,” *Phys. Rev. D* **107** no. 7, (2023) 075011, [arXiv:2301.03640 \[hep-ph\]](#).
- [124] **ATLAS** Collaboration, G. Aad *et al.*, “A detailed map of Higgs boson interactions by the ATLAS experiment ten years after the discovery,” *Nature* **607** no. 7917, (2022) 52–59, [arXiv:2207.00092 \[hep-ex\]](#). [Erratum: *Nature* 612, E24 (2022)].
- [125] **CMS** Collaboration, A. Tumasyan *et al.*, “A portrait of the Higgs boson by the CMS experiment ten years after the discovery,” *Nature* **607** no. 7917, (2022) 60–68, [arXiv:2207.00043 \[hep-ex\]](#). [Erratum: *Nature* 623, (2023)].
- [126] C.-S. Chen, C.-Q. Geng, D. Huang, and L.-H. Tsai, “New Scalar Contributions to $h \rightarrow Z\gamma$,” *Phys. Rev. D* **87** (2013) 075019, [arXiv:1301.4694 \[hep-ph\]](#).
- [127] **CMS** Collaboration, A. M. Sirunyan *et al.*, “Measurements of Higgs boson production cross sections and couplings in the diphoton decay channel at $\sqrt{s} = 13$ TeV,” *JHEP* **07** (2021) 027, [arXiv:2103.06956 \[hep-ex\]](#).
- [128] **ATLAS** Collaboration, G. Aad *et al.*, “Measurement of the properties of Higgs boson production at $\sqrt{s} = 13$ TeV in the $H \rightarrow \gamma\gamma$ channel using 139 fb⁻¹ of pp collision data with the ATLAS experiment,” *JHEP* **07** (2023) 088, [arXiv:2207.00348 \[hep-ex\]](#).
- [129] **ATLAS** Collaboration, G. Aad *et al.*, “A search for the $Z\gamma$ decay mode of the Higgs boson in pp collisions at $\sqrt{s} = 13$ TeV with the ATLAS detector,” *Phys. Lett. B* **809** (2020) 135754, [arXiv:2005.05382 \[hep-ex\]](#).
- [130] **CMS** Collaboration, A. Tumasyan *et al.*, “Search for Higgs boson decays to a Z boson and a photon in proton-proton collisions at $\sqrt{s} = 13$ TeV,” *JHEP* **05** (2023) 233, [arXiv:2204.12945 \[hep-ex\]](#).
- [131] **ATLAS, CMS** Collaboration, G. Aad *et al.*, “Evidence for the Higgs Boson Decay to a Z Boson and a Photon at the LHC,” *Phys. Rev. Lett.* **132** no. 2, (2024) 021803, [arXiv:2309.03501 \[hep-ex\]](#).
- [132] **ATLAS** Collaboration, G. Aad *et al.*, “Higgs boson production cross-section measurements and their EFT interpretation in the 4ℓ decay channel at $\sqrt{s} = 13$ TeV with the ATLAS detector,” *Eur. Phys. J. C* **80** no. 10, (2020) 957, [arXiv:2004.03447 \[hep-ex\]](#). [Erratum: *Eur.Phys.J.C* 81, 29 (2021), Erratum: *Eur.Phys.J.C* 81, 398 (2021)].

- [133] T. G. Rizzo, “Decays of Heavy Higgs Bosons,” *Phys. Rev. D* **22** (1980) 722.
- [134] W.-Y. Keung and W. J. Marciano, “HIGGS SCALAR DECAYS: $H \rightarrow W^\pm X$,” *Phys. Rev. D* **30** (1984) 248.
- [135] A. Djouadi, “Decays of the Higgs bosons,” in *International Workshop on Quantum Effects in the Minimal Supersymmetric Standard Model*, pp. 197–222. 12, 1997. [arXiv:hep-ph/9712334](#).
- [136] A. Djouadi, “The Anatomy of electro-weak symmetry breaking. I: The Higgs boson in the standard model,” *Phys. Rept.* **457** (2008) 1–216, [arXiv:hep-ph/0503172](#).
- [137] A. Djouadi, “The Anatomy of electro-weak symmetry breaking. II. The Higgs bosons in the minimal supersymmetric model,” *Phys. Rept.* **459** (2008) 1–241, [arXiv:hep-ph/0503173](#).
- [138] **ATLAS** Collaboration, “Improved W boson Mass Measurement using 7 TeV Proton-Proton Collisions with the ATLAS Detector,”.
- [139] **LHCb** Collaboration, R. Aaij et al., “Measurement of the W boson mass,” *JHEP* **01** (2022) 036, [arXiv:2109.01113 \[hep-ex\]](#).
- [140] **D0** Collaboration, V. M. Abazov et al., “Measurement of the W boson mass,” *Phys. Rev. Lett.* **103** (2009) 141801, [arXiv:0908.0766 \[hep-ex\]](#).
- [141] **D0** Collaboration, V. M. Abazov et al., “Measurement of the W boson mass with the D0 detector,” *Phys. Rev. D* **89** no. 1, (2014) 012005, [arXiv:1310.8628 \[hep-ex\]](#).
- [142] **ATLAS** Collaboration, M. Aaboud et al., “Measurement of the W -boson mass in pp collisions at $\sqrt{s} = 7$ TeV with the ATLAS detector,” *Eur. Phys. J. C* **78** no. 2, (2018) 110, [arXiv:1701.07240 \[hep-ex\]](#). [Erratum: *Eur.Phys.J.C* 78, 898 (2018)].
- [143] **ALEPH, DELPHI, L3, OPAL, LEP Electroweak** Collaboration, S. Schael et al., “Electroweak Measurements in Electron-Positron Collisions at W -Boson-Pair Energies at LEP,” *Phys. Rept.* **532** (2013) 119–244, [arXiv:1302.3415 \[hep-ex\]](#).
- [144] **LHC-TeV MW Working Group** Collaboration, S. Amoroso et al., “Compatibility and combination of world W -boson mass measurements,” *Eur. Phys. J. C* **84** no. 5, (2024) 451, [arXiv:2308.09417 \[hep-ex\]](#).
- [145] J. de Blas, M. Pierini, L. Reina, and L. Silvestrini, “Impact of the Recent Measurements of the Top-Quark and W -Boson Masses on Electroweak Precision Fits,” *Phys. Rev. Lett.* **129** no. 27, (2022) 271801, [arXiv:2204.04204 \[hep-ph\]](#).
- [146] **ATLAS** Collaboration, G. Aad et al., “Measurement of the W -boson mass and width with the ATLAS detector using proton-proton collisions at $\sqrt{s} = 7$ TeV,” [arXiv:2403.15085 \[hep-ex\]](#).
- [147] **CMS** Collaboration, “Measurement of the W boson mass in proton-proton collisions at $\sqrt{s} = 13$ TeV,”.
- [148] **ATLAS** Collaboration, G. Aad et al., “Search for direct stau production in events

- with two hadronic τ -leptons in $\sqrt{s} = 13$ TeV pp collisions with the ATLAS detector,” *Phys. Rev. D* **101** no. 3, (2020) 032009, [arXiv:1911.06660 \[hep-ex\]](#).
- [149] CMS Collaboration, A. M. Sirunyan *et al.*, “Search for direct pair production of supersymmetric partners to the τ lepton in proton-proton collisions at $\sqrt{s} = 13$ TeV,” *Eur. Phys. J. C* **80** no. 3, (2020) 189, [arXiv:1907.13179 \[hep-ex\]](#).
- [150] CMS Collaboration, A. Tumasyan *et al.*, “Search for direct pair production of supersymmetric partners of τ leptons in the final state with two hadronically decaying τ leptons and missing transverse momentum in proton-proton collisions at $\sqrt{s} = 13$ TeV,” *Phys. Rev. D* **108** no. 1, (2023) 012011, [arXiv:2207.02254 \[hep-ex\]](#).
- [151] ATLAS Collaboration, G. Aad *et al.*, “Search for electroweak production of supersymmetric particles in final states with two τ -leptons in $\sqrt{s} = 13$ TeV pp collisions with the ATLAS detector,” *JHEP* **05** (2024) 150, [arXiv:2402.00603 \[hep-ex\]](#).
- [152] CMS Collaboration, A. M. Sirunyan *et al.*, “Search for physics beyond the standard model in multilepton final states in proton-proton collisions at $\sqrt{s} = 13$ TeV,” *JHEP* **03** (2020) 051, [arXiv:1911.04968 \[hep-ex\]](#).
- [153] CMS Collaboration, “Inclusive nonresonant multilepton probes of new phenomena at $\sqrt{s} = 13$ TeV,”.
- [154] ATLAS Collaboration, G. Aad *et al.*, “Search for supersymmetry in events with four or more charged leptons in 139 fb^{-1} of $\sqrt{s} = 13$ TeV pp collisions with the ATLAS detector,” *JHEP* **07** (2021) 167, [arXiv:2103.11684 \[hep-ex\]](#).
- [155] ATLAS Collaboration, G. Aad *et al.*, “Search for new phenomena in three- or four-lepton events in pp collisions at $\sqrt{s} = 13$ TeV with the ATLAS detector,” *Phys. Lett. B* **824** (2022) 136832, [arXiv:2107.00404 \[hep-ex\]](#).
- [156] ATLAS Collaboration, G. Aad *et al.*, “A search for new resonances in multiple final states with a high transverse momentum Z boson in $\sqrt{s} = 13$ TeV pp collisions with the ATLAS detector,” *JHEP* **06** (2023) 036, [arXiv:2209.15345 \[hep-ex\]](#).
- [157] ATLAS Collaboration, G. Aad *et al.*, “Search for type-III seesaw heavy leptons in leptonic final states in pp collisions at $\sqrt{s} = 13$ TeV with the ATLAS detector,” *Eur. Phys. J. C* **82** no. 11, (2022) 988, [arXiv:2202.02039 \[hep-ex\]](#).
- [158] ATLAS Collaboration, G. Aad *et al.*, “Search for doubly charged Higgs boson production in multi-lepton final states using 139 fb^{-1} of proton-proton collisions at $\sqrt{s} = 13$ TeV with the ATLAS detector,” *Eur. Phys. J. C* **83** no. 7, (2023) 605, [arXiv:2211.07505 \[hep-ex\]](#).
- [159] ATLAS Collaboration, G. Aad *et al.*, “Measurements of differential cross-sections in four-lepton events in 13 TeV proton-proton collisions with the ATLAS detector,” *JHEP* **07** (2021) 005, [arXiv:2103.01918 \[hep-ex\]](#).
- [160] R. Frederix, S. Frixione, V. Hirschi, D. Pagani, H. S. Shao, and M. Zaro, “The

- automation of next-to-leading order electroweak calculations,” *JHEP* **07** (2018) 185, [arXiv:1804.10017 \[hep-ph\]](#). [Erratum: *JHEP* 11, 085 (2021)].
- [161] T. Sjöstrand, S. Ask, J. R. Christiansen, R. Corke, N. Desai, P. Ilten, S. Mrenna, S. Prestel, C. O. Rasmussen, and P. Z. Skands, “An introduction to PYTHIA 8.2” *Comput. Phys. Commun.* **191** (2015) 159–177, [arXiv:1410.3012 \[hep-ph\]](#).
- [162] **DELPHES 3** Collaboration, J. de Favereau, C. Delaere, P. Demin, A. Giammanco, V. Lemaitre, A. Mertens, and M. Selvaggi, “DELPHES 3, A modular framework for fast simulation of a generic collider experiment,” *JHEP* **02** (2014) 057, [arXiv:1307.6346 \[hep-ex\]](#).
- [163] M. Cacciari, G. P. Salam, and G. Soyez, “The anti- k_t jet clustering algorithm,” *JHEP* **04** (2008) 063, [arXiv:0802.1189 \[hep-ph\]](#).
- [164] M. Cacciari, G. P. Salam, and G. Soyez, “FastJet User Manual,” *Eur. Phys. J. C* **72** (2012) 1896, [arXiv:1111.6097 \[hep-ph\]](#).
- [165] M. Cepeda et al., “Report from Working Group 2: Higgs Physics at the HL-LHC and HE-LHC,” *CERN Yellow Rep. Monogr.* **7** (2019) 221–584, [arXiv:1902.00134 \[hep-ph\]](#).
- [166] **ATLAS** Collaboration, M. Aaboud et al., “Measurements of Higgs boson properties in the diphoton decay channel with 36 fb⁻¹ of pp collision data at $\sqrt{s} = 13$ TeV with the ATLAS detector,” *Phys. Rev. D* **98** (2018) 052005, [arXiv:1802.04146 \[hep-ex\]](#).
- [167] G. Cowan, K. Cranmer, E. Gross, and O. Vitells, “Asymptotic formulae for likelihood-based tests of new physics,” *Eur. Phys. J. C* **71** (2011) 1554, [arXiv:1007.1727 \[physics.data-an\]](#). [Erratum: *Eur.Phys.J.C* 73, 2501 (2013)].
- [168] H. Georgi and M. Machacek, “DOUBLY CHARGED HIGGS BOSONS,” *Nucl. Phys. B* **262** (1985) 463–477.
- [169] **ATLAS** Collaboration, G. Aad et al., “Inclusive and differential cross-sections for dilepton $t\bar{t}$ production measured in $\sqrt{s} = 13$ TeV pp collisions with the ATLAS detector,” *JHEP* **07** (2023) 141, [arXiv:2303.15340 \[hep-ex\]](#).
- [170] S. Inoue, G. Ovanessian, and M. J. Ramsey-Musolf, “Two-Step Electroweak Baryogenesis,” *Phys. Rev. D* **93** (2016) 015013, [arXiv:1508.05404 \[hep-ph\]](#).
- [171] P. M. Ferreira, R. Santos, and A. Barroso, “Stability of the tree-level vacuum in two Higgs doublet models against charge or CP spontaneous violation,” *Phys. Lett. B* **603** (2004) 219–229, [arXiv:hep-ph/0406231](#). [Erratum: *Phys.Lett.B* 629, 114–114 (2005)].
- [172] A. Barroso, P. M. Ferreira, and R. Santos, “Charge and CP symmetry breaking in two Higgs doublet models,” *Phys. Lett. B* **632** (2006) 684–687, [arXiv:hep-ph/0507224](#).
- [173] P. M. Ferreira and B. L. Gonçalves, “Stability of neutral minima against charge

- breaking in the Higgs triplet model,” *JHEP* **02** (2020) 182, [arXiv:1911.09746 \[hep-ph\]](#).
- [174] D. Azevedo, P. Ferreira, H. E. Logan, and R. Santos, “Vacuum structure of the \mathbb{Z}_2 symmetric Georgi-Machacek model,” *JHEP* **03** (2021) 221, [arXiv:2012.07758 \[hep-ph\]](#).
- [175] R. S. Hundi, “Study on the global minimum and $H \rightarrow \gamma\gamma$ in the Dirac scotogenic model,” *Phys. Rev. D* **108** no. 1, (2023) 015006, [arXiv:2303.04655 \[hep-ph\]](#).